Inaugural dissertation

for

obtaining the doctoral degree

of the

Combined Faculty of Mathematics, Engineering and Natural Sciences

of the

Ruprecht-Karls-University

Heidelberg

Presented by:

B.Sc. Hui Ting Zhang

Born in Singapore

Oral examination: September 15, 2022

Coordination of growth and morphogenesis

in the mouse peri-implantation embryo

Referees: Jun.-Prof. Dr. Steffen Lemke

Dr. Aissam Ikmi

SUMMARY

In contrast to the majority of animals, mammalian embryonic development is highly regulative, beginning from one or several functionally-identical cells and sequentially acquiring increasing complexity over a relatively short period of time. During this period, the embryo also undergoes significant changes in morphology so as to accommodate the increase in complexity, especially during the landmark developmental event of gastrulation. How these morphological changes are enacted, coordinated, and controlled at the supra-cellular scale is yet unclear. The study of this question, and indeed this scientifically interesting period of development, has been historically difficult. This is partially due to the fact that unlike in other animals such as the zebrafish or the fruit fly, most mammalian embryos – including that of mice, the most common model organism in which such studies are conducted – are undergoing or have already undergone implantation into the uterine tissues during this period.

To facilitate the study the peri-implantation development of mouse embryos, I have developed a 3D *ex vivo* culture system that is compatible with long-term light-sheet imaging, jointly with colleagues and collaborators. I characterised the development of embryos in this culture system and optimised it so that it supported the physiological growth and morphogenesis of embryonic and several extra-embryonic lineages. After validating this culture system, I used it to investigate the cell- and tissue-scale changes that occurred in the embryonic tissues during the peri-implantation period. In the mouse embryo, this period is associated with significant growth and differentiation of both embryonic and extra-embryonic tissues. For example, the epiblast (an embryonic cell lineage) adopts a pseudo-stratified epithelium organisation, while a subpopulation of the visceral endoderm (an extra-embryonic cell lineage) specialises into a distinct lineage that patterns the underlying embryonic ectoderm to lay down the first embryonic body axis. I demonstrated that the 3D *ex vivo* culture system supports live imaging at sufficient spatial and temporal resolution to visualise these processes. In addition, using an automatic 3D segmentation pipeline developed by colleagues and collaborators, I showed that the culture system can be used to study cell- and tissue-scale dynamics.

The regulative nature of early mammalian development is also evident in the fact that the early mammalian embryo can tolerate drastic deviations in tissue size and cell number during development and correct these deviations so that at birth, embryos are once again within the stereotypical range of sizes for the species. The early mouse embryo can tolerate at least

four-fold changes in cell number, brought about by removal or addition of blastomeres; however, these size deviations are reportedly resolved by the time gastrulation is initiated, with embryos all undergoing gastrulation with the epiblast cell number at a certain threshold. I observed discrepancies between my findings and those previously reported, demonstrating that this process is still poorly understood despite decades of study, and identify cell- and tissue-scale parameters that may play a role in the sensing and correction of size deviations in the embryo.

ZUSAMMENFASSUNG

Im Gegensatz zu den meisten Tieren verläuft die Embryonalentwicklung bei Säugetieren hochgradig regulativ. Sie beginnt mit einer oder mehreren funktionell identischen Zellen und nimmt innerhalb eines relativ kurzen Zeitraums immer mehr an Komplexität zu. Während dieser Zeit durchläuft der Embryo auch bedeutende morphologische Veränderungen, um der zunehmenden Komplexität Rechnung zu tragen, insbesondere während des wegweisenden Entwicklungsereignisses der Gastrulation. Wie diese morphologischen Veränderungen auf der suprazellulären Ebene in Gang gesetzt, koordiniert und kontrolliert werden, ist noch unklar. Die Untersuchung dieser Frage und dieses wissenschaftlich interessanten Entwicklungsabschnitts war in der Vergangenheit schwierig. Dies liegt zum Teil daran, dass im Gegensatz zu anderen Tieren wie dem Zebrafisch oder der Fruchtfliege die meisten Säugetierembryonen - auch die der Maus, dem häufigsten Modellorganismus, an dem solche Studien durchgeführt werden - in diesem Zeitraum die Einnistung in das Gebärmuttergewebe durchlaufen oder bereits abgeschlossen haben.

Um die Untersuchung der Peri-implantationsentwicklung von Mäuseembryonen zu erleichtern, habe ich gemeinsam mit Kollegen und Mitarbeitern ein 3D-Ex-vivo-Kultursystem entwickelt, das mit Langzeit-Lichtschnittaufnahmen kompatibel ist. Ich habe die Entwicklung von Embryonen in diesem Kultursystem charakterisiert und es so optimiert, dass es das physiologische Wachstum und die Morphogenese von embryonalen und verschiedenen extra-embryonalen Linien unterstützt. Nach der Validierung dieses Kultursystems untersuchte ich damit die zell- und gewebebezogenen Veränderungen, die in den embryonalen Geweben während der Periimplantationszeit auftreten. Beim Mausembryo ist dieser Zeitraum mit einem bedeutenden Wachstum und einer bedeutenden Differenzierung sowohl der embryonalen als auch der extraembryonalen Gewebe verbunden. So nimmt beispielsweise der Epiblast (eine embryonale Zelllinie) eine pseudo-stratifizierte Epithelorganisation an, während eine Subpopulation des viszeralen Endoderms (eine extraembryonale Zelllinie) sich zu einer bestimmten Linie spezialisiert, die das darunter liegende embryonale Ektoderm strukturiert, um die erste embryonale Körperachse zu bilden. Ich habe gezeigt, dass das 3D-Ex-vivo-Kultursystem Live-Bildgebung mit ausreichender räumlicher und zeitlicher Auflösung ermöglicht, um diese Prozesse sichtbar zu machen. Darüber hinaus habe ich mit Hilfe einer automatischen 3D-Segmentierungspipeline, die von Kollegen und Mitarbeitern entwickelt

wurde, gezeigt, dass das Kultursystem zur Untersuchung der Dynamik auf Zell- und Gewebeskala verwendet werden kann.

Die regulative Natur der frühen Säugetierentwicklung zeigt sich auch darin, dass der frühe Säugetierembryo drastische Abweichungen in der Gewebegröße und Zellzahl während der Entwicklung tolerieren und diese Abweichungen korrigieren kann, so dass die Embryonen bei der Geburt wieder innerhalb des stereotypen Größenbereichs für die jeweilige Art liegen. Der frühe Mausembryo kann mindestens vierfache Veränderungen der Zellzahl tolerieren, die durch die Entfernung oder Hinzufügung von Blastomeren verursacht werden; diese Größenabweichungen werden jedoch Berichten zufolge bis zum Beginn der Gastrulation behoben, wobei alle Embryonen die Gastrulation mit einer bestimmten Zellzahl des Epiblasten durchlaufen. Ich habe Diskrepanzen zwischen meinen Ergebnissen und den zuvor berichteten festgestellt, was zeigt, dass dieser Prozess trotz jahrzehntelanger Studien noch immer schlecht verstanden wird, und ich habe Parameter auf Zell- und Gewebeskala identifiziert, die bei der Erkennung und Korrektur von Größenabweichungen im Embryo eine Rolle spielen könnten.

TABLE OF CONTENTS

ABBREVIATIONS

2D	two-dimensional
3D	three-dimensional
3D-geec	3D gel-embedded embryo culture
ANOVA	analysis of variance
AP	anterior-posterior
AR	aspect ratio
a.u.	arbitrary unit
ASE	asymmetric enhancer
AVE	anterior visceral endoderm
bp	base pairs
BSA	bovine serum albumin
Cdh1	Cadherin 1
Cdx2	Caudal type homeobox 2
Cer1	Cerberus 1
D	day
DNA	deoxyribonucleic acid
Dusp4	Dual specificity protein phosphatase 4
DV	dorsal-ventral
DVE	distal visceral endoderm
E	embryonic day
EDTA	ethylenediaminetetraacetic acid
EGFP	enhanced green fluorescent protein
EPI	epiblast
EpiSC	Epiblast-derived stem cell
ExE	extraembryonic ectoderm
FGF	fibroblast growth factor
Gata4	GATA binding protein 4
gDNA	genomic DNA
H2B	histone 2B
hCG	human chorionic gonadotropin

HEPES	4-(2-hydroxyethyl)-1-piperazineethanesulfonic acid
Hex	homeobox protein
ICM	inner cell mass
IKNM	interkinetic nuclear migration
IU	international unit
IVC	*in vitro* culture
KO	knockout
KSOM	potassium simplex optimisation medium
KSOM-H	KSOM with HEPES
LR	left-right
M	molar
micro-CT	micro-computed tomorgraphy
min	minute
MPM	multiphoton microscopy
MRI	magnetic resonance imaging
mTE	mural trophectoderm
NaCl	sodium chloride
OCT	optical coherence tomography
Oct4	Octamer-binding transcription factor 4
PBS	phosphate-buffered saline
PCR	polymerase chain reaction
Pdgfra	platelet-derived growth factor receptor A
pERM	phosphorylated Ezrin/Radixin/Moesin
pET	post-embryo transfer
PFA	paraformaldehyde
PMSG	pregnant mare serum gonadotropin
ppMRLC	bi-phosphorylated myosin regulatory light chain
PrE	primitive endoderm
pTE	polar trophectoderm
rpm	rounds per minute
S.D.	standard deviation
SDS	sodium dodecyl sulphate
Sox2	SRY-box containing gene 2

SPIM	single plane illumination microscopy
SSR	Sum of Squared Residuals
TE	trophectoderm
TF	transcription factor
Tg	transgenic
Tris-HCl	tris(hydroxymethyl)aminomethane hydrochloride
VE	visceral endoderms
VP+	vaginal plug positive
WLS	Weighted Least Squares (Pearson's chi-squared statistic)
w/v	weight per volume
WT	wild-type
YAP	yes-associated protein
YFP	yellow fluorescent protein
ZP	zona pellucida

1. INTRODUCTION

Unlike invertebrates, many of which display drastically-different larval and adult forms, the vast majority of vertebrates lay down the adult body plan entirely during embryonic development. Crucial events such as the breaking of initial symmetry, the establishment of the body axes, and the formation of the germ layers through gastrulation, take place during early embryonic development. Mammalian embryos, exemplars of regulative development, display a remarkable ability to accomplish most of these processes without much external input. The regulative nature of mammalian development extends to the ability to tolerate and compensate for drastic deviations from normal embryo size so that embryos which started with significantly different cell numbers and tissue sizes will end up indistinguishable in size by birth. Study of these processes have been hindered by the relative inaccessibility of the mammalian embryo once it implants. Recent advancements in embryo culture, imaging, and manipulation promise to shed light on this extremely interesting period of development.

EARLY EMBRYONIC DEVELOPMENT IN MAMMALS

Early embryonic development is highly conserved across mammalian species (**Figure 1.1**). While differences in the size of the embryo, the timing of developmental events, and, eventually, the morphology of the embryos can vary across taxa, the broad strokes of early embryonic development are conserved. This makes it possible to study general principles of early mammalian development using model organisms such as the mouse, *Mus musculus*.

One of the most striking features of early embryonic development in mammals is its highly regulative nature (Louvet-Vallée et al., 2005; Posfai et al., 2017; Rossant and Lis, 1979; Rossant and Vijh, 1980; Tarkowski, 1959, 1961; Tarkowski and Wróblewska, 1967). In direct contrast to the deterministic development in invertebrates and some non-mammalian vertebrates, the early mammalian embryo is homogenous with respect to its ability to develop into the foetus proper. Despite extensive investigation, no maternal determinants have been found in the mammalian oocyte (Antczak and Van Blerkom, 1997; Littwin and Denker, 2011; Schulz and Roberts, 2011); there is no animal or vegetal pole for mammals, unlike in other vertebrates such as the African clawed frog, *Xenopus laevis,* or the zebrafish, *Danio rerio* (Alarcón and Marikawa, 2005; Kurotaki et al., 2007; Motosugi et al., 2005; Rossant and Tam, 2009; Solter, 2016). The question of how blastomeres arising from such a homogeneous structure go on to adopt different cell fates and identities has long been under investigation.
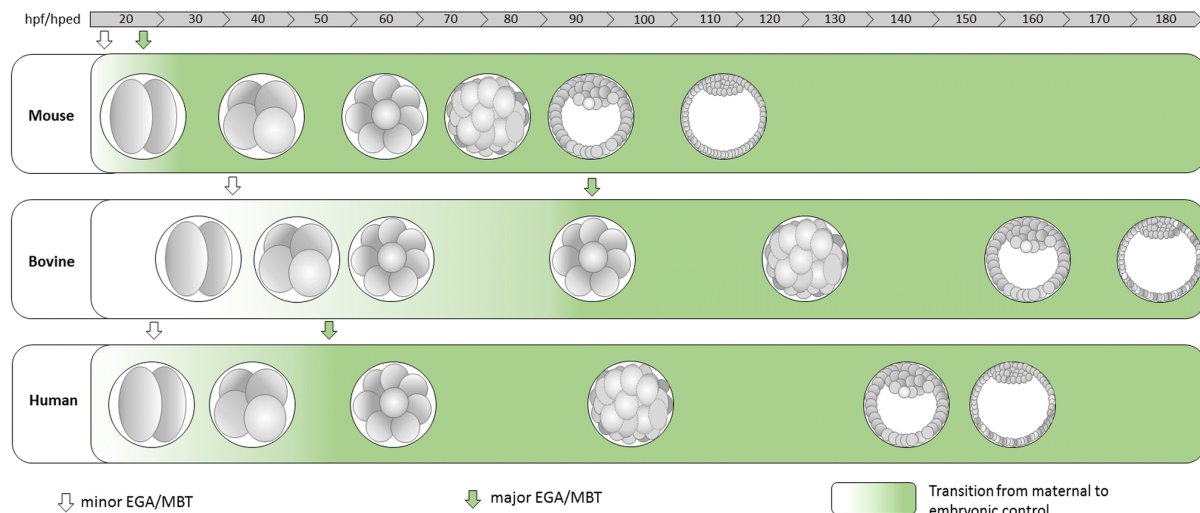
Figure 1.1: Early embryonic development from 2-cell to blastocyst stage in the mouse, bovine, and human contexts. The sequential cleavage-type cell divisions, the differentiation of cell lineages, the handover of genetic expression and control from maternal transcripts to the embryo, and the organisation of the embryo into a morula that later cavitates into a blastocyst is highly conserved. Figure adapted from (Toralova et al., 2020). hpf: hours post fertilisation; EGA/MBT: Embryonic genome activation/mid-blastula transition.

The mouse embryo as a model for mammalian early embryonic development

The mouse, *Mus musculus*, has traditionally been used as a model for the study of mammalian embryonic development. In the mouse, development from fertilisation to implantation takes place over the span of four days, beginning as a single-celled zygote in the oviduct and developing into a blastocyst, a structure comprised of a single layer of cells encapsulating a fluid-filled cavity and a mass of cells (**Figure 1.2**). The embryonic development of the mouse embryo has been extensively reviewed in the past (Arnold and Robertson, 2009; Artus and Chazaud, 2014; Chazaud and Yamanaka, 2016; Hermitte and Chazaud, 2014; Johnson and McConnell, 2004; Rossant and Tam, 2004, 2009; Stower and Srinivas, 2018; Wennekamp et al., 2013; Yamanaka et al., 2006; Zhang and Hiiragi, 2018). Here, I present a brief introduction to the key events that occur during the period of development leading up to implantation, and place them in the context of regulative development.
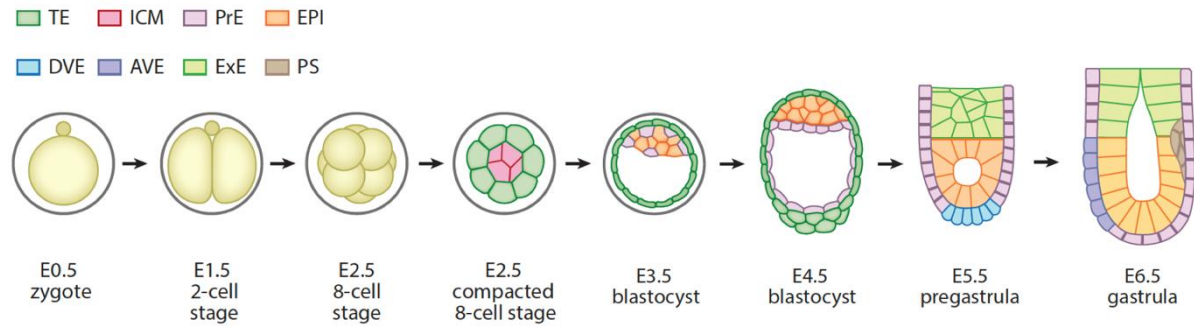
Figure 1.2: Progressive increase in complexity through self-organised symmetry-breaking events during early embryonic development in the mouse. The symmetrical zygote gives rise to a morula that is at first homogenous with respect to potency, but which spontaneously acquires asymmetry during compaction at E2.5 and specifies the first cell lineage with restricted potency, the trophectoderm (TE). Further differentiation of the inner cell mass (ICM) from E2.5 to E4.5 gives rise to the primitive endoderm (PrE) while maintaining the embryonic lineage, the epiblast (EPI). Finally, from E5.5 to E6.5, the establishment of the anterior-posterior axis occurs, ending with the onset of gastrulation where ingression and migration of cells at the posterior primitive streak eventually gives rise to the three germ layers of the foetus. Figure adapted from (Zhang and Hiiragi, 2018). Figure prepared by Hui Ting Zhang.

The first lineage segregation at the 8-cell stage

During the first two days of development, the zygote undergoes three rounds of cleavage-type cell divisions to give rise to a morula with eight blastomeres. Up until this point, all cells of the mouse embryo are functionally identical, with all blastomeres capable of giving rise to both embryonic and extra-embryonic lineages (Guo et al., 2010; Tarkowski and Wróblewska, 1967). With the initiation of compaction, asymmetries in the embryo arise for the first time, and the embryo specifies its first extra-embryonic lineage, the trophectoderm (TE) (**Figure 1.3**).
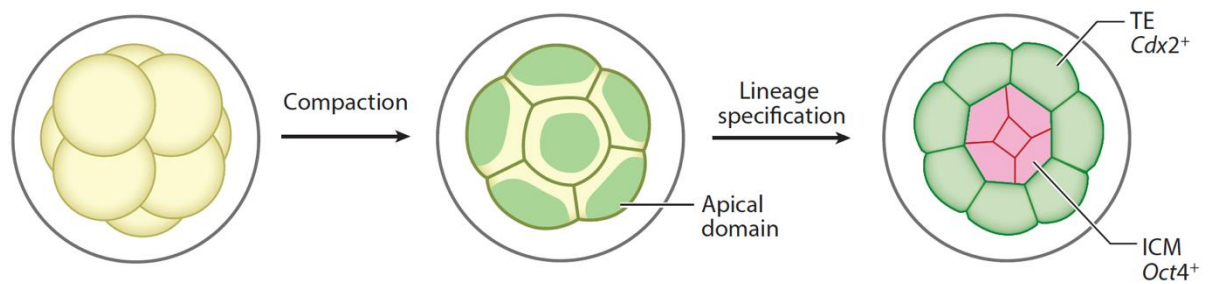
Figure 1.3: The first lineage segregation event occurs concurrently with the first major morphogenetic event in the early mouse embryo. Figure adapted from (Zhang and Hiiragi, 2018). Figure prepared by Hui Ting Zhang.

Naturally, much attention has been paid to how the first lineage segregation occurs in the mouse embryo. Two hypotheses have been put forth to explain how blastomeres in the embryo adopt a TE identity, or, in contrast, maintain an inner-cell mass (ICM) that is capable of differentiating into both embryonic and extra-embryonic lineages: the inside-outside model (Tarkowski and Wróblewska, 1967) and the cell polarity model (Johnson and Ziomek, 1981). The inside-outside model emphasises the role that positional information plays in lineage segregation, where cells exposed to the external environment differentiate into the TE, and cells shielded from the external environment become ICM cells. In contrast, the cell polarity model identifies the acquisition of apico-basal polarity during the 8-cell stage to 16-cell stage, and the differential inheritance of the apical domain through asymmetric and symmetric divisions, as the key factor, with apolar cells, generated by asymmetric divisions, becoming the ICM.
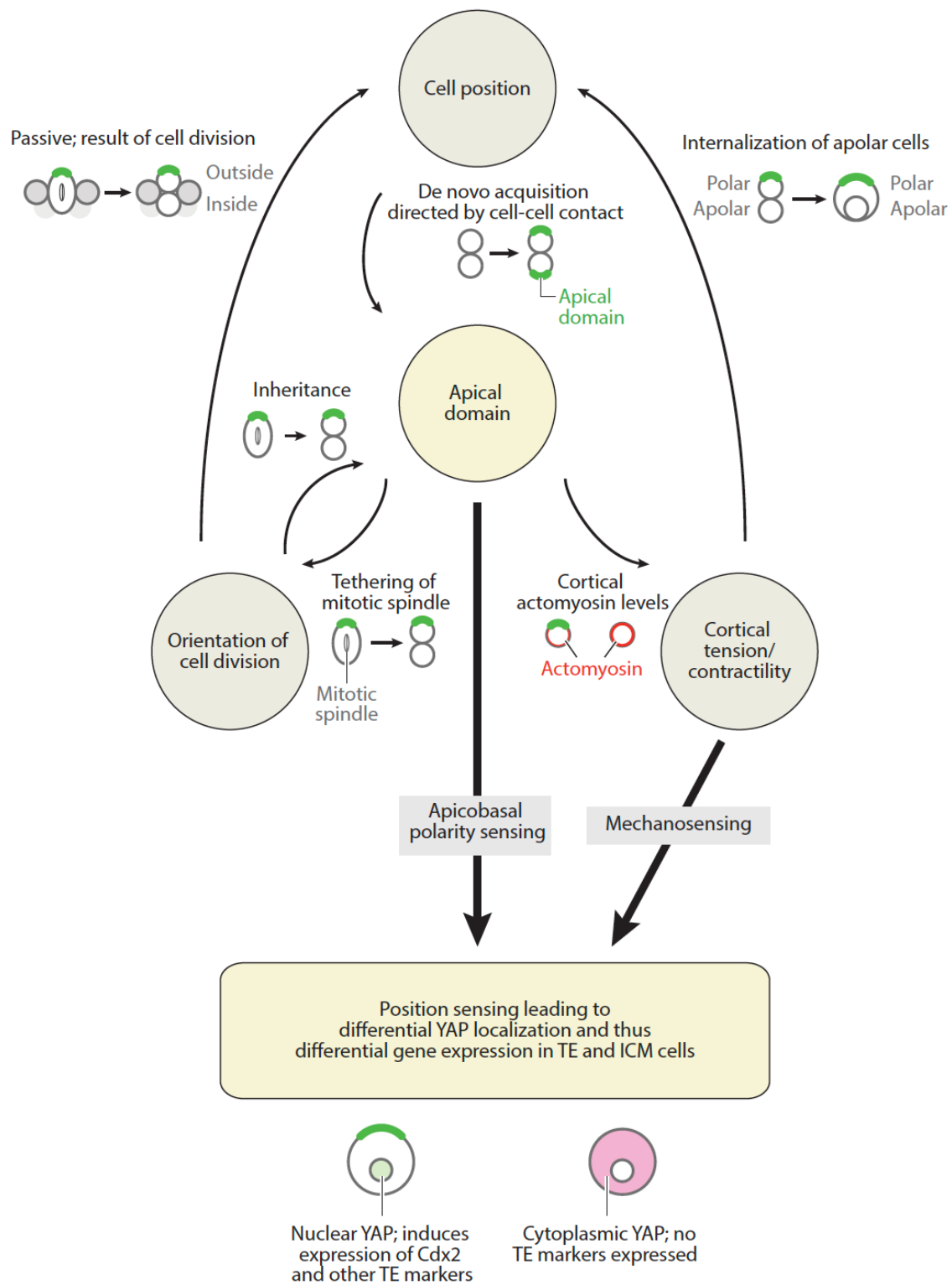
Figure 1.4: The apical domain acts to coordinate positional information and cell polarity information to ensure robust symmetry-breaking and lineage specification. Figure adapted from (Zhang and Hiiragi, 2018). Figure prepared by Hui Ting Zhang.

More recent works have revealed that rather than being dictated by one model or the other, the first symmetry-breaking event and specification of ICM versus TE occurs through the integration and synthesis of multiple inputs, coordinated by the acquisition, positioning, and inheritance of the apical domain (**Figure 1.4**) (Anani et al., 2014; Korotkevich et al., 2017; Maître et al., 2015, 2016). The differential localisation of YAP in future TE and ICM cells led to the expression of different genetic programmes, resulting in lineage specification (Hirate et al., 2013; Korotkevich et al., 2017; Nishioka et al., 2009). A remarkable fact is that the apical domain itself feeds back onto its own inputs – cell positioning and inheritance of the apical domain – by tethering mitotic spindles to orient cell divisions (Korotkevich et al., 2017; Maître et al., 2016), and by restricting the contractile cell cortex to non-apical surfaces (Anani et al., 2014; Maître et al., 2015, 2016; Samarage et al., 2015; Zhu et al., 2017). This complexity of interactions stands in stark contrast to systems where asymmetry is largely imparted by a single external input, as in *Drosophila* or *C. elegans*, and highlights how mammalian development is both regulative and robust.

Specification of the embryonic lineage within the inner cell mass

Following the first lineage segregation event and the formation of the blastocyst, the ICM undergoes further differentiation into the primitive endoderm (PrE) and the epiblast (EPI) (**Figure 1.5**). The former gives rise to extra-embryonic lineages that support and pattern the embryo, while the latter is the embryonic lineage from which the foetus proper is derived. The phenomenon of how ICM cells are specified to these lineages – and furthermore, how they two lineages segregate spatially – has been studied extensively over the past decades.
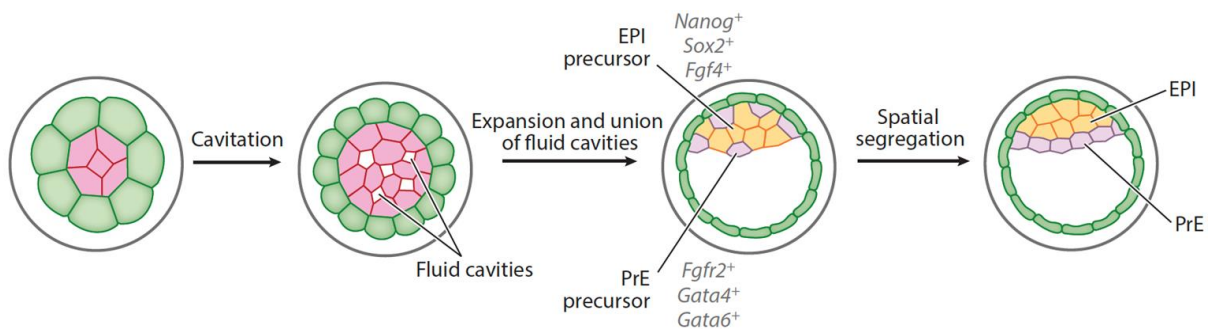
Figure 1.5: The specification ICM-derived lineages is sequential and involves coordination between commitment to different cell fates and spatial segregation of cells. Figure adapted from (Zhang and Hiiragi, 2018). Figure prepared by Hui Ting Zhang.

The first question that must be addressed was if ICM cells were initially equivalent, or if a subpopulation were biased *a priori* towards either PrE or EPI fates even before blastocyst formation. Expression of markers for PrE and EPI arise asynchronously in a salt-and-pepper pattern (Chazaud et al., 2006; Koutsourakis et al., 1999; Mitsui et al., 2003). It had been hypothesised that the time of internalisation during compaction, or the round of division that gave rise to the ICM cell, introduced a bias: ICM cells internalised earlier, or derived from an earlier round of cell division, were predisposed towards an EPI fate, while the converse was true for ICM cells derived from later rounds of division (Chazaud et al., 2006; Chisholm and Houliston, 1987; Krupa et al., 2014; Morris et al., 2010; Yamanaka et al., 2010). However, transcriptomic studies were unable to find evidence to support this hypothesis (Ohnishi et al., 2014a). Instead, ICM cells appeared to express genes reflecting one lineage or the other stochastically (Ohnishi et al., 2014a; Plusa et al., 2008; Yamanaka, 2011; Yamanaka et al., 2010). The ICM always arrives at roughly the same proportion of EPI and PrE cells, and all cells are both committed to a lineage and spatially sorted into the correct position. The question is therefore how apparently-equivalent ICM cells are able to robustly differentiate and sort into separate domains. The question of cell sorting is under intense investigation; the blastocoelic cavity has been implicated in this process (Ryan et al., 2019), though it has yet to be conclusively shown.

More attention has been paid to the specification of cell fates in the ICM in terms of gene expression and signalling. Several studies pointed to signalling through the FGF pathway as a key player in the specification of the PrE and EPI lineages (Kang et al., 2013, 2017; Krawchuk et al., 2013; Molotkov et al., 2017). Stochastic variations in FGF4 expression were enhanced by feedback loops that stabilised fate choice (Plusa et al., 2008; Saiz et al., 2016; Yamanaka et al., 2010). A recent work showed that the asynchronicity of lineage specification within the ICM facilitates the maintenance of the proportions of EPI and PrE cells (Saiz et al., 2020), once again highlighting the regulative nature of mammalian development.

Peri-implantation development is marked by extensive morphogenesis

At this point, the mammalian embryo has adopted the classical blastocyst structure. Up until now, mammalian development looks much the same across species in terms of gross morphology and organisation. However, as the embryo prepares for implantation, species-dependent differences become increasingly evident (Frankenberg et al., 2013; Sheng, 2015).

Strikingly, the rodent embryo undergoes drastic changes in epiblast morphology upon implantation. The EPI adopts a pseudostratified epithelial structure (Ichikawa et al., 2013), and a cavity, known as the pro-amniotic cavity, forms *de novo* within the EPI tissue (Christodoulou et al., 2018); the entire embryo adopts an elongated, cylindrical structure termed the egg cylinder (**Figure 1.6**). While this egg cylinder is unique to rodents, similar principles drive its development and morphogenesis as in other mammalian systems. A complex interplay of signals between the EPI and surrounding extra-embryonic tissues establish the first body axis and prepare the EPI for gastrulation (reviewed in Arnold and Robertson, 2009; Rossant and Tam, 2004; Zhang and Hiiragi, 2018). It is yet unknown how much this complex landscape depends on biochemical or mechanical inputs from the maternal environment.
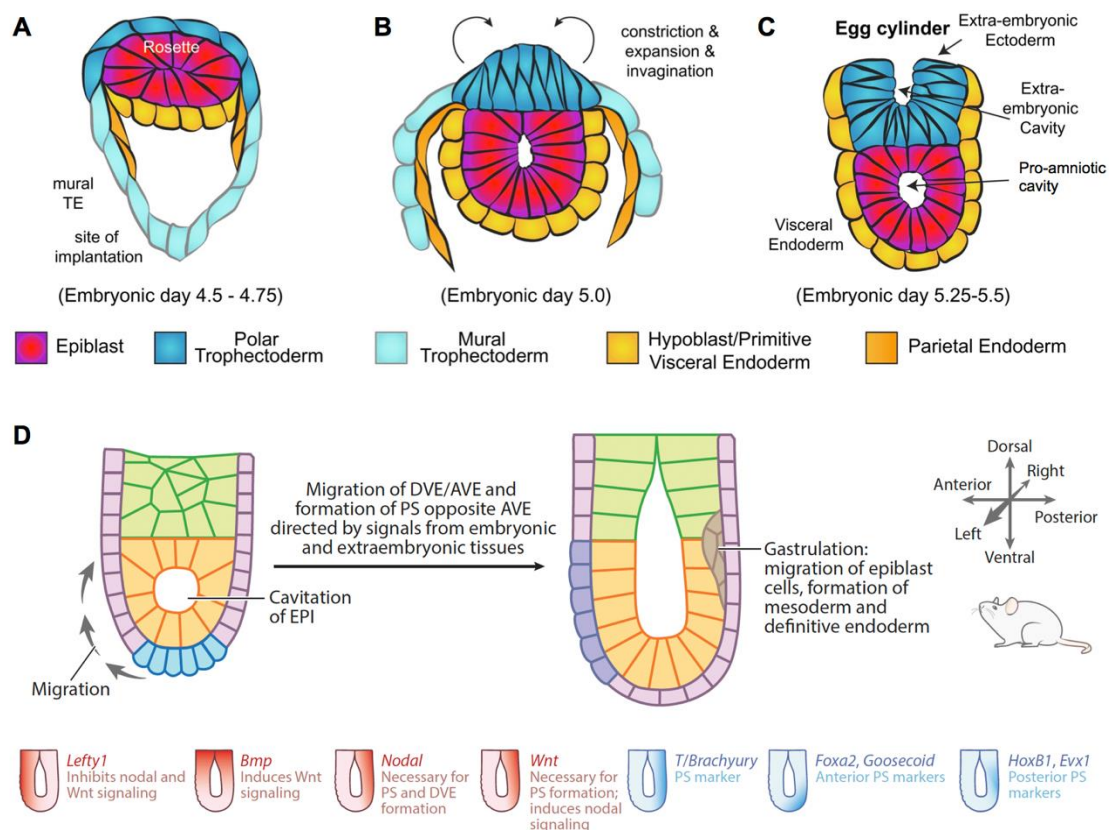
Figure 1.6: Morphogenesis and axis establishment in the peri-implantation mouse embryos.

(A—C) Morphogenesis of the mouse embryo from just before implantation (A) to just after implantation (B), followed by peri- to early-post-implantation morphogenesis (C). Figure adapted from (Molè et al., 2020).

(D) The complex signalling landscape that guides establishment of the anterior-posterior body axis as well as onset of gastrulation in the mouse embryo. Figure adapted from (Zhang and Hiiragi, 2018).

PERI-IMPLANTATION DEVELOPMENT OF THE MOUSE EMBRYO

The implantation process is a hallmark of development in placental mammals

Like in other true placental mammals, the mouse embryo undergoes a characteristic event during early embryonic development where embryo and maternal tissues come into close contact – implantation. During implantation, drastic changes occur in the embryo as well as the maternal uterine environment; new lineages arise, existing lineages mature, and cells undergo tissue-scale reorganisation (Cha et al., 2012; Skreb et al., 1991; Wang and Dey, 2006).

Implantation strategies differ between species, though general principles are conserved (Wang and Dey, 2006) (**Figure 1.7**). First, the uterus itself must be receptive to implantation. Hormone-induced changes in the mother (Cha et al., 2012; Ma et al., 2003; Paria et al., 1998; Song et al., 2007) prime the uterine endometrium for receiving the embryo (Dey et al., 2004; Fazleabas and Strakova, 2002; Yoshinaga, 1988). In parallel, embryo development must proceed so that the tissue crucial for implantation, the TE, is mature by the time the embryo is ready to implant; mouse embryos transferred into foster mothers that have a more advanced uterine age fail to implant and develop (Paria et al., 1993). The pre-implantation embryo is encased in the zona pellucida; just before implantation, the embryo breaches this physical barrier by enzymatic digestion of its constituents and mechanical forces exerted by the blastocoelic cavity (Cole, 1967; Mishra and Seshagiri, 2000; Negrón-Pérez and Hansen, 2017; O'Sullivan et al., 2001; Perona and Wassarman, 1986; Sawada et al., 1990; Seshagiri et al., 2009). The embryo, now exposed directly to the uterine environment, can then initiate implantation. In different species, implantation sites are either restricted to a fixed domain within the uterus, as in humans and bovines (Bulletti and de Ziegler, 2005; Valadão et al., 2018), or develop *de novo* in response to the embryo, as in rodents (Arora et al., 2016; Flores et al., 2020; O'Grady and Heald, 1969).

Reciprocal signals between the embryo and the uterus are crucial for implantation and further development of both the embryo and the uterus. A full discussion of the complex maternal-embryo interactions that occur before and during implantation is outside of the scope of this study; reviews on the current state of the field can be found at (Carson et al., 2000; Cha et al., 2012; Kierszenbaum, 2001; Matsumoto, 2017; Paria et al., 2002). In the rest of the thesis, I focus on the developmental events that occur in the embryo proper, and in select extra-embryonic lineages originating from the zygote.
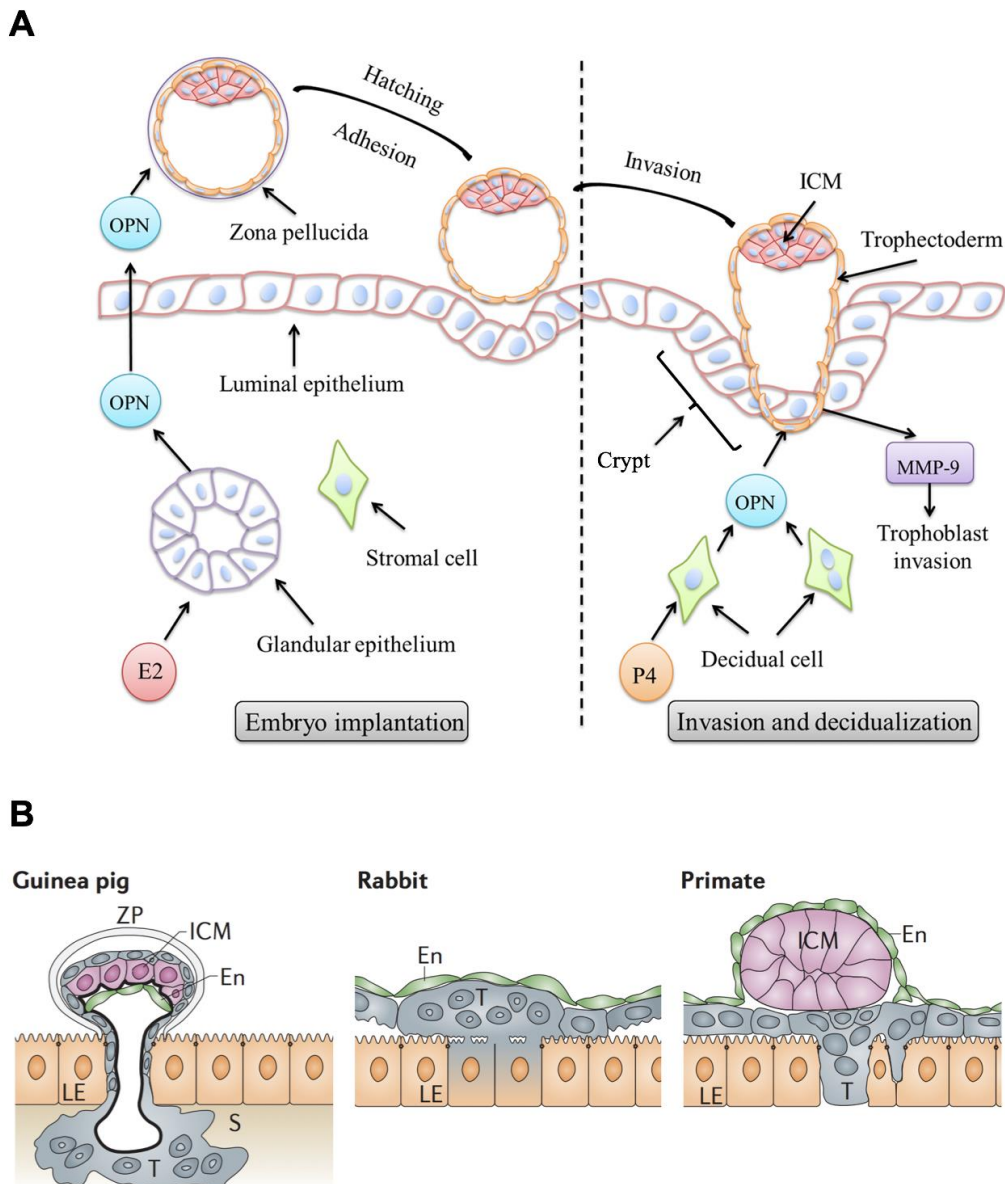
Figure 1.7: Implantation in the mouse and other species. Figures adapted from (Qi et al., 2014; Wang and Dey, 2006).

(A) Implantation of the mouse embryo. The blastocyst hatches from the zona pellucida and attaches to the luminal epithelium, which triggers the formation of the crypt. The invasion of the trophoblasts and the proliferation of stromal cells lead to the folding of the crypt over the embryo, resulting in an embryo almost completely enclosed by uterine tissue. Figure adapted from (Qi et al., 2014).

(B) Non-murine strategies for implantation. Syncytial trophoblast (T) in guinea pigs anchor the embryo, still within the zona pellucida (ZP) to the luminal endothelium (LE) of the uterus. In rabbits, trophoblast cells (T) undergo cell fusion with LE to form symplasma. Primate implantation is triggered by trophoblast near the inner cell mass (ICM), which forms trophoblastic knobs (T) with which they penetrate the LE. Figure adapted from (Wang and Dey, 2006).

Challenges and strategies to studying the peri-implantation period

Despite the multitude of interesting and crucial developmental processes taking place during peri-implantation development, this period remains severely under-studied for a simple reason: the relative inaccessibility of the embryo. The pre-implantation mammalian embryo is a largely self-enclosed and independent system (Austin, 1961). The post-implantation embryo, while attached to the maternal tissues, is nevertheless still tolerant to *ex vivo* culture, observation, and perturbation for a short time, especially in rodent species (Harris, 2012). In stark contrast, implanting embryos are difficult to observe and almost impossible to manipulate *in utero*. As a result, study of early mammalian embryonic development has therefore traditionally been divided into pre-implantation and post-implantation, with the peri-implantation period remaining a "black box". While the corresponding chronological period can be studied in other systems, such as in non-mammalian embryos such as fish, amphibians, or avians, or in *in vitro* models reconstituted from mammalian cells (**Figure 1.8**) (reviewed in Shahbazi and Zernicka-Goetz, 2018; Simunovic and Brivanlou, 2017; Vianello and Lutolf, 2019), insights gained from these systems are not necessarily applicable to the *in utero* mammalian context.   strategy for studying mammalian embryonic development through implantation is still required.

Mouse	EpiLC Micropatterns	Embryoid Bodies	ETS embryo-like structures	ETX embryo-like structures	(3D) Gastruloids
Ø:	1000µm	~500µm	100x200µm	100x200µm	800µm
Axes:	AP (radial)	AP	AP	AP	AP (+Hox), DV, bilateral
EMT:	yes	yes	yes	yes	yes
Matrix:	Matrigel/Laminin		Matrigel		
Cell types:	EPI Mesoderm Definitive endo. ExEmb mesoderm	Ectoderm Mesendoderm	EPI Mesoderm PGCs	EPI Mesoderm Endoderm PGCs AVE Definitive endo.	Ectoderm Mesoderm Definitive endo.
Models:	Symmetry break AP-axis formation Gastrulation Germ Layer spec.	Symm. break AP-axis Gastrulation Germ Layer	Symm. break AP-axis Gastrulation Germ Layer Lumen PGC	Symm. break AP-axis Gastrulation Germ Layer spec. Lumen PGC Visceral Endo.	Symmetry break AP/DV/ML-axis Gastrulation Germ Layer spec. Hox patterning Axial extension Cardiac development

Human	(2D) gastruloids	Synthetic human epiblast
Ø:	500µm	50-120µm
Axes:	AP (radial)	AP
EMT:	yes	yes
Matrix:	Laminin	Matrigel +hydrogel*
Cell types:	Ectoderm Mesoderm Definitive endoderm ExEmb (mesoderm?)	EPI Mesendoderm
Models:	Symmetry break AP-axis Gastrulation Germ Layer spec.	Symmetry break AP-axis Gastrulation Cell sorting

Figure 1.8: *In vitro* **systems of studying mammalian peri-implantation development.** These systems involve the aggregation of one or more cell types in an attempt to reconstitute *in vivo* embryo cell lineages and organisation, coupled with biochemical or mechanical cues to induce differentiation and morphogenesis. Figure adapted from (Vianello and Lutolf, 2019).

Various attempts have been made to overcome this break-point and connect pre- and post-implantation development, and to make inroads into the study of the peri-implantation period. Recovery of *in utero*-developed embryos (either by dissection or *in situ* fixation and cryo-sectioning) at a series of time points around the time of implantation presents one solution, but this precludes the study of dynamics of development. Furthermore, natural developmental variability between litters can confound attempts to construct a timeline of peri-implantation development. Therefore, live-imaging of peri-implantation development is necessary.

Multiple *in vivo* imaging modalities have been developed for the study of biological processes *in vivo* and/or *in situ*, often originally for a clinical setting. Some of these have been adapted to study laboratory animals and embryonic development, with varying degrees of success (**Figure 1.9**) (reviewed in Gregg and Butcher, 2012; Lauber et al., 2017). One significant limitation is the trade-off between depth of field and resolution. Mammalian embryos, especially in commonly-used small animal models at the early stages, are small (ranging tens or hundreds of micrometres in diameter), and often deeply embedded within the maternal body, where dense tissues cause scattering and limit the working distance and spatial resolution. Furthermore, not all imaging modalities are compatible with live, highly-sensitive embryos, for example if they require tissue clearance or the addition of a contrasting agent, or if they cause damage to the tissue through phototoxicity. Finally, the study of many developmental processes has traditionally relied on the usage of fluorescent that mark specific tissues, cells, or subcellular complexes (Korotkevich et al., 2017; Saiz et al., 2020; Takaoka et al., 2011). If an imaging modality not compatible with these reporters has been chosen, different tools and techniques must be developed for visualising these processes (Hsieh et al., 2008; Sun et al., 2004) – perhaps with the application of machine learning (Rad et al., 2018; Shen et al., 2022).
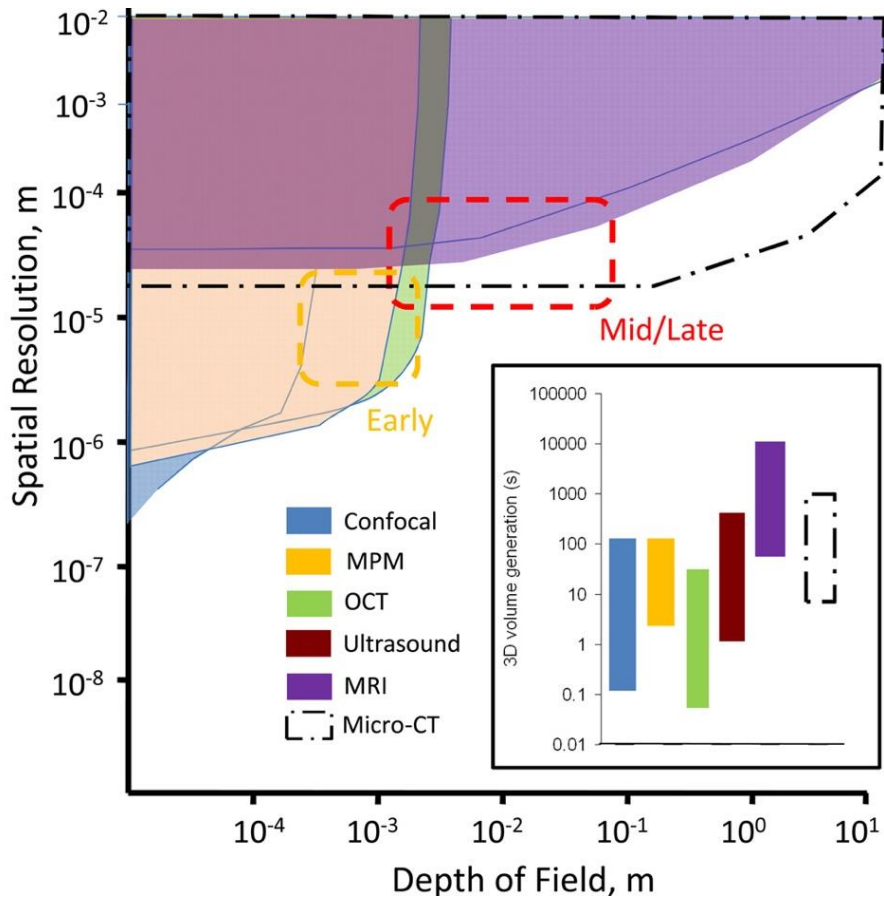
Figure 1.9: *In vivo* **imaging modalities and their applicability to early, mid, or late gestation in animal models.** Figure adapted from (Gregg and Butcher, 2012). MPM: multiphoton microscopy; OCT: optical coherence tomography; MRI: magnetic resonance imaging; Micro-CT: micro-computed tomography.

Taking into consideration the unique challenges of the system, confocal microscopy, multi-photon microscopy, and optical coherence tomography remain relatively more applicable to studying early mammalian embryonic development (Jones et al., 2004; Kyvelidou et al., 2011; Larina et al., 2009; McMullen et al., 2009). One approach that has been explored in the recent years, to make the mammalian embryo more accessible for these imaging techniques, has been intravital imaging (Huang et al., 2020; Wang and Larina, 2021), which has already seen wide usage in the study of other biological systems (**Figure 1.10**). However, the application of this technique to embryo development is still a recent advancement, and imaging of embryos during implantation has hitherto not been reported.
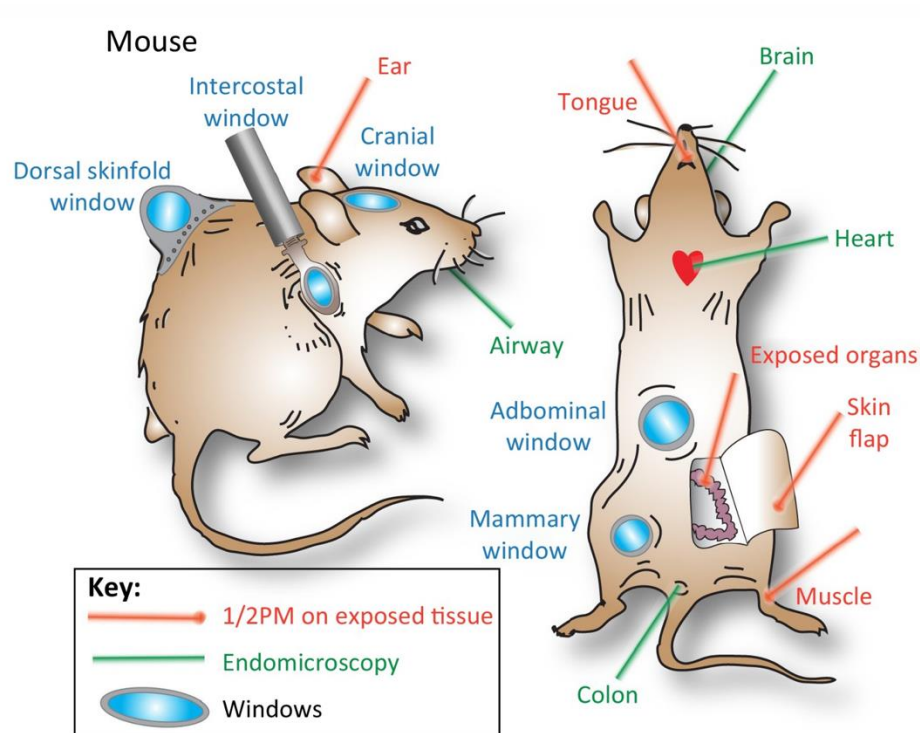
Figure 1.10: Intravital imaging in the mouse. Abdominal windows would allow access to the mouse oviduct and uterus. Figure adapted from (Karreman et al., 2016).

Ex vivo culture of mouse embryos through the peri-implantation period

Owing to the difficulties encountered in the *in situ* study of mammalian embryos, one complementary strategy has been to culture peri-implantation embryos *ex vivo*, much as has been done for pre- and post-implantation embryos. Over decades, many attempts have been made to culture mouse embryos through peri-implantation development, but have met with far less success than for pre- and post-implantation embryos. Initial attempts to culture mouse blastocysts through implantation involved the use of rat tail collagen to mimic uterine tissue and trigger implantation, coated on a 2D surface (Hsu, 1971). Embryos cultured using this methodology were able to form egg cylinders, yolk sacs, and even cardiac muscle and vasculature, though morphology was variable and there was a significant developmental delay (Hsu, 1971, 1972, 1973). Later works refined the culture medium and surface substrate composition, but largely relied on the same setup of allowing blastocysts to attach to a 2D surface (Bedzhov et al., 2014a; Morris et al., 2012a), and were seemingly able to support egg cylinder development.

While 2D culture systems can produce an egg cylinder from a blastocyst after several days of culture, these egg cylinders may not have developed through the same mechanisms that are in play in development *in utero*. Closer inspection of 2D-cultured embryos revealed that the TE of the blastocyst undergoes massive proliferation and spreading, which causes the blastocyst to collapse and the ICM to lose structure (**Figure 1.11A, 1.11B**). From this disorganised mass of cells, an egg cylinder sometimes forms *de novo*. Clearly, even though the end result is similar, embryos in normal *in utero* development do not undergo this catastrophic loss of organisation, and the mechanisms that direct *de novo* egg cylinder development in these systems are not necessarily the same mechanisms that are in play during *in utero* development. Indeed, amorphous embryos often arise in 2D culture where there is incomplete separation of Cdx2$^+$ TE and Oct3/4$^+$ EPI (**Figure 1.11C**; see also Panavaite, 2018). Therefore, a 3D culture system that would avoid blastocyst collapse and egg cylinder reformation was a logical next step.

This 3D culture system also necessitated the development of a compatible imaging setup; the working distance of a conventional confocal or spinning disc light microscope is insufficient if enough space between the embryo and any 2D surface has to be preserved to avoid attachment. While embryos can be removed from culture for fixed sample analysis, it is paramount that live-imaging be possible so as to study the dynamics of developmental events, as mentioned above. The search for a 3D culture system that fulfils these requirements had been underway in the laboratory before the initiation of the study presented in this thesis (Panavaite, 2018).
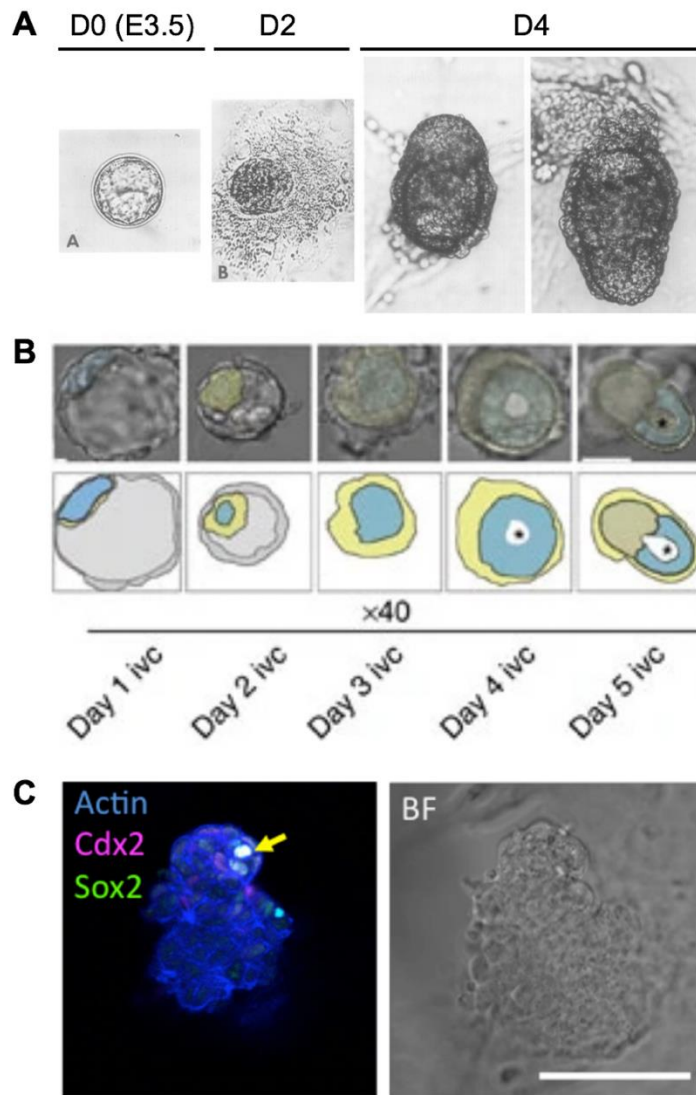
Figure 1.11: Existing 2D culture protocols for peri-implantation embryos do not recapitulate *in utero* egg cylinder formation. Figures adapted from (Hsu, 1973; Morris et al., 2012a; Panavaite, 2018).

(A) 2D culture system from Hsu, 1973. Embryos show loss of organisation at D2. Figure adapted from (Hsu, 1973).

(B) 2D culture system from Morris et al., 2012. Embryos show loss of organisation at D3. Figure adapted from (Morris et al., 2012a).

(C) Example of an amorphous embryo at D4 of *ex vivo* culture using culture system from (Bedzhov et al., 2014a). Yellow arrow indicates Cdx2/Sox2 double positive cells. Figure adapted from (Panavaite, 2018).

Scale bars = 100 μm.

COORDINATION OF GROWTH WITH MORPHOGENESIS IN REGULATIVE DEVELOPMENT

Regulation of body and organ size in nature

The question of how organisms control their sizes has been a long-standing one (Gomer, 2001; Horiguchi and Tsukaya, 2011; Raff, 1996). The variation in adult body size – spanning 8 orders of magnitude from 1.5 g to 150000 kg – in animals is not accounted for by changes in cell volume, but in cell number and tissue shape (Penzo-Méndez and Stanger, 2015; Raff, 1996). Somehow, organisms are able to sense their size, or their cell number, and limit their growth and coordinate with morphogenetic events (Lui and Baron, 2011). Not only that, they must also ensure that their body parts are proportional with each other; organ size control is also involved (Gokhale and Shingleton, 2015; Penzo-Méndez and Stanger, 2015; Stanger, 2008). A loss of regulation of body and organ size, or a decoupling thereof, can result in visually impressive phenotypes (**Figure 1.12**; Harrison, 1924).
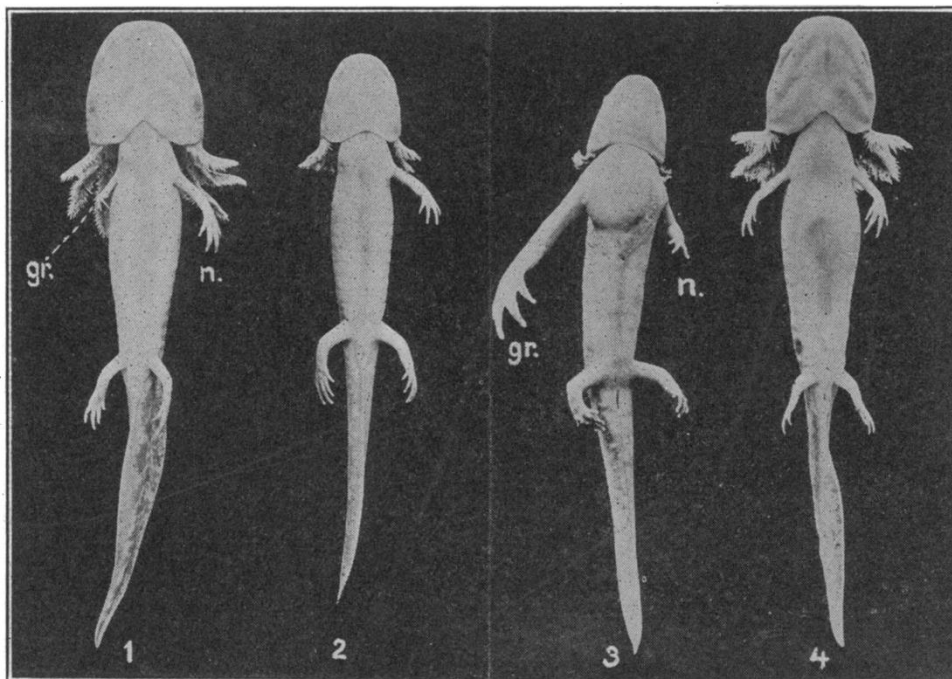
Figure 1.12: A mismatch between organ and body size in two species of salamanders with reciprocal limb bud transplants. Figure adapted from (Harrison, 1924).

Size regulation is a complex question. A significant proportion of the body of work on this topic has been targeted towards the sub-topics of post-natal body and organ size regulation, including in the context of regeneration or parabiosis; these have been reviewed extensively (Conlon and Raff, 1999; Gokhale and Shingleton, 2015; Lui and Baron, 2011; Penzo-Méndez and Stanger, 2015; Raff, 1996), and fall outside of the scope of this study. In this work, I focus on size regulation during the early embryonic development in the mouse. Despite being restricted in scope to a single system and a short time frame, the question is by no means trivial. Despite many decades of study, little is known about the mechanisms and dynamics of compensatory growth programmes in the mouse embryo, and even less about how they are triggered. Indeed, whether embryo size regulation necessitates the *sensing* of size in all cases is still an open question.

Size regulation in early mammalian development

The early mammalian embryo can tolerate drastic changes in cell number without disruption to normal development. Mammalian embryos can be experimentally induced to increase or decrease its size by more than two-fold, and yet recover to near normal body size by the time of birth (Markert and Petters, 1978; Mintz, 1964, 1965; Moore et al., 1968; Petters and Mettus, 1984; Tarkowski, 1959, 1961). How this can be achieved has been the subject of decades of work, utilising a variety of experimental tools and analysis methods (**Table 1.1**). Remarkably, this degree of size compensation is achieved only after implantation begins – pre-implantation embryos do not show compensatory growth (Tarkowski, 1959) – although the exact time frame and dynamics of size regulation is still not well-defined.

Part of the confusion regarding the contradictory findings between studies and how they should be interpreted is likely due to the significant differences in methodology that exist between studies, on account of technological advances over these decades. As of yet, there has been no comprehensive study to characterise the full scope of compensatory growth during peri-implantation development using quantitative methods that have become available in recent years.

Study	Manipulations	Analysis	Key findings
(Tarkowski, 1959)	Undersized	Volumes	Morphogenesis is determined by time, not cell number, in under-sized embryos. Compensatory growth in under-sized embryos occurs between E10.5 and E11.5. Persistently-under-sized embryos resorbed after implantation, and after E10.5.
(Tarkowski, 1961)	Oversized	Volumes	Compensatory growth in over-sized embryos is complete by E10.
(Buehr and McLaren, 1974)	Oversized	Volumes, cell counts (limited)	Compensatory growth in over-sized embryos occurs between E5.5 and E5.8. (Of note is that pro-amniotic cavity formation is noted to be at E5.8, which differs from other studies.)
(Lewis and Rossant, 1982)	Oversized and undersized	Cell count estimates	Compensatory growth in over-sized embryos occurs between E5.67 and E6.67, accomplished by lengthening of the cell cycle and suppressing a proliferative burst at E6.33. Pro-amniotic cavity formation is determined by cell number, not time, and is delayed in undersized embryos until E5.67—E6.0.
(Rands, 1986a) (I)	Oversized	Volumes, cell counts (limited)	Pro-amniotic cavity formation is determined by time, not cell number, in over-sized embryos. Gastrulation onset is delayed in over-sized embryos until correct time is reached.
(Rands, 1986b) (II)	Undersized	Volumes, cell counts (limited)	Gastrulation is further delayed in under-sized embryos until correct cell number is attained. Under-sized embryos undergo two phases of compensatory growth.
(Power and Tam, 1993)	Undersized	Volumes, cell count estimates	Gastrulation onset is determined by cell number. Compensatory growth in under-sized embryos occurs between E6.5 and E11.5. Rate of somitogenesis adjusted for smaller-sized embryo.
(Orietti et al., 2020)	Oversized	Cell counts	Size regulation in over-sized embryos is completed during pro-amniotic cavity formation through increased apoptosis.

Table 1.1: An overview of key studies investigating size regulation in the mouse embryo.

Mechanisms of compensatory growth

Several mechanisms of compensatory growth have been proposed. (Lewis and Rossant, 1982) identified a wave of mitotic activity at E6.33 that is suppressed in over-sized embryos. Their survey of mitotic indices has found no difference in proportion of cells undergoing mitosis between control and double-sized embryos. (Lewis and Rossant, 1982) have also proposed that lengthening of the cell cycle in double-sized embryos may contribute as well to the progressive lessening of the disparity between over-sized and control embryos. Finally, (Orietti et al., 2020) suggested that increased apoptosis is necessary for size regulation in double-sized embryos.

Under-sized embryos seem to take longer to achieve full compensation (Power and Tam, 1993; Rands, 1986b; Tarkowski, 1959). Interestingly, (Rands, 1986b) identified two waves of compensatory growth in under-sized embryos, wherein the embryo manages a significant amount of compensation in terms of cell number before gastrulation, but falls behind again during gastrulation; this lag is corrected during the second, post-gastrulation and organogenesis wave, so that by birth the embryos reach control size again.

A point to note is that it may not be the same mechanism(s) for size regulation acting in under- and over-sized embryos. Over-sized embryos simply need to eliminate excess cells, whereas under-sized embryos must produce extra material to make up for the deficit. While it has been found that a degree of apoptosis naturally occurs in the mouse peri-implantation EPI (Bowling et al., 2018), suppressing apoptosis entirely is still not enough to rescue the two-fold reduction in cell number and tissue size in half-sized and smaller embryos.

Finally, it must be highlighted that mouse embryos do not only need to reach a certain size; they must reach a certain size *by a certain developmental time*. This distinguishes them from other systems in which growth simply stops once a certain size is attained (Lui and Baron, 2011).

Coordination between embryo growth and morphogenetic events

The formation of the pro-amniotic cavity is suggested to be delayed in under-sized or over-sized embryos (Lewis and Rossant, 1982; Orietti et al., 2020); similarly, gastrulation onset only occurs once the epiblast reaches a set number of cells, even if chronologically, the embryo is of the right age (Power and Tam, 1993; Rands, 1986a). A long-standing question in field has therefore been how the embryo is able to enact this level of regulation, whereby tissue growth is coordinated with the commencement of landmark events that shape the embryo throughout embryonic development.

Past studies mostly focused on the processes by which compensatory growth is enacted, instead of how such size deviations are detected. In addition, due to the technical limitations of the time, most studies were unable to pinpoint specific mechanisms, or describe how size compensation takes place in real time. With recent technological advancements in embryo culture, imaging, and analysis, it is now possible to return to this interesting topic and investigate it in more detail.

2.AIMS & STRATEGY

My overarching aim was to investigate the coordination of developmental events with changes in embryo size and shape during early mouse embryonic development. To this end, I conducted a review of the landmark developmental events during this time and found that most significant changes in embryo architecture, especially with respect to the embryonic cell lineages, took place during the peri-implantation period. Therefore, I decided to focus on the peri-implantation mouse embryo.

In my literature review, I observed that while large bodies of work have been built upon investigations into both pre- and post-implantation embryos, the peri-implantation period is comparatively less well-studied. This was perhaps owing to the difficulty of supporting embryo development through implantation without disruptions to its normal developmental programmes. While robust *ex vivo* culture systems existed for both pre-implantation and post-implantation mouse embryos, none of these systems were able to support embryo development through the implantation period. While it is possible to recover embryos at all stages of embryonic development, morphogenetic events cannot be studied as they occur in real time by using only fixed samples acquired at separate time points. As a culture system for peri-implantation mouse embryos was under development in the lab, my first sub-objective was to verify whether this system was suitable for my purposes, i.e. whether it supported the morphogenesis of the embryonic tissues in a physiological manner. To this end, my approach was to come up with a rubric for assessing embryonic development quantitatively and independently of chronological time.

My second sub-objective was to study the peri-implantation period using the validated culture system, at both a cell and tissue level. The light-sheet microscope previously developed for pre-implantation mouse embryos was suitable for adaptation to peri-implantation embryos, due to the low phototoxicity and high compatibility with the culture setup. My approach is to optimise the microscope for imaging *ex vivo* cultured peri-implantation embryos in high spatio-temporal resolution, as well as for sufficiently-long periods of time so as to follow the developmental process from egg cylinder formation to establishment of the anterior pole. With this setup, I hope to study how individual cells behaved and interacted with each other, as well as how the embryonic tissues were changing overall.

Finally, my third sub-objective was to investigate how embryos were able to sense and correct for deviations in tissue size during development. Size deviations in the embryo naturally result in impacts on the morphogenetic landscape, and must be either tolerated or compensated for to ensure robust embryonic development. While compensatory growth had been observed

in mouse peri-implantation development and attempts had been made to investigate this phenomenon, these earlier studies, due to technological limitations at the time, were unable to draw conclusions about the mechanisms of compensatory growth. I sought to first establish that the observations reported in past literature can be recapitulated, and then to provide mechanistic insight as to how size deviations could be detected and how compensatory growth programmes were enacted in response. To this end, I combined classical embryological techniques with modern imaging and analysis setups, perturbing embryo size by doubling or halving cell number and following these embryos through peri-implantation development. I aimed to characterise the time frame in which compensatory growth is enacted, and, by investigating how the cell and tissue parameters were affected by size deviations, identify candidate parameters that could be sensed by the cells as a trigger to induce compensatory growth.

3.MATERIALS AND METHODS

ANIMAL AND EMBRYO WORK

Animal husbandry

For the majority of the work described in this thesis, animal work was performed at the Laboratory Animal Resources (LAR) facility at the European Molecular Biology Laboratory (EMBL), Heidelberg, Germany. Permission for animal work was granted from the Institutional Animal Care and Use Committee (IACUC), under IACUC number TH11 00 11. Animals at the LAR facility were housed under specific pathogen-free (SPF) conditions with a 12-12 hours light-dark cycle.

Animal work was also performed at the animal facility of the Hubrecht Institute (HI), Royal Netherlands Academy of Arts and Sciences (KNAW), Utrecht, the Netherlands. Permission for animal work was granted from the Centrale Commissie Dierproeven (CCD), under CCD licence number AVD 80100 2021 15238. Animals at the HI animal facility were housed under SPF conditions with a 14-10 hours light-dark cycle.

All animals used for experiments were between the age of 8 to 35 weeks and housed under standard group housing conditions, with feed and water provided *ad libitum*.

Mouse lines and genotyping

Transgenic mouse lines used are presented in **Table 3.1**. Mice were genotyped using standard PCR techniques. Briefly, tail tip or ear punch tissue was digested in 400 µl lysis buffer (50 mM Tris-HCl (Sigma, T2663), 100 mM EDTA (Fluka, 03690), 100 mM NaCl, 1% SDS (Serva, 39575.02), and 0.5 mg/ml Proteinase K (Sigma P2308)) overnight at 56°C with gentle agitation. An equal volume of isopropanol was added to precipitate the genomic DNA (gDNA), which was precipitated by centrifugation at 12000 rpm for 5 mins. The gDNA pellet was washed in 80% ethanol and resuspended in water. Resuspended gDNA was used for genotyping by Taq polymerase (Thermo Fisher Scientific, EP0402). Primers used for genotyping each line are presented in **Table 3.2**.

A F1 hybrid between C57BL/6 and C3H (B6C3F1) was used as wild-type (WT) controls and as foster mothers for embryo transfer in HI. CD1 was used as foster mothers in EMBL, as well as vasectomised males (to induce pseudopregnancy) in both EMBL and HI.

Mouse line	Reference	Purpose
A$_7$-Venus	(Takaoka et al., 2017)	Signalling activity reporter
ASE-YFP	(Granier et al., 2011)	Signalling activity reporter
Cdx2-GFP	(McDole and Zheng, 2012)	Trophectoderm marker
Cdh1-GFP	(Gong et al., 2003)	Tight junction marker
Dusp4-T2A-3xmVenus	(Ichikawa et al., 2022)	Signalling activity reporter
Ezrin-mCherry	(Ichikawa et al., 2022)	Apical domain marker
GFP-Myh9	(Zhang et al., 2012)	Cell-cell junction marker
H2B-GFP	(Hadjantonakis and Papaioannou, 2004)	Nucleus marker
Lefty1-mVenus	(Takaoka et al., 2011)	Distal/Anterior visceral endoderm marker
mTmG	(Muzumdar et al., 2007)	Membrane marker
Pdgfra-EGFP	(Plusa et al., 2008)	Primitive endoderm marker
TCF/Lef:H2B-GFP	(Ferrer-Vaquer et al., 2010)	Signalling activity reporter

Table 3.1: Transgenic mouse lines used in this work.

Mouse line	Primers	Target bands
A₇-Venus	ACGTAAACGGCCACAAGTTC TGTCGGCGGTGATATAGACG	Tg: 400 bp
ASE-YFP	TGCAGTGCTTCAGCCGCTAC CCAGCAGGACCATGTGATCG	Tg: 420 bp
Cdx2-GFP	ATGGTTCCGTTCCCTGGTTC GCGGACTTGAAGAAGTCGTGCTGCTT AGGCTTGTTTGGCTCGTTACAC	Tg: 750 bp WT: 1400 bp
Cdh1-GFP	CTGCTAAATTCGAACGCCAGC CGTCCATGCCGAGAGTGATC	Tg: 800 bp
Dusp4-T2A-3xmVenus	GCCCGCCAAGGTCCCTAATC GGGGGCCGACTCTGGATTTG ACGCTGAACTTGTGGCCGTT	Tg: 639 bp WT: 464 bp
Ezrin-mCherry	TGGCCATCATCAAGGAGTTCATG TGTAGATGAACTCGCCGTCCTG	Tg: 348 bp
GFP-Myh9	CTGTCACATGGCTCATGTTC GCCGGACACGCTGAACTTGT GCCCTGAGTAGTATCGCTCC	Tg: 200 bp WT: 400 bp
H2B-GFP	GGCTTCTGGCGTGTGACCGGC GTCTTGTAGTTGCCGTCGTC	Tg: 900 bp
Lefty1-mVenus	CAGGCATCAAGCAGAGAACG TCCTTGAAGAAGATGGTGCG CTAGGCCACAGAATTGAAAGATCT GTAGGTGGAAATTCTAGCATCATCC	Tg: 880 bp WT: 324 bp
mTmG	CTCTGCTGCCTCCTGGCTTCT CGAGGCGGATCACAAGCAATA TCAATGGGCGGGGGTCGTT	Tg: 250 bp WT: 330 bp
Pdgfra-EGFP	CCCTTGTGGTCATGCCAAAC GCTTTTGCCTCCATTACACTG ACGAAGTTATTAGGTCCCTCGAC	Tg: 242 bp WT: 451 bp
TCF/Lef:H2B-GFP	ACAACAAGCGCTCGACCATCAC AGTCGATGCCCTTCAGCTCGAT CTAGGCCACAGAATTGAAAGATCT	Tg: 530 bp WT: 324 bp

Table 3.2: Primers used for genotyping the mouse lines above.

Superovulation and natural mating

To obtain 4-cell stage embryos for size manipulation and embryo transfer, female WT mice were superovulated with IP injections of 5—7.5 IU of PMSG (Intervet, Intergonan; ProSpec, PMSG) and, after 48 hours, 5—7.5 IU of hCG (Intervet, Ovogest 1500; MSD, Chorulon). Females were put together with males after hCG injection and noon on the next day was defined as embryonic day 0.5 (E0.5), with E0, the time of fertilisation, being the midpoint of the dark period immediately following the hCG injection.

To obtain mouse embryos for *ex vivo* peri-implantation culture or analysis of *in utero* development, mice were naturally mated, and noon on the day when a vaginal plug was detected was defined as embryonic day 0.5 (E0.5), with E0, the time of fertilisation, being the midpoint of the dark period immediately prior to plug detection.

Embryo recovery and culture

Pregnant female mice were humanely euthanised by cervical dislocation under anaesthesia, and the reproductive organs (oviducts or uterine horns) were dissected out immediately after euthanasia, placed in pre-warmed KSOM with HEPES (oviducts) or dissection medium (uterine horns), and kept in incubators until embryo recovery.

Recovery of embryos was performed under a stereomicroscope (Zeiss, StreREO Discovery.V8) equipped with a thermo plate (Tokai Hit) at 37°C. Embryos were handled with rubber aspirators (Sigma, A5177) mounted with hand-pulled and flame-polished glass needles (Blaubrand intraMark 708744). Embryo culture was performed in incubators with a humidified atmosphere of 5% CO_2 at 37 °C (Thermo Scientific, Heracell 240i).

Pre-implantation embryos were recovered by flushing dissected oviducts or uterine horns with KSOM with HEPES. Peri- and post-implantation embryos were recovered by dissecting uterine horns in dissection medium (DMEM (Gibco, 11880028) with 15% heat-inactivated FBS (PAA, A15-080), 2 mM GlutaMAX (Gibco, 35050061), 10 mM HEPES (Sigma, H0887), 25 units/mL Penicillin and 25 μg/mL Streptomycin (Gibco, 15070063)).

Blastocyst Immunosurgery and Culture

Blastocysts were recovered at E3.5 and their zona pellucida (ZP) was removed by brief incubation in 0.5% (w/v) Protease (Sigma, P8811) at 37°C. They were subsequently cultured for 24 hours in KSOM drops under mineral oil on 35 mm glass-bottom dishes (MatTek, P35G-1.5-14-C). The TE layer was removed by immunosurgery according to (Ohnishi et al., 2014b).

Embryos then recovered for 30 minutes in IVC1 medium before further *ex vivo* culture (described below). Embryos were fixed after 24-28 hours of culture and subjected to immunofluorescence staining and imaging.

3D-gel embedded embryo culture (3D-geec)

The detailed protocol for 3D-gel embedded embryo culture (3D-geec) was described in (Ichikawa et al., 2022). In brief, 3D-geec gel mix was prepared on ice, and 15 µL gel mix was added into the inner well of one well in an µ-Slide Angiogenesis dish (Ibidi, 81506). For 3D-geec using E4.5 embryos, the mural trophectoderm (mTE) of these embryos was microsurgically removed after recovery, and the embryos were quickly rinsed with the gel mix and carefully embedded in the gel droplet so that they touched neither the surface of the dish nor the air-gel interface. After solidification of the gel upon 30 minutes incubation in the incubator, 50 µL IVC1 medium (Bedzhov et al., 2014b) was added to fill the outer well. After the first 24 hours of culture, the IVC1 medium was carefully aspirated, and 50 µL IVC2 medium was added (Bedzhov et al., 2014b).

Derivation of optimal initial cell number threshold for 3D-geec

Derivation of the optimal initial cell number threshold was performed as described in (Ichikawa et al., 2022). In brief, a confusion matrix for threshold levels ranging from 0—230 cells was constructed, and the threshold level that yielded the highest Accuracy (110 cells) was determined to provide the best trade-off between minimising sample loss and maximising egg cylinder formation success rate.

Embryo size manipulation

Pre-implantation embryos were recovered at the 4-cell stage and and their zona pellucida (ZP) was removed by brief incubation in 0.5% (w/v) Protease at 37°C. For half-sized embryo studies, ZP-less embryos were then dissociated by a short incubation in calcium-free KSOM into 2-cell doublets and individually cultured in KSOM microdrops under mineral oil. For double-sized embryo studies, two ZP-less embryos were aggregated and cultured together in a single microdrop of KSOM under mineral oil. Aggregation of blastomeres was encouraged by depositing cells in micro-wells in the Petri dishes so that they adhered to each other and did not drift apart. Embryos are cultured until day E3.5, when a clear blastocyst cavity and coherent inner cell mass (ICM) can be seen; aberrant embryos, such as those with multiple cavities or ICMs, or those that did not aggregate, are discarded at this point.

Embryo transfer surgery

Pseudopregnancy was induced in foster mothers by natural mating with vasectomised males. Pseudopregnant foster mothers, as indicated by vaginal plug detection and corpus luteum presence in the ovaries, were used for embryo transfer surgeries. Noon on the day when a vaginal plug was detected was defined as E0.5, or in this case, vaginal plug positive day 0.5 (VP+0.5).

Bilateral oviduct transfers were performed, where control embryos were transferred into one uterine horn and manipulated embryos were transferred into the other. 5—10 embryos, with an average of 8 embryos, were transferred per oviduct, to increase implantation efficiency and to prevent crossing-over into the other uterine horn during implantation. Embryos were allowed to implant and develop until the relevant post-implantation time point, counted based on the foster mother; i.e., 4 days after embryo transfer at VP+0.5 would be pET4.5. Post-embryo transfer embryos were recovered as described for post-implantation embryos.

Embryo transfer surgeries were performed according to standard operating procedures at the EMBL LAR and the HI animal facility under anaesthesia and analgesia. Welfare checks were conducted 1—2 times daily post-surgery and animals determined to be experiencing more than moderate discomfort were humanely euthanised and excluded from the experiment.

IMMUNOFLUORESCENT AND LIVE IMAGING

Immunostaining for fluorescence imaging

Embryos were fixed with 4% paraformaldehyde (Electron microscopy sciences 19208) in PBS for 15 minutes at room temperature and permeabilized with 0.5% Triton X-100 (Sigma, T8787) in PBS for 35—60 minutes (depending on size of embryo) at room temperature. Embryos were incubated in blocking buffer (5% donkey serum (Sigma, D9663), 5% BSA (Sigma, A9647), 0.05% Triton X-100 in PBS) overnight at 4°C with gentle agitation. Embryos were then incubated with primary antibodies overnight at 4°C or for 2 hours at room temperature, washed, and incubated with secondary antibodies and dyes overnight at 4°C or for 2 hours at room temperature. Antibodies and dyes were diluted in blocking buffer to recommended concentrations. Embryos were washed and mounted in PBS for imaging.

Primary and secondary antibodies used are presented in **Tables 3.3** and **3.4** respectively. All secondary antibodies were used at 1:200. Dyes used were DAPI (Thermo Fisher Scientific, D3571, 10 µg/ml), Rhodamine Phalloidin (Invitrogen, R415, 1:200), and Streptavidin-conjugated Alexa Fluor 555 (Thermo Fisher Scientific, D3571, 10 µg/ml) against biotinylated goat anti-Brachyury antibody.

Confocal and light-sheet fixed sample imaging

Fixed and immunostained embryos were imaged using a confocal microscope, the LSM880 equipped with a C-Apochromat 40x/1.2 NA water immersion objective (Zeiss), or an inverted light-sheet microscope, the InVi SPIM (Bruker, Luxendo). When Airyscan Fast mode was used, raw Airyscan images were post-processed by ZEN black software (Zeiss).

Target	Host	Source and catalogue number	Dilution
Brachyury	Goat	R&D Systems, AF2085	1:25
activated caspase-3	Rabbit	Cell Signaling Technology, 9664	1:50
Cdx2	Mouse	Biogenex Laboratories, MU392AUC	1:200
Cerberus1	Rat	R&D systems, MAB1986	1:50
Collagen IV	Rabbit	Millipore, AB756P	1:200
Gata4	Goat (biotin-conjugated)	R&D systems, AF2606	1:200
phosphorylated ERM (pERM)	Rabbit	Cell Signaling Technology, 3726	1:100
phosphorylated histone H3 (pH3)	Mouse	Millipore, 05-806, Lot 3485893	1:50
Id1	Rabbit	Biocheck, BCH-1/195-14	1:50
Lefty	Goat	R&D systems, AF746	1:50
bi-phosphorylated myosin regulatory light chain (ppMRLC)	Rabbit	Cell Signaling Technology, 3674	1:100
Oct3/4	Mouse	Santa Cruz Biotechnology, sc-5279	1:50
Sox2	Rabbit	Cell Signaling Technology, 23064	1:200

Table 3.3: Primary antibodies used in this work.

Target	Host	Source and catalogue number	Fluorophore
Goat IgG	Donkey	Invitrogen, A11055	Alexa Fluor 488
Goat IgG	Donkey	Invitrogen, A32860	Alexa Fluor Plus 680
Rabbit IgG	Donkey	Invitrogen, A32790	Alexa Fluor Plus 488
Mouse IgG	Donkey	Invitrogen, A32744	Alexa Fluor Plus 594
Mouse IgG	Donkey	Jackson ImmunoResearch, 715-175-150	Cy5 AffiniPure
Rat IgG	Donkey	Jackson ImmunoResearch, 712-175-153	Cy5 AffiniPure

Table 3.4: Secondary antibodies used in this work.

Confocal live-imaging

For counting of initial cell numbers prior to 3D-geec, E4.5 embryos after mTE removal were incubated in IVC1 with 5 µg/mL Hoechst 33342 (Invitrogen, H21492) for 30 minutes at 37°C, washed, and mounted in IVC1 drops covered with mineral oil on 35 mm glass-bottom dishes. Live-imaging was performed on the confocal microscope described above, with environmental controls for temperature and humidity. Images were acquired with Airyscan Fast mode to reduce photodamage.

For imaging of polar trophectoderm (pTE) invagination, E4.5 Cdx2-GFP embryos after mTE removal were mounted in IVC1 drops covered with mineral oil on 35 mm glass-bottom dishes. Live-imaging was performed on the confocal microscope described above, with environmental controls for temperature and humidity.

Light-sheet live-imaging and laser ablation

The detailed protocol for 3D-geec, live-imaging, and laser ablation in the InVi SPIM setup was described in (Ichikawa et al., 2022). In brief, embryos were embedded in gel mix and covered with IVC1 medium and mineral oil within an InVi SPIM imaging chamber, carefully positioned so that they are close to the bottom of the chamber but non-adherent, and imaged for up to 48 hours in the case of 3D-geec embryos, and up to 72 hours in the case of embryos embedded at E3.5 (pertinent only to preliminary studies during method development). Short-term live-imaging of post-implantation embryos was performed with gel embedding as above, and covered with IVC2 medium instead of IVC1 medium.

For laser ablation of cell-cell junctions, an additional photomanipulation module on the InVi SPIM was used (Bruker, Luxendo) (de Medeiros et al., 2020). GFP-Myh9 was used as a live marker of cell-cell junctions, and circular ROIs were drawn around GFP-Myh9 foci to ablate them. Post-ablation viability was assessed by following embryo development for 6 hours after the ablation experiment, with embryos showing wound responses excluded from analysis.

IMAGE AND DATA ANALYSIS

Image analysis

Dimension measurements, cell counts, cell coordinates analysis, and cell parameters measurements were performed with Imaris v9.2.1 (Bitplane). Signal intensity measurements were performed with Fiji (Schindelin et al., 2012). Cell tracking was performed with Fiji, Mov-IT (Faure et al., 2016), and Imaris.

Analysis of cell and embryo morphology

Dimension measurements were performed in using the Measurement Points tool in Imaris. Diameter is defined as the mean of the long and short transverse axes of the inner cell mass (ICM) including primitive endoderm (PrE) layer, or the egg cylinder including visceral endoderm (VE) layer. Length is defined as the distance between the epiblast (EPI)-polar trophectoderm (pTE) boundary and the distal point of the ICM, or the distance between the EPI-extraembryonic ectoderm (ExE) boundary and the distal tip of the egg cylinder including the VE layer. EPI cell length is defined as the length between the apical and basal cell surfaces.

Cell volume, cavity volume, and tissue volume was measured in Imaris using the Surfaces tool. Cell volume was obtained by manually segmenting a cell based on Phalloidin staining or membrane signal. The total EPI volume, including the pro-amniotic cavity, was manually segmented as one single Surface based on Phalloidin staining or membrane signal. The pro-amniotic cavity was similarly segmented out, and EPI tissue volume was obtained by subtracting cavity volume from the total EPI volume.

Counting of embryo cell numbers

Cell counts were performed using the Spots tool in Imaris, with manual correction after one round of automatic Spots detection. Initial cell number was based on all nuclei. VE was defined as the visceral endoderm overlying EPI, and total cell number was defined as the sum of VE and EPI. VE and EPI identity was assigned based on lineage marker expression as seen in immunofluorescence imaging as well as cell morphology.

Evaluation of embryo development

Evaluation of embryo development overall was performed as described in (Ichikawa et al., 2022). In brief, an "*in utero* age" was calculated for *ex vivo*-cultured embryos by mapping their total cell numbers onto a linear regression line derived from total cell numbers of *in utero*

embryos. Another regression line derived from EPI cell number of in utero embryos was used in cases pertaining specifically to the EPI.

In addition, D2 embryos were also evaluated for establishment of the anterior-posterior axis by the degree of asymmetry of their AVE cells. In brief, polar plots were generated of the VE cells, each annotated for expression of AVE markers, of *in utero* E5.25, E6.0, and *ex vivo*-cultured D2 embryos. An AVE Asymmetry Index was computed for each embryo, defined as the distance of the AVE centroid from the distal tip (centre of the polar plot) divided by the radius of the polar plot. E5.25 and E6.0 embryos were first manually classified as Symmetric, Asymmetric. To miminise bias, the same set of embryos was classified independently by two experimenters. Embryos classified differently by the experimenters, or could not be decisively classified, were assigned as Borderline. The highest AVE Asymmetry Index amongst the Symmetric embryos was taken as the threshold for AVE asymmetry, i.e. the lowest AVE Asymmetric Index an embryo could have without being classified as Symmetric. This value was then applied to D2 embryos to evaluate degree of AVE asymmetry and thus establishment of the anterior pole.

Analysis of pro-amniotic cavity formation

Apical domain detection was performed using the Spots tool in Imaris. Spots objects were manually placed based on Ezrin-mCherry reporter signal, and their linear distance from the centre of the egg cylinder was divided by the radius of the EPI tissue to derive their scaled distance from embryo centre.

Analysis of cell dynamics and the signalling landscape of the EPI

Analysis of cell dynamics and the signalling landscape of the EPI was performed as described in (Ichikawa et al., 2022). In brief, to evaluate cell dynamicity in the EPI, a cluster of ten EPI cells was tracked for 16 hours through ExE invagination. The displacement of the cells from their centroid was used as an indicator of cell dispersion.

To evaluate signalling activity in the EPI, a combination of immunostaining and fluorescent reporters was used. Id1 expression was used as a reporter for BMP signalling activity and was analysed by immunofluorescence imaging. A7-Venus and Dusp4-T2A-mVenus expression were used as reporters for Nodal-Foxh1 and FGF-Dusp4 signalling activities respectively and were analysed by fluorescence imaging of the fluorophores. To account for heterogeneity in signalling activity in the EPI, the proportion of cells expressing these reporters in the proximal versus the distal halves of the EPI was used as a readout of the

signalling landscape. For embryos post-immunosurgery, which lack a proximal and a distal half, signal intensity was measured in a linear ROI swept radially around the centre of the embryo and plotted against the angle of the ROI to display the signalling landscape of the EPI.

Machine-learning-based image segmentation and analysis

The segmentation pipeline used, and the development of this pipeline, was described in (Ichikawa et al., 2022). In brief, images acquired on the InVi SPIM were pre-processed and fed into PlantSeg (Wolny et al., 2020), which generated a probability map based on membrane signal and segmented the image according to the probability map. After exploring the algorithms and their hyperparameters, the best segmentation output was chosen by visual inspection, manually corrected for remaining errors, and used for measurement of cell parameters, lineage tracing, and other further analyses.

Analysis of cell parameters was performed with Python 3.8. Aspect ratio is calculated by fitting an ellipsoid to the cell and dividing its longest axis by the average of its two shorter axes. Alignment is defined as the angle between the long axis of the cell and a line segment connecting the outermost voxel of the cell to the centre of the cell, and a low angle indicates that the cell is radially-aligned.

Lineage tracing was performed with Mov-IT based on nuclear and membrane signals with manual correction. Daughter cells that cannot be traced with confidence through mitosis are excluded from the lineage trees. For analysis of neighbour effects, two lineages were identified, in which one lineage had daughter cells that remained in a cluster, and the other lineage had daughter cells that dispersed. One cell from the second lineage came into proximity with the cluster from the first lineage and was used to analyse the effects of lineage versus proximity.

Evaluation of embryo transfer success rate

Embryo transfer surgeries were scored on several metrics: number of decidua observed out of total number of embryos transferred; number of embryos recovered out of number of decidua observed; and number of embryos recovered out of total embryos transferred. The first metric indicates the number of implantation sites triggered in the uterine epithelium and indirectly, the competency of the uterus to support implantation; if no decidua were seen at all, pseudopregnancy may not have been successfully induced in the foster mother. The second metric indicates the number of successful implantations – embryos implanted and later resorbed

would yield only empty decidua. The third metric indicates the overall efficiency of embryo transfer.

Inclusion and exclusion criteria for post-embryo transfer (pET) embryos

Due to the embryo transfer procedure, post-embryo transfer (pET) embryos exhibited a greater degree of developmental variation in comparison with *in utero* embryos. Firstly, it was determined that to control for inter-litter variation, only complete litters with control and manipulated littermates would be used for analysis. Secondly, inclusion and exclusion criteria were derived for pET embryos in two steps.

In the first step, only control embryos that fell within 50% to 200% of the expected mean EPI cell number of *in utero* embryos for chronological time at which they are recovered were included for further analysis. At this point, any litters that had less than two control embryos remaining were also excluded from further analysis, as a low sample size for controls could significantly skew further analyses.

In the second step, exclusion was performed on a per-litter basis to account for inter-litter variation. The theoretical mean EPI cell numbers for uncompensated half- and double-sized embryos were calculated using 50% and 200% of the mean EPI cell number of the control littermates respectively, and two standard deviations (S.D.s) away from these means was taken as acceptable variation. S.D.s were scaled to EPI cell number. Equations for deriving the upper and lower for each condition based on the mean EPI cell number of the control littermates are as follows:

$$\text{Upper bound for half-sized embryos (HUB)} = 1.4203x - 4.0554$$

$$\text{Lower bound for half-sized embryos (HLB)} = 0.2898x + 2.0277$$

$$\text{Upper bound for double-sized embryos (DUB)} = 2.8407x - 8.1107$$

$$\text{Lower bound for double-sized embryos (DLB)} = 0.5797x + 4.0554$$

where x is the mean EPI cell number of the control littermates.

Evaluation of compensatory growth

Embryos were evaluated for compensation in terms of EPI cell number. The mean control EPI cell number and the mean manipulated EPI cell number for each litter were derived, and a litter-based EPI cell number ratio (manipulated:control) was computed as a readout for whether compensatory growth had taken place. In addition, individual EPI cell number ratios were also computed for each manipulated embryo in the litter against the mean control EPI cell number. Embryos were also evaluated for compensation in terms of physical dimensions, EPI tissue volume, and pro-amniotic cavity volume.

Evaluation of correlation of parameters

Regression lines were constructed for pooled *in utero*-developed and control pET embryos. Only embryos with a pro-amniotic cavity, in the case of *in utero*-developed embryos, were used. EPI cell number, EPI tissue volume, and pro-amniotic cavity volume were log-transformed during calculations. The Sum of Squared Residuals (SSR) of each manipulated pET embryo from the regression lines was then calculated, as well as Weighted Least Squares (WLS), as a measure of goodness of fit for each regression line to the manipulated pET embryos:

$$SSR = \sum_{i=1}^{N}(Y_i^{observed} - Y_i^{predicted})^2$$

$$WLS = \sum_{i=1}^{N}\frac{(Y_i^{observed} - Y_i^{predicted})^2}{Y_i^{predicted}}$$

Evaluation of cell proliferation and cell death

Evaluation of cell proliferation and cell death was performed through immunofluorescence imaging. Phosphorylated histone H3 (pH3) was used as a marker for cells in mitosis, while activated caspase-3 was used as a marker for apoptotic cells. Immunostaining was performed as described above, and mitotic and apoptotic cells were counted on Imaris using the Spots tool.

Data visualisation and statistical analysis

Data analysis and visualisation were performed in Rstudio. Boxes in box-and-whisker plots represent the interquartile range, while the whiskers represent 1.5x of the interquartile range. Each dataset was first tested for normality by the Shapiro-Wilk test. If the data followed a normal distribution, a Student's *t*-test or a one-way analysis of variance (ANOVA) and Tukey's post-hoc test was performed. If the data did not follow a normal distribution, a non-parametric Kruskal-Wallis ANOVA and Mann-Whitney's *U*-test was performed. For testing significance of difference between slopes, a two-way ANOVA was used. For testing goodness of fit, Least Squares and Weighted Least Squares were used.

4.RESULTS

ESTABLISHMENT OF A 3D EX VIVO CULTURE SYSTEM FOR MOUSE PERI-IMPLANTATION EMBRYOS

The work described in the first two sections of Results had been initiated by Laura Panavaite, with the first section describing method establishment and the second section describing biological insights obtained from the method. Together with my contributions, and those of my co-authors, it forms part of a publication (Ichikawa et al., 2022). Here, I describe my contributions to the project, including the validation, revision, and optimisation of a 3D *ex vivo* culture system, the collection and analysis of *in utero*-developed and *ex vivo*-cultured embryos throughout peri-implantation development, the establishment of a quantitative rubrics for evaluating embryonic development *in utero* and *ex vivo*, and the new insights pertaining to the peri-implantation epiblast gained from live-imaging of this *ex vivo* culture system.

Existing ex vivo culture systems exhibit non-physiological morphogenesis of the egg cylinder

To investigate the coordination of growth and morphogenesis in mouse peri-implantation development, we required a system that was able to recapitulate peri-implantation development outside of the uterine environment. While *ex vivo* culture methodologies had already been published, prior work in our laboratory had found that culture on a 2D surface led to the collapse of the embryo and the complete loss of epiblast (EPI) 3D structure before the egg cylinder was reformed *de novo* (**Figure 1.11**; see also Panavaite, 2018). To avoid this phenomenon, a 3D culture system based on Matrigel was under development in the laboratory (**Figure 4.1A**; see also Panavaite, 2018). I aimed to validate this culture system in terms of its capability to recapitulate *in utero* morphogenesis of the embryonic tissues.

While the 3D gel matrix was able to support the formation of egg cylinders (**Figure 4.1B**), many embryos exhibited signs of impeded growth, where distinct clusters Oct3/4$^+$ cells remained adjacent to Gata4$^+$ cells, but the ICM fails to develop into an egg cylinder (**Figure 4.1C**). I found that the efficiency at which embryos cultured in such an environment formed egg cylinders was much lower than expected (17%, n = 8 out of 47 embryos from 7 experiments), and egg cylinders were variable in morphology. I hypothesised that the culture system in its current setup was impeding the growth and morphogenesis of the embryo. In addition, the lack of live-imaging throughout the culture period meant that whether the embryos that formed egg cylinders were able to do so through physiological morphogenetic processes remained yet unclear.
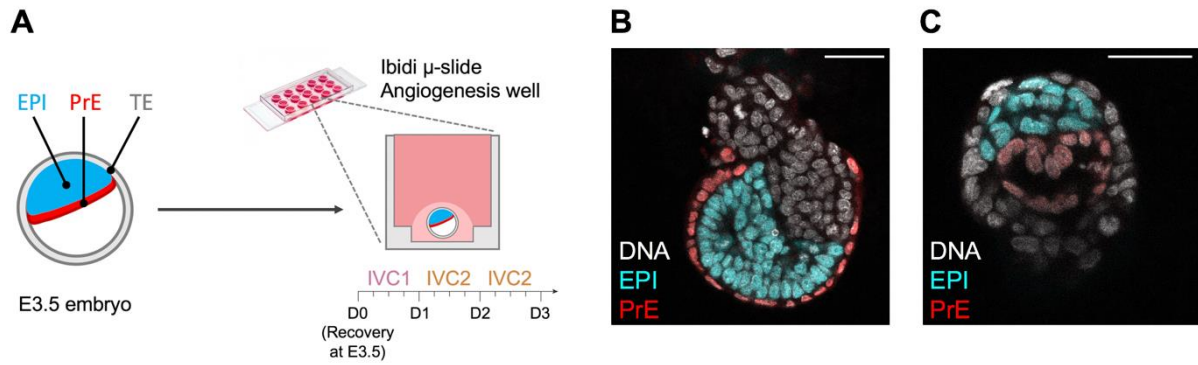
Figure 4.1: Existing *ex vivo* culture systems do not efficiently support egg cylinder morphogenesis. Culture method conceptualised by Laura Panavaite. Experiments performed by Hui Ting Zhang. Figure prepared by Hui Ting Zhang.

(A) A proposed Matrigel-based culture system for the mouse embryos during peri-implantation development. Mouse embryos recovered at E3.5 are embedded into a Matrigel-based gel mix. After the gel has solidified, in vitro culture 1 (IVC1) medium is added; after 24 hours of culture, it is replaced by *in vitro* culture 2 (IVC2) medium, and after a further 24 hours, the old medium is aspirated and fresh IVC2 medium is added. Only embryos that have naturally hatched from their zona pellucidae are used.

(B) Immunofluorescence image of an egg cylinder developed from an E3.5 mouse embryo after 48 hours of culture in the Matrigel-based culture system, stained for Oct3/4[+] EPI, Gata4^{+} VE, and DNA.

(C) Immunofluorescence image of an embryo after 48 hours of culture in the Matrigel-based culture system, stained for Oct3/4[+] EPI, Gata4^{+} PrE, and DNA.

Scale bars = 50 µm.

High tension in mural trophectoderm impedes extraembryonic ectoderm and egg cylinder morphogenesis in ex vivo-cultured embryos

To understand why growth was impeded in *ex vivo*-cultured embryos, I imaged E3.5 embryos during *the ex vivo* culture period on an inverted light-sheet microscope, the Luxendo InVi SPIM (Bruker, Luxendo) (Ichikawa et al., 2022; Strnad et al., 2016). I found that in the embryos that succeeded in forming egg cylinders, the inner cell mass (ICM), distinguishable by the Pdgfra-GFP$^+$ primitive endoderm (PrE) layer surrounding it, invariably breached the mural trophectoderm (mTE) (**Figure 4.2A**). Notably, breaching of the mTE allowed for an invaginating movement in pTE cells (**Figure 4.2B**), which was absent in embryos that did not form egg cylinders. In these embryos that did not form egg cylinders, limited proliferation took place, and the ICM does not breach the mTE layer (**Figure 4.2C**).

During peri-implantation development *in utero*, the single-layered pTE undergoes elongation along the apico-basal axis, invagination, and proliferation to develop into the multi-layered extraembryonic ectoderm (ExE) (**Figure 4.3A**) (Christodoulou et al., 2019; Copp, 1979). I hypothesised that this pTE invagination process must be recapitulated in *ex vivo* culture for normal development of the embryo; breaching of the mTE, seen in the Matrigel-based *ex vivo* culture system, may be a non-physiological attempt to satisfy the prerequisite of pTE invagination. Together with my colleague Takafumi Ichikawa, we performed additional experiments to address this hypothesis (reported in (Ichikawa et al., 2022)). We found that "cortical tension of pTE cells increases during this period [of development]", accompanied by "[enrichment of] actin and bi-phosphorylated myosin regulatory light chain (ppMRLC) at the apical surface", suggesting that "pTE cells invaginate from the surface layer by the apical constriction" (Ichikawa et al., 2022).

We also observed that in the *ex vivo* culture system, pTE cells remained highly stretched throughout the culture period, and did not adopt the columnar morphology of pTE cells in *in utero*-developed embryos at the corresponding developmental stage. We concluded that pTE cells are under high tension in the *ex vivo* culture system, most likely from the mTE, and this prevented their invagination; release of this tension should allow invagination to proceed. Release of the tension by laser ablation of cortical junctions between the pTE and the mTE allowed pTE cells to "[shorten] apically and [elongate] along their apico-basal axis" (Ichikawa et al., 2022). Based on these observations, we concluded that "excess tension acting on pTE cells, as induced by this culture method, prevents pTE invagination and subsequent ExE formation" (Ichikawa et al., 2022).
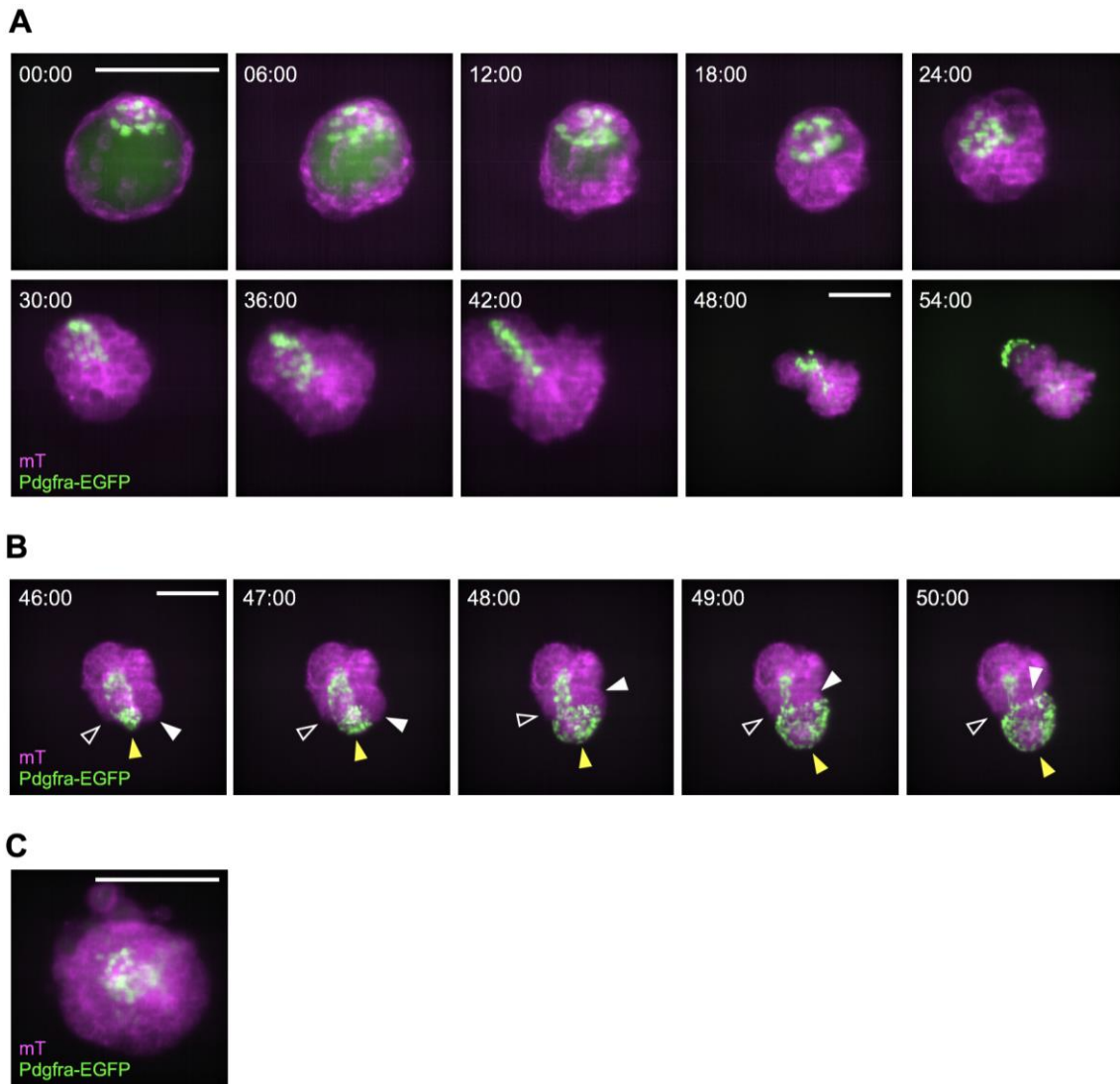
Figure 4.2: mTE impedes egg cylinder morphogenesis and elongation in *ex vivo*-cultured embryos.

(A) Time-lapse images of a Pdgfra-EGFP;mT mouse embryo developing from E3.5 in the Matrigel-based culture system with inverted light-sheet microscopy. Magnification change at 48:00 to accommodate increased size in growing embryo.

(B) Time-lapse images of a Pdgfra-EGFP;mT mouse embryo showing invagination of the polar trophectoderm (pTE) and breaching of the mural trophectoderm (mTE). Open white arrowheads indicate the mTE, while solid white arrowheads indicate the pTE, and solid yellow arrowheads indicate Pdgfra-EGFP⁺ PrE cells.

(C) A representative image of a mouse embryo whose inner cell mass (ICM) does not breach the TE layer.

Time = hours:minutes. Scale bars = 50 µm.

The mTE contributes to the formation of the Reichert's membrane, together with the parietal endoderm, a descendent of the PrE that arises during the late pre-implantation period (Salamat et al., 1995). I noted that removal of the mTE/Reichert's membrane (depending on the stage of development) for *ex vivo* culture of mouse embryos has been previously reported (Bedzhov et al., 2014b; Copp, 1981; McDole et al., 2018). When the mTE was microsurgically excised, pTE invagination proceeded (**Figure 4.3B**). In these embryos, proliferation and egg cylinder morphogenesis took place without loss of structure and organisation; the PrE remained on the surface of the EPI and extended to cover the ExE as *in utero* (**Figure 4.3C**), and EPI cells adopted the elongated morphology seen in *in utero* peri-/post-implantation embryos (**Figure 4.3D**). Therefore, I incorporated the excision of the mTE into the 3D *ex vivo* culture protocol.

Efficiency of egg cylinder formation increases when initial cell number is higher

I tested mTE excision and subsequent ICM culture and found that development into egg cylinder was more successful when embryos started with larger ICMs (**Figure 4.4A**). This may be because embryos with larger ICMs represented healthier embryos in a litter, which are more tolerant to the recovery and excision process and to injuries resulting from technical errors. Due to natural variation associated with the natural mating process, litters recovered at the same *in utero* time point often had a range of ICM sizes in terms of cell number, with up to four-fold difference between the largest and smallest ICMs at E4.5 (55—232 cells, **Figure 4.4B**). To ensure robustness of the culture system, I introduced a quality check before embedding. In this step, embryos with ICM numbers under a specific threshold will be discarded, as they will be highly unlikely to develop into egg cylinders. The optimal threshold was determined to be 110 cells or greater, as at this threshold level, sample loss is minimised against maximising the proportion of embryos developing into egg cylinders in the remaining samples (**Figure 4.4B**). A detailed description of how this threshold was determined, based on the application of a confusion matrix, can be found in (Ichikawa et al., 2022).
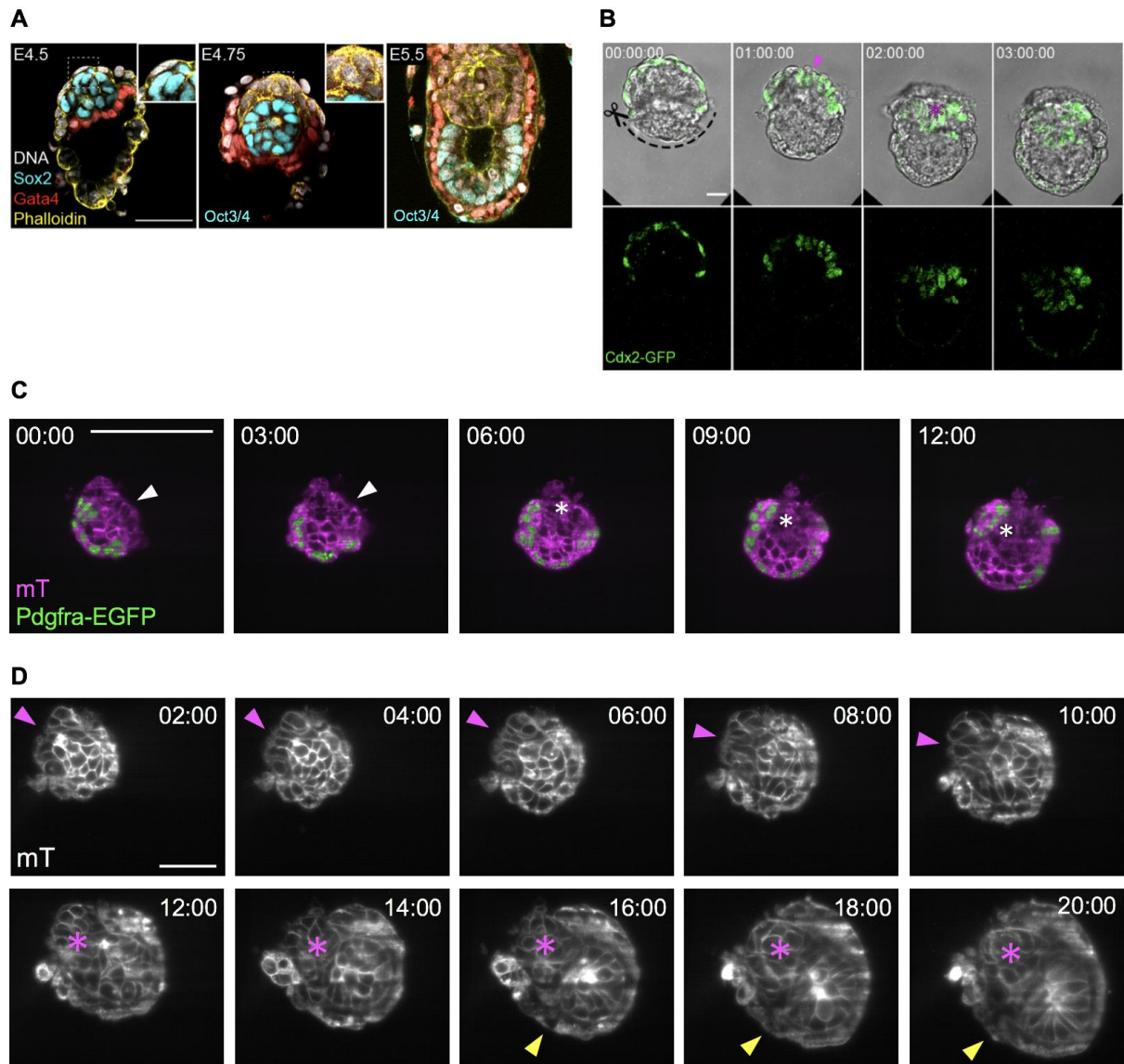
Figure 4.3: Excision of mTE allows for the invagination of the pTE, leading to unimpeded ExE and egg cylinder morphogenesis.

(A) Immunofluorescence images of *in utero*-developed embryos at E4.5, E4.75, and E5.5, showing the change in pTE morphology and the formation of the ExE. Embryos are stained for DNA, Sox2+ or Oct3/4+ EPI, Gata4+ VE, and Actin. Figure adapted from (Ichikawa et al., 2022). Sample collection and image analysis performed by Takafumi Ichikawa and Hui Ting Zhang. Figures prepared by Takafumi Ichikawa and Hui Ting Zhang.

(Legends continue on next page)

(Legends continued from previous page)

(B) Time-lapse images of a representative E4.5 Cdx2-GFP embryo after mTE excision. The solid magenta arrowhead indicates apically-constricting pTE cells, and the magenta asterisk indicates the invaginated ExE cells. Pdgfra-EGFP⁺ PrE cells remain on the surface of the EPI and the ExE. Figure adapted from (Ichikawa et al., 2022). Live-imaging performed by Takafumi Ichikawa and Hui Ting Zhang. Figures prepared by Takafumi Ichikawa.

(C) Time-lapse images of a representative E4.5 Pdgfra-EGFP;mT embryo after mTE excision. The solid white arrowhead indicates apically-constricting pTE cells, and the white asterisk indicates the invaginated ExE cells.

(D) Time-lapse images of a representative E4.5 mT embryo after mTE excision. The solid magenta arrowhead indicates apically-constricting pTE cells, and the magenta asterisk indicates the invaginated ExE cells. The solid yellow arrowhead indicates the developing egg cylinder with EPI cells adopting elongated morphology.

Time = hours:minutes:seconds (A), hours:minutes (B and C). Scale bars = 50 µm (A, C and D), 20 µm (B).
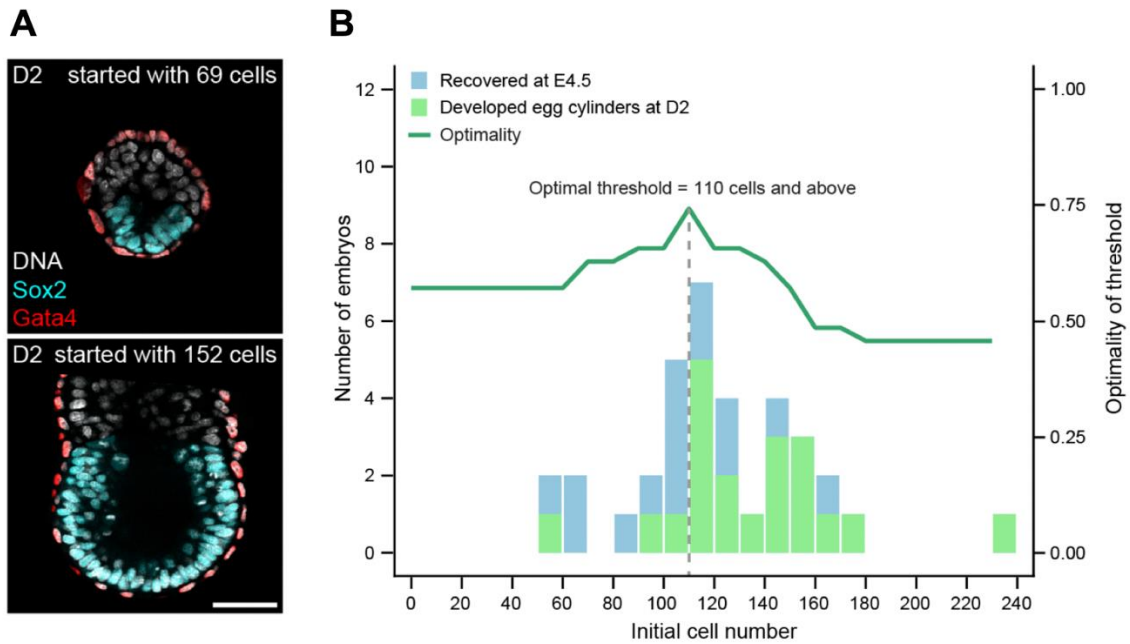
Figure 4.4: An optimal threshold of initial cell number maximises efficiency of egg cylinder development and minimises sample loss.

(A) Immunofluorescence images of 3D-geec embryos at D2, starting from different initial cell numbers (69, upper panel; 152, lower panel). Embryos are stained for Oct3/4⁺ EPI, Gata4⁺ VE, and DNA. Figure adapted from (Ichikawa et al., 2022). Sample collection, image analysis, cell counting, data analysis, and data visualisation performed by Hui Ting Zhang. Figure prepared by Hui Ting Zhang.

(B) Derivation of the optimal initial cell number threshold. Blue histograms show number of embryos recovered at E4.5 within each bin of initial cell number (sum of ICM cells and pTE cells), while green histograms show the subset of these embryos that developed egg cylinders at D2 of *ex vivo* culture. The green line chart shows optimality (i.e. Accuracy) for a threshold set at each initial cell number. Bin size = 10. A threshold of ≥110 cells gives the best optimality of 0.74. *n* = 35 embryos. Figure adapted from (Ichikawa et al., 2022).

Scale bar = 50 μm.

A revised 3D ex vivo culture system, 3D-geec, supports development of E4.5 embryos into egg cylinders without loss of epiblast organisation

Based on these findings, I modified the 3D *ex vivo* culture protocol to incorporate the excision of the mTE and the initial quality check before gel embedding (**Figure 4.5**). The full 3D-gel embedded embryo culture (3D-geec) protocol can be found at (Ichikawa et al., 2022). In brief, mouse embryos are recovered at E4.5, and their mTE is removed microsurgically with fine needles. Embryos with initial cell number greater than or equal to 110 cells are selected and embedded in a Matrigel-based gel mix for up to 48 hours of *ex vivo* culture. IVC1 medium is added once the gel has solidified, and exchanged for IVC2 medium after 24 hours of culture (Bedzhov et al., 2014b).
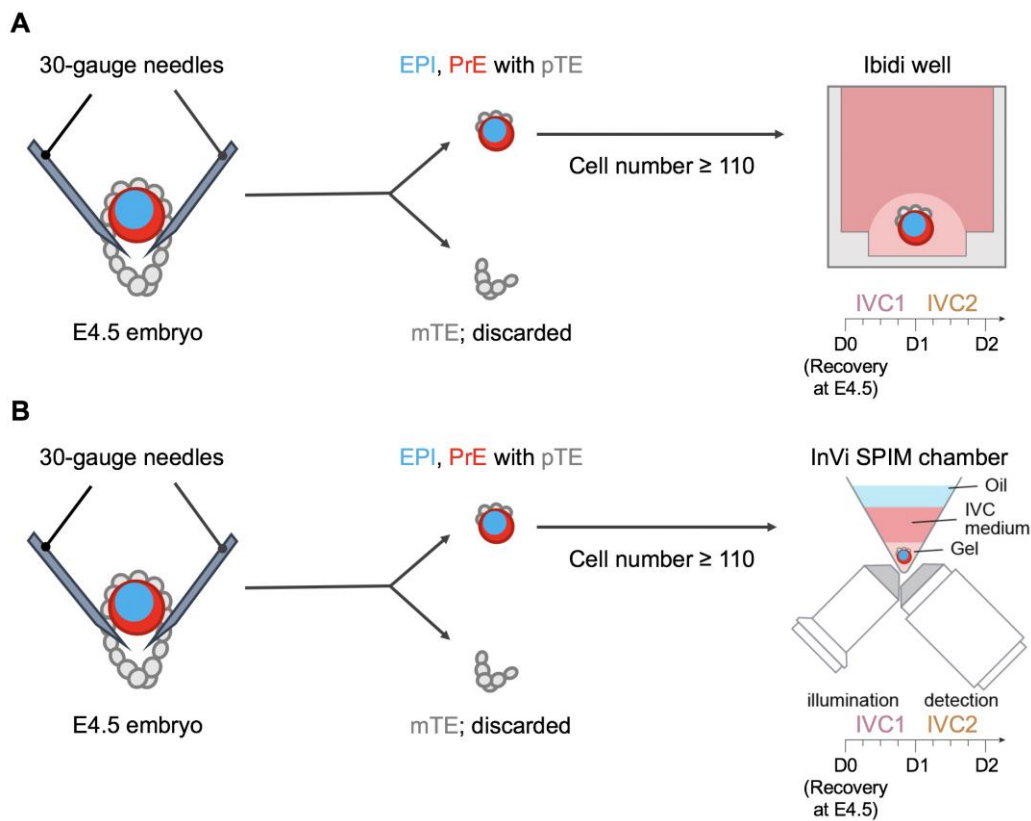
Figure 4.5: A revised 3D *ex vivo* culture system, 3D-gel embedded embryo culture (3D-geec), supports physiological morphogenesis of the egg cylinder (A) and is compatible with live-imaging in the InVi SPIM (B). InVi SPIM chamber schematic in (B) adapted from (Ichikawa et al., 2022).

3D-GEEC RECAPITULATES IN UTERO PERI-IMPLANTATION EGG CYLINDER DEVELOPMENT

3D-geec embryos successfully form the egg cylinder and specify cell lineages

I characterised embryos cultured *ex vivo* for up to 48 hours by the 3D-geec protocol. 3D-geec embryos recapitulated *in utero* development in terms of embryo morphology (**Figure 4.6A**), including spatial arrangement of the epiblast (EPI) and visceral endoderm (VE) tissues, as evidenced by immunostaining for markers expressed by those lineages. EPI organisation is well-preserved in 3D-geec embryos. EPI cells are arranged as a single, pseudo-stratified layer, with the apico-basal axis of the cells oriented radially and mitotic cells positioned at the apical surface (**Figure 4.6B**). In addition, 3D-geec embryos also recapitulated *in utero* morphogenetic processes of the EPI, such as the formation of the pro-amniotic cavity.

3D-geec embryos also recapitulated *in utero* cell lineage specification. Expression of the DVE/AVE marker Lefty1 is observed in a subpopulation of VE cells of 3D-geec embryos at D2, and the expression range of this marker is notable asymmetric about the proximal-distal axis of the egg cylinder, similar to its expression pattern *in utero* in E6.0 embryos (**Figure 4.6A'**). I concluded that, based on inspection of embryo gross morphology and expression pattern of marker genes, 3D-geec embryos were able to recapitulate *in utero* peri-implantation development.

A rubric to assess embryo development independently of chronological time facilitates comparison of in utero and ex vivo embryos

I sought to construct a more quantitative rubric by which 3D-geec embryo development can be assessed. I noted that when peri- and post-implantation embryos were cultured *ex vivo*, some degree of developmental delay was always observed. As such, comparing cultured embryos to in utero developed embryos purely based on chronological age was not always feasible or informative. Therefore, I identified key parameters that could be used to describe the extent of embryo development, such as: the number of cells in the EPI, VE overlying the EPI, and the total number of cells in the egg cylinder (**Figure 4.7A**); the proximal-distal length and diameter of the egg cylinder (**Figure 4.7B**); and the expression pattern of fate markers (**Figure 4.7C**).
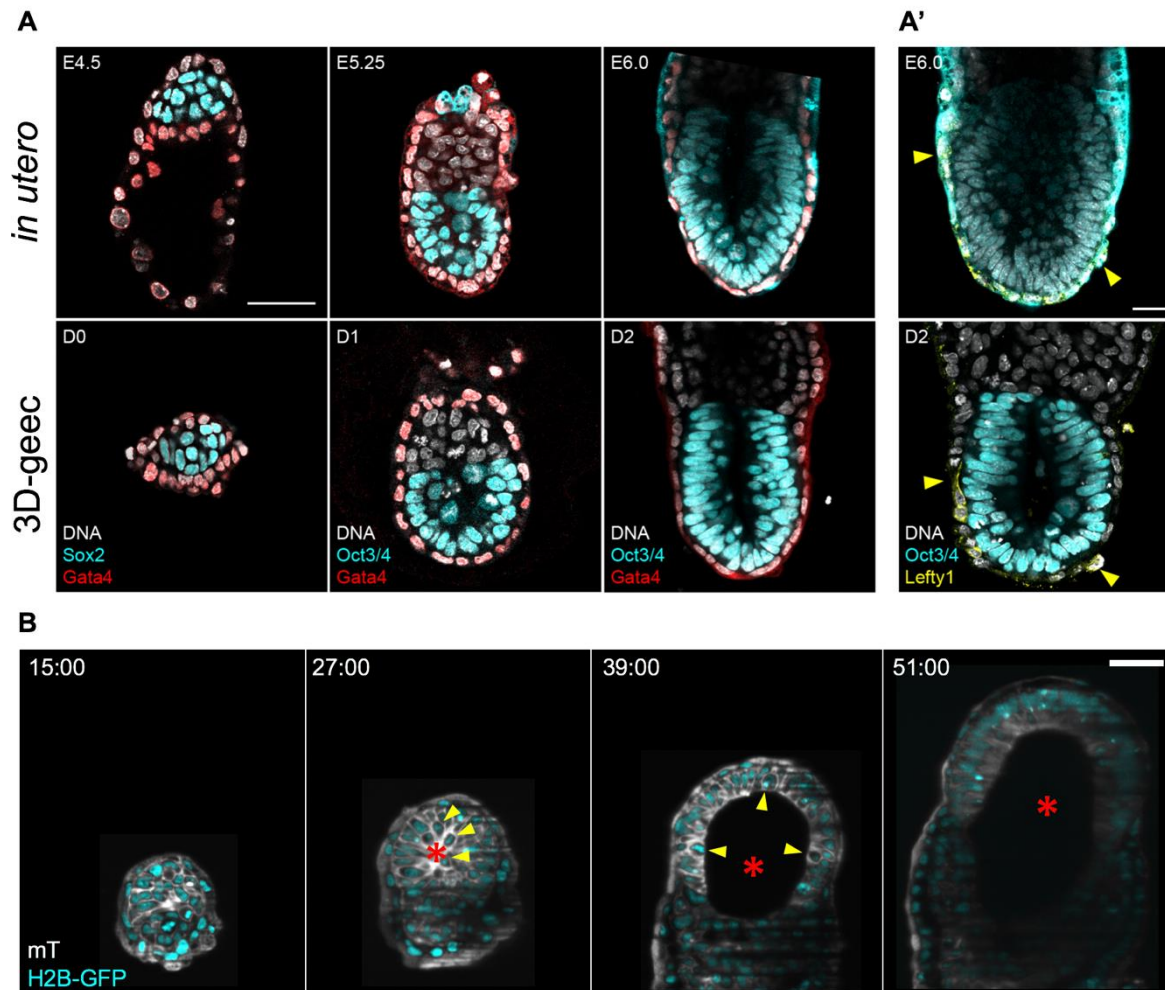
Figure 4.6: 3D-geec embryos successfully form the egg cylinder and specify cell lineages within 48 hours of *ex vivo* culture.

(A) Immunofluorescence images of representative *in utero*-developed embryos from E4.5 to E6.0 (upper panels) and 3D-geec embryos from day 0 (D0) to day 2 (D2) (lower panels). Embryos are stained for Sox2^{+} or Oct3/4[+] EPI, Gata4^{+} VE, and DNA. Figure adapted from (Ichikawa et al., 2022). Sample collection and image analysis performed by Hui Ting Zhang. Figure prepared by Hui Ting Zhang.

(A') *In utero* embryos at E6.0 (upper panel) and 3D-geec embryo at D2 (lower panel) exhibiting asymmetrically-localised anterior visceral endoderm (AVE domain). Embryos are stained for Oct3/4[+] EPI, Lefty1^{+} AVE, and DNA. The solid yellow arrowheads mark the boundaries of the Lefty1^{+} AVE domain.

(B) Time-lapse images of a 3D-geec H2B-GFP;mT embryo. The solid yellow arrowheads indicate apically-positioned mitotic cells in the EPI, and the red asterisk indicates the nascent and expanding pro-amniotic cavity.

Time = hours:minutes. Scale bars = 50 μm.

I first collected embryos at different time points in *in utero* development. I ensured that each time point contained embryos from multiple litters, so as to account for inter-litter variation in development due to natural mating. From these samples, I excluded embryos damaged during recovery, and measured the parameters identified above. In parallel, I collected samples from 3D-geec embryos at D1 and D2, and measured the parameters of these embryos. This allowed me to directly compare the development in terms of these parameters between 3D-geec and *in utero* embryos, and to quantify the developmental delay, if any, that existed in 3D-geec embryos.
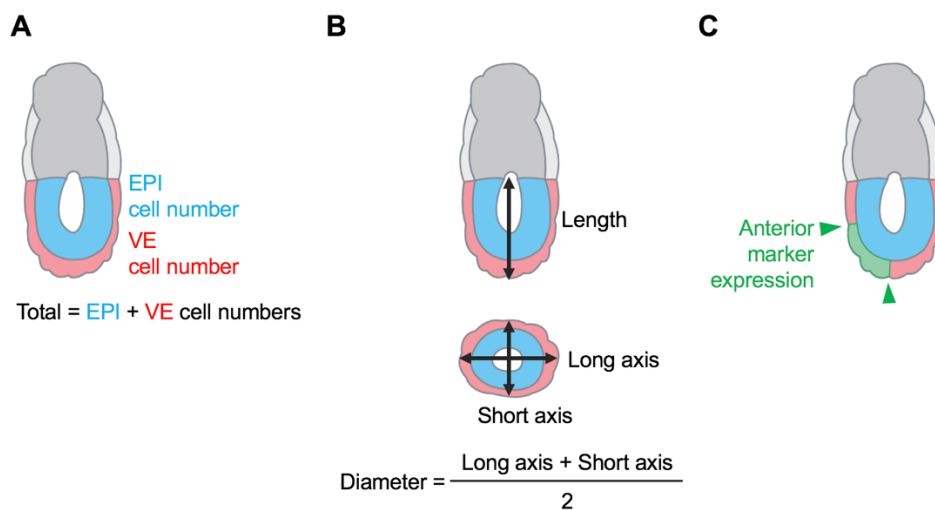
Figure 4.7: Identification of cell- and tissue-scale parameters (A, B and C) as a rubric for assessing embryo development.

3D-geec embryos recapitulate in utero growth, tissue organisation, cell differentiation, and body axis specification until E6.0

I compared the physical dimensions of 3D-geec embryos at D1 and D2 with *in utero*-developed embryos collected from E4.5 to E6.0 (**Figure 4.8A**). 3D-geec embryos follow a similar growth pattern to *in utero*-developed embryos, though when compared to *in utero*-developed counterparts of the same proximal-distal egg cylinder length, they consistently exhibit a larger egg cylinder diameter ($P < 0.05$, $n = 22$ and 26 embryos) (**Figure 4.8B**). I performed a comparison of slopes of the trends in *in utero*-developed and in 3D-geec embryos, and observed that while the trends are significantly different ($P < 0.05$), 3D-geec embryos are increasingly similar to *in utero* embryos over time, in terms of length-to-diameter ratio (**Figure 4.8C**).
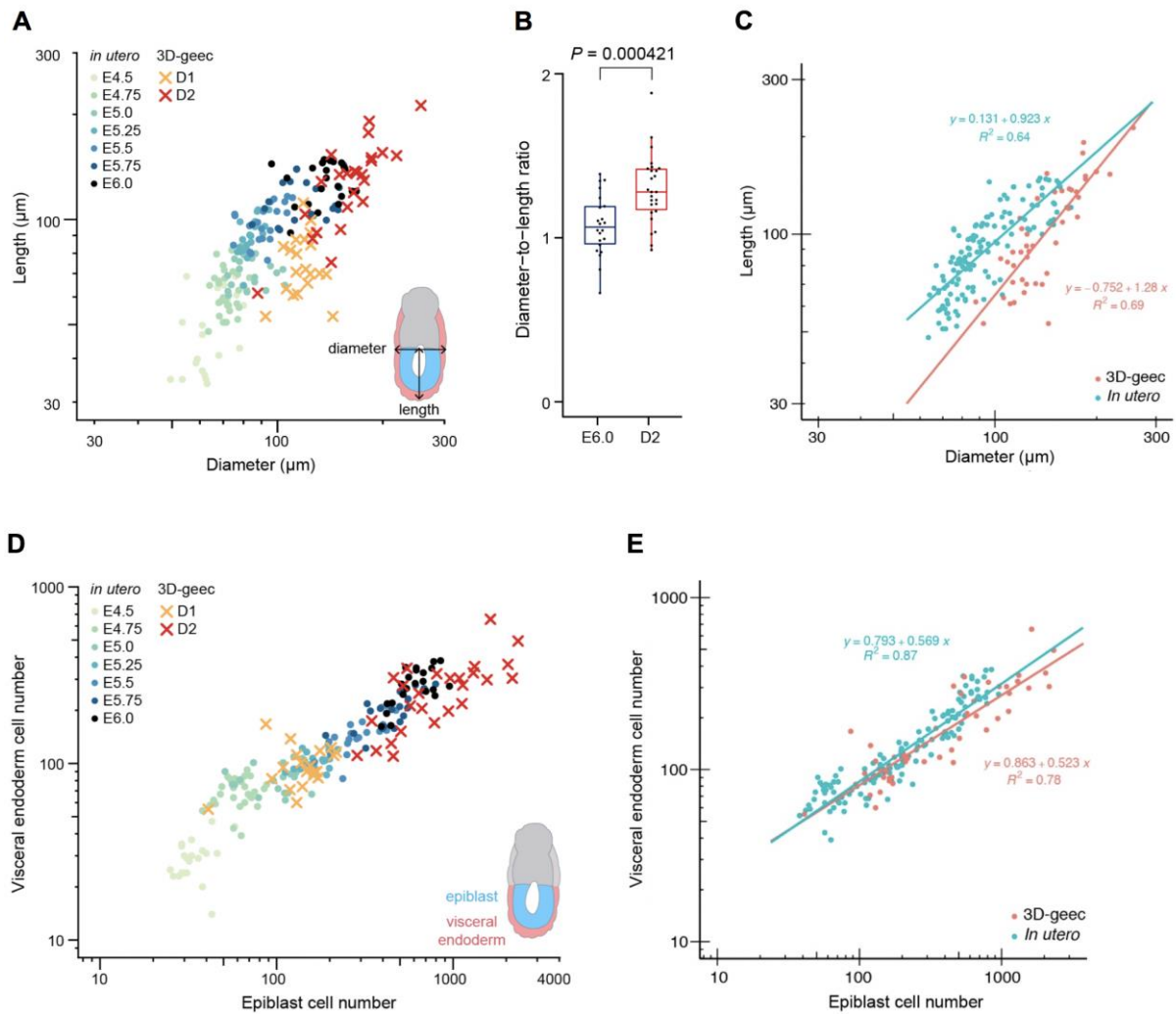
Figure 4.8: 3D-geec embryos recapitulate *in utero* development in terms of tissue size and cell number. Figure adapted from (Ichikawa et al., 2022). Data produced jointly with Takafumi Ichikawa. Sample collection and imaging performed by Takafumi Ichikawa and Hui Ting Zhang. Image analysis, cell counting, dimension measurements, data analysis, and data visualisation performed by Hui Ting Zhang. Figure prepared by Hui Ting Zhang.

(A) Scatter plot of egg cylinder proximal-distal length against egg cylinder diameter (defined as the average of long and short transverse axes of the egg cylinder) of 3D-geec embryos and *in utero*-developed embryos. Axes are in log scale.

(B) Diameter-to-length ratios of *in utero*-developed embryos at E6.0 and 3D-geec embryos at D2. P = 0.000421.

(C) Comparison of trends of embryos shown in (A). P = 0.0076. Axes are in log scale.

(D) Scatter plot of visceral endoderm (VE) cell numbers against epiblast (EPI) cell numbers of 3D-geec embryos and *in utero*-developed embryos. Axes are in log scale.

(Legends continue on next page)

(Legends continued from previous page)

(E) Comparison of trends of embryos shown in (D). $P = 0.2451$. Axes are in log scale.

$n = 21$ (E4.5), 28 (E4.75), 20 (E5.0), 20 (E5.25), 21 (E5.5), 21 (E5.75), 22 (E6.0), 20 (D1), and 26 (D2) embryos.

I also compared 3D-geec embryos and *in utero*-developed embryos in terms of cell number (**Figure 4.8D**). 3D-geec embryos maintained a similar proportion of EPI to VE cells as *in utero*-developed embryos and mapped well to the *in utero* embryos; a comparison of slopes for the trends showed no significant difference ($P = 0.2451$) (**Figure 4.8E**). In terms of both physical dimensions and cell numbers, 3D-geec embryos are more variable in terms of development than *in utero* embryos, with a greater spread of points as evident in **Figures 4.8A** and **4.8D**.

Apart from physical dimensions and cell numbers, I sought to characterise 3D-geec embryos in terms of ability to differentiate cell lineages and specify the first body axis, the anterior-posterior axis. In mouse embryos at E6.0, the expression of anterior fate markers such as Lefty1 and Cerberus1 are already radially asymmetric, caused by the distal-to-proximal migration of a subpopulation of VE cells expressing these markers known as the anterior visceral endoderm (AVE) (Brennan et al., 2001a; Thomas et al., 1998), and which we were able to observe in live-imaging of 3D-geec embryos (Ichikawa et al., 2022). *In utero*-developed embryos can be qualitatively classified into "Asymmetric" or "Symmetric" categories based on immunofluorescence images by experimenters experienced in mouse embryo development, but 3D-geec embryos posed a problem due to the increased variability in embryo size, shape, and aspect ratio. Therefore, I developed a method to quantitatively characterise the degree of migration of these cells in 3D-geec embryos (**Figure 4.9A**).

I classified VE cells as "AVE" or simply "VE" depending on whether each cell expressed Lefty1/Cerberus1. I calculated the linear distance in 3D of each cell from the distal tip of the egg cylinder, as well as its angle radially *around* the proximal-distal axis of the egg cylinder. This allowed me to plot the VE and AVE cells in each embryo as a polar plot with the distal tip of the egg cylinder as the origin of the plot. The inclusion of distance *along* the proximal-distal axis provided more information about the migration of AVE cells than simply performing a projection off the egg cylinder along that axis, and is more tolerant to variations in embryo shape. I scaled each polar plot by the maximum linear distance among all AVE and VE cells to facilitate comparison across embryos of different sizes. From the scaled polar plots, I calculated the linear distance in 2D of the centroid of AVE cells from the origin of the polar plot. This distance, which I termed the AVE Asymmetry Index took a value from 0 to 1. I performed these calculations for a set of *in utero*-developed embryos recovered at E5.25 and E6.0, as well as 3D-geec embryos at D2 (**Figure 4.9B**).
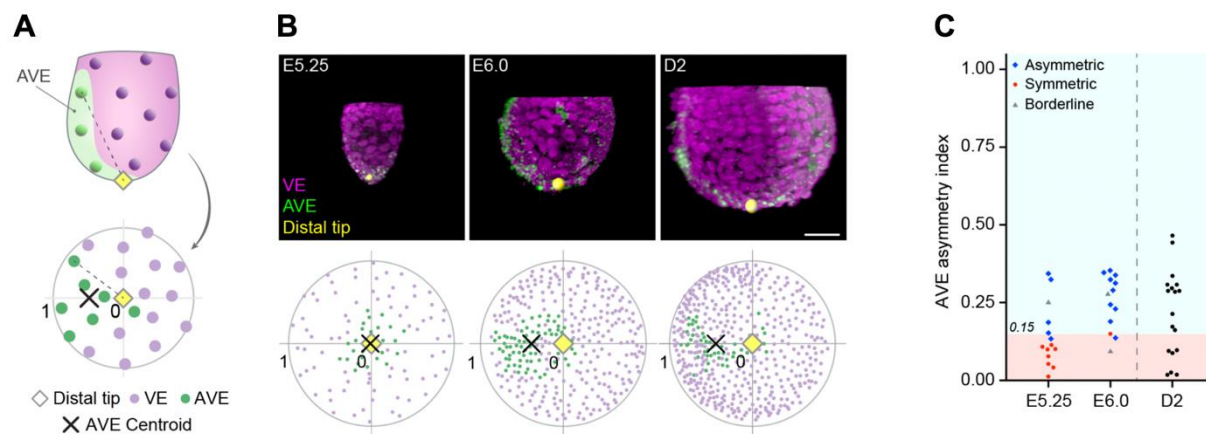
Figure 4.9: 3D-geec embryos recapitulate anterior-posterior body axis establishment by D2. Figure adapted from (Ichikawa et al., 2022). Data produced jointly with Takafumi Ichikawa. Sample collection and imaging performed by Takafumi Ichikawa and Hui Ting Zhang. Image analysis (classification of embryos) performed by Takafumi Ichikawa and Hui Ting Zhang. Image analysis (classification of cells), data analysis, and data visualisation (generation of polar plots and calculation of AVE Asymmetry Index) performed by Hui Ting Zhang. Figure prepared by Hui Ting Zhang.

(A) Schematic showing how the AVE Asymmetry Index was calculated. 3D-coordinates of VE cells, assigned as AVE (green) or VE (purple), are plotted on a polar plot. The black cross indicates the centroid of the AVE cells calculated from their spread on the polar plot, and the yellow diamond indicates the distal tip of the egg cylinder. Polar plots are scaled by the maximum linear distance of any AVE or VE cell for that embryo.

(B) Representative *in utero*-developed embryos recovered at E5.25 and E6.0, and a 3D-geec embryo at D2 (upper panels), and their polar plots (lower panels). Embryos are stained for Lefty1+ or Cer1+ AVE, Gata4+ VE, and DNA.

(C) AVE Asymmetry Indices of *in utero*-developed embryos recovered at E5.25 and E6.0, and 3D-geec embryos at D2. The blue diamonds indicate Asymmetric embryos, the red circles indicate Symmetric embryos, and the grey triangles indicate Borderline embryos. The threshold for AVE asymmetry was determined to be 0.15. *n* = 15 (E5.25), 13 (E6.0), and 18 (D2) embryos.

Scale bar = 50 μm.

In parallel, I had manually classified *in utero*-developed embryos into "Asymmetric" or "Symmetric" categories as described above. To miminise bias, the same set of embryos was classified independently by my colleague Takafumi Ichikawa, and we found good agreement in classification of *in utero*-developed embryos. Embryos that had different classifications, or could not be classified confidently, were assigned as "Borderline", and consisted of 3 out of 28 embryos (11%). I found that all embryos classified as Symmetric had an AVE Asymmetry Index below 0.15 (**Figure 4.9C**). Therefore, I took this value as the threshold, and found that 67% of 3D-geec embryos at D2 showed AVE asymmetry.

As 3D-geec and *in utero*-developed embryos exhibited similar trends in EPI and VE cell numbers, I decided to use total egg cylinder cell number as the primary parameter for assessing embryo development (**Figure 4.10A**). I fitted a regression line to the total egg cylinder cell numbers of *in utero*-developed embryos (**Figure 4.10B**); the equation of this regression line allowed me to find the theoretical *in utero* age for an embryo of any given egg cylinder cell number. Based on this regression line, 3D-geec embryos at D1 corresponded to E5.20 in *in utero* age, while 3D-geec embryos at D2 corresponded to E6.04 in *in utero* age. This method of deriving the theoretical *in utero* age provides a way to assess development in embryos that exhibit a developmental delay due to *ex vivo*-culture or other manipulations.

Scaling the developmental timeline of 3D-geec embryos to that of *in utero*-developed embryos showed that 3D-geec embryos were able to recapitulate 36 hours of *in utero* development after 48 days of *ex vivo* culture (**Figure 4.10C**). This is corroborated by the comparable AVE domain establishment and embryonic body axis specification in 3D-geec embryos at D2 and in *in utero* embryos at E6.0.
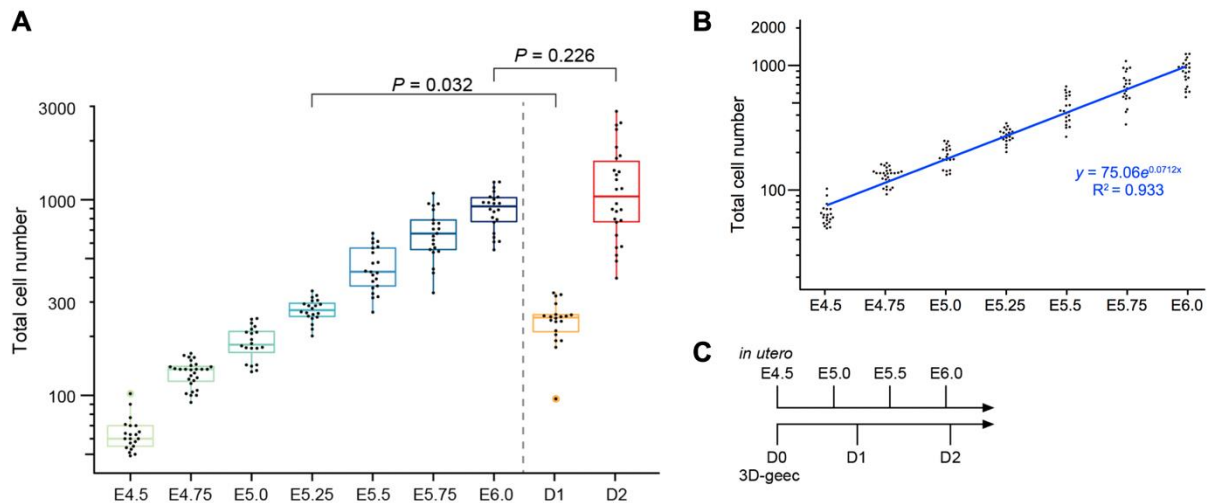
Figure 4.10: A scaled timeline of 3D-geec development based on total egg cylinder cell numbers allows for comparison between *ex vivo*-cultured and *in utero*-developed embryos. Figure adapted from (Ichikawa et al., 2022). Data produced jointly with Takafumi Ichikawa. Sample collection and imaging performed by Takafumi Ichikawa and Hui Ting Zhang. Image analysis, cell counting, dimension measurements, data analysis, and data visualisation performed by Hui Ting Zhang. Figure prepared by Hui Ting Zhang.

(A) Boxplots of total egg cylinder cell numbers of *in utero*-developed and 3D-geec embryos. 3D-geec embryos at D1 are least significantly different from E5.25 embryos ($P = 0.032$), and 3D-geec embryos at D2 are least significantly different from E6.0 embryos ($P = 0.336$). *y*-axis in log scale.

(B) Dot plots of total egg cylinder cell numbers of *in utero*-developed embryos from E4.5 to E6.0. A regression line ($y = 75.061e^{0.0712x}$, where x = number of hours after E4.5 and y = total egg cylinder cell number) allows the calculation of a theoretical *in utero* age corresponding to a known total egg cylinder cell number. *y*-axis in log scale.

(C) Scaled timeline of 3D-geec development against *in utero* development. 3D-geec embryos at D1 corresponded to E5.20 in *in utero* age, while 3D-geec embryos at D2 corresponded to E6.04 in *in utero* age.

n = 21 (E4.5), 28 (E4.75), 20 (E5.0), 20 (E5.25), 21 (E5.5), 21 (E5.75), 22 (E6.0), 20 (D1), and 26 (D2) embryos.

3D-geec is a robust ex vivo culture system for mouse peri-implantation embryos

The quality checks that have been introduced to evaluate embryo competence for *ex vivo* culture as well as embryo development after *ex vivo* culture have resulted in the elimination of a subpopulation of embryos. While the elimination of aberrant embryos will have improved the robustness of the culture system, I wanted to know the final expected success rate for *ex vivo* culture using 3D-geec. The first quality check includes 66% of embryos with greater than or equal to 110 cells in the ICM and pTE, 74% of which will develop into egg cylinders (**Figure 4.4B**); of these, 67% will exhibit AVE asymmetry to a sufficient degree to be considered as having established the anterior pole (**Figure 4.9C**). In sum, 3D-geec has a 49% efficiency of supporting peri-implantation embryo development up to an extent comparable to *in utero*-developed embryos at E6.0 (**Figure 4.11**).

Taken together, 3D-geec is a robust *ex vivo* culture system for mouse embryos that supports peri- and early post-implantation development until specification of the first body axis.
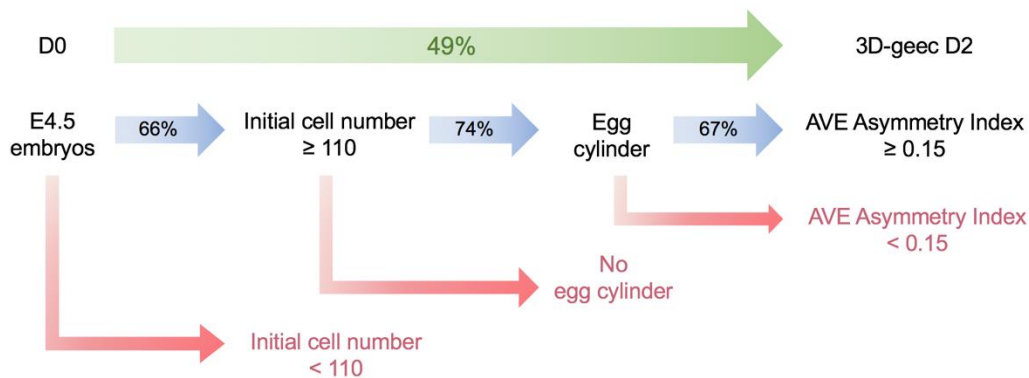
Figure 4.11: 3D-geec achieves 49% efficiency in supporting embryo growth and morphogenesis for at least 48 hours.

CELLULAR DYNAMICS IN THE PERI-IMPLANTATION EPIBLAST

The establishment and validation of an *ex vivo* culture protocol for peri-implantation mouse embryos opens new inroads to studying this exciting period of embryonic development. In particular, the compatibility of this culture system, 3D-geec, with live-imaging in an inverted light-sheet microscope, the InVi SPIM (Bruker, Luxendo), allows one to follow development in real time over days without photodamage to the embryos (Ichikawa et al., 2022), or to study cell- and tissue-scale phenomena with high spatial and temporal resolution. In conjunction with a machine-learning-based image segmentation and analysis pipeline constructed by my colleagues and collaborators (Ichikawa et al., 2022), I was able to study cellular dynamics in the peri-implantation epiblast.

The mouse epiblast undergoes significant changes in cell shape and arrangement during peri-implantation development

During early peri-implantation development, over a period of 24 hours, the mouse epiblast (EPI) changes drastically in structure. Within this period, a new compartment within the embryo, the pre-amniotic cavity, forms *de novo*. I had previously observed that EPI cells undergo rapid and significant elongation during the time of pro-amniotic cavity formation ($P <$ 0.00001, n = 16 and 18 embryos) (**Figure 4.12A**). At around the same time, EPI cells also progressively align their long axis with each other, which begins before pro-amniotic cavity formation (**Figure 4.12B**). I also observed that the formation of the pro-amniotic cavity involved the emergence and localisation of apical components at the centre of the embryo (**Figure 4.12C, D**). However, some of these observations were made from fixed time points and could reveal little about the dynamics of these cell-level changes in the EPI, and others, while based on live-imaging data, lacked the spatio-temporal resolution for quantitative analysis.

Using a combination of long-term live-imaging followed by machine-learning based image segmentation, cell tracking, and analysis, I was able to measure the change in cellular parameters such as cell volume, cell shape, and cell alignment in the EPI up until pro-amniotic cavity formation (**Figure 4.13A—C**). Furthermore, the ability to track cells allows me to follow the changes in these parameters for individual cells, not just the EPI as a whole (**Figure 4.13D— F, 4.13G—I, 4.13J—L**). These analyses were performed on two representative embryos. Data from one embryo is presented here; the full dataset can be found at (Ichikawa et al., 2022).
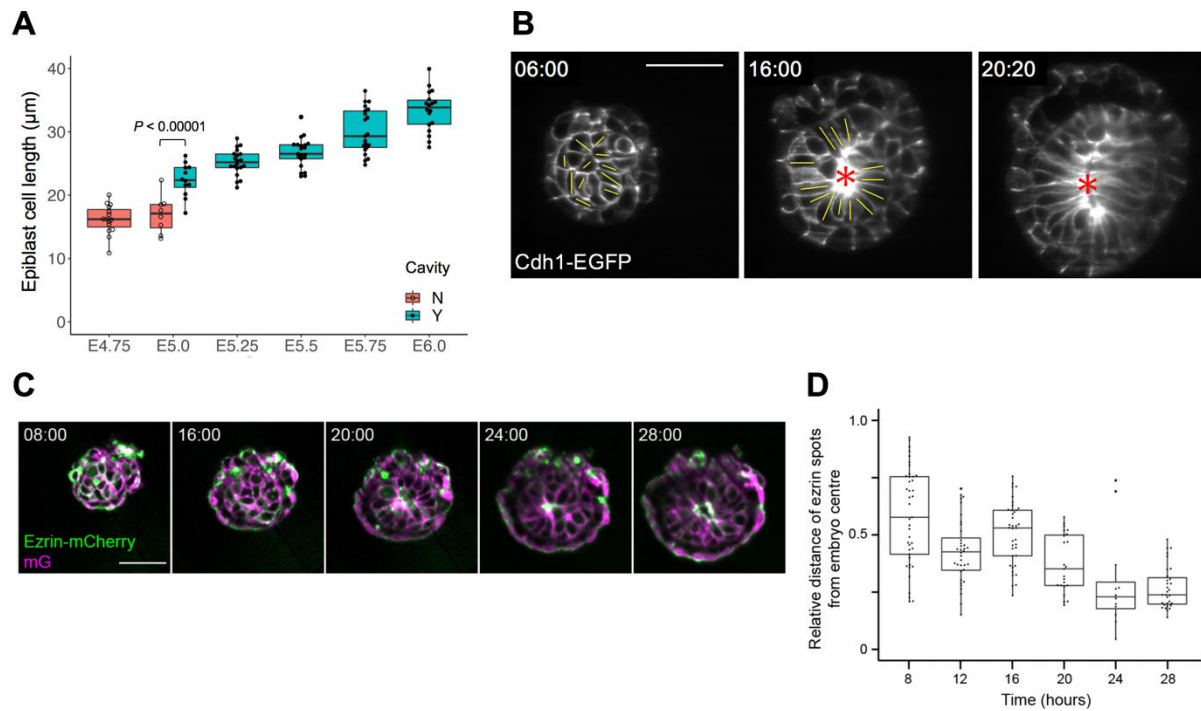
Figure 4.12: EPI cells undergo elongation, alignment, and acquisition of apico-basal polarity during early peri-implantation development. Data produced jointly with Takafumi Ichikawa. Sample collection and imaging performed by Takafumi Ichikawa and Hui Ting Zhang. Image analysis, data analysis, and data visualisation performed by Hui Ting Zhang. Figure prepared by Hui Ting Zhang.

(A) Rapid elongation of EPI cells during pro-amniotic cavity formation *in utero* is followed by progressive elongation at a slower pace. $P < 0.00001$, $n = 16$ (E5.0 without cavity) and 18 (E5.0 with cavity) embryos.

(B) Time-lapse images of a representative Cdh1-GFP embryo in 3D-geec from just before until just after pro-amniotic cavity formation. Progressive alignment of EPI cells' long axes precedes pro-amniotic cavity formation. The yellow lines indicate the long axes of EPI cells, and the red asterisk indicates the nascent and expanding pro-amniotic cavity.

(C) Time-lapse images of a representative Ezrin-mCherry;mG embryo in 3D-geec until pro-amniotic cavity formation. Figure adapted from (Ichikawa et al., 2022).

(D) Relative distance of Ezrin-mCherry spots from the centre of the embryo in (C). Figure adapted from (Ichikawa et al., 2022).

Scale bars = 50 μm.
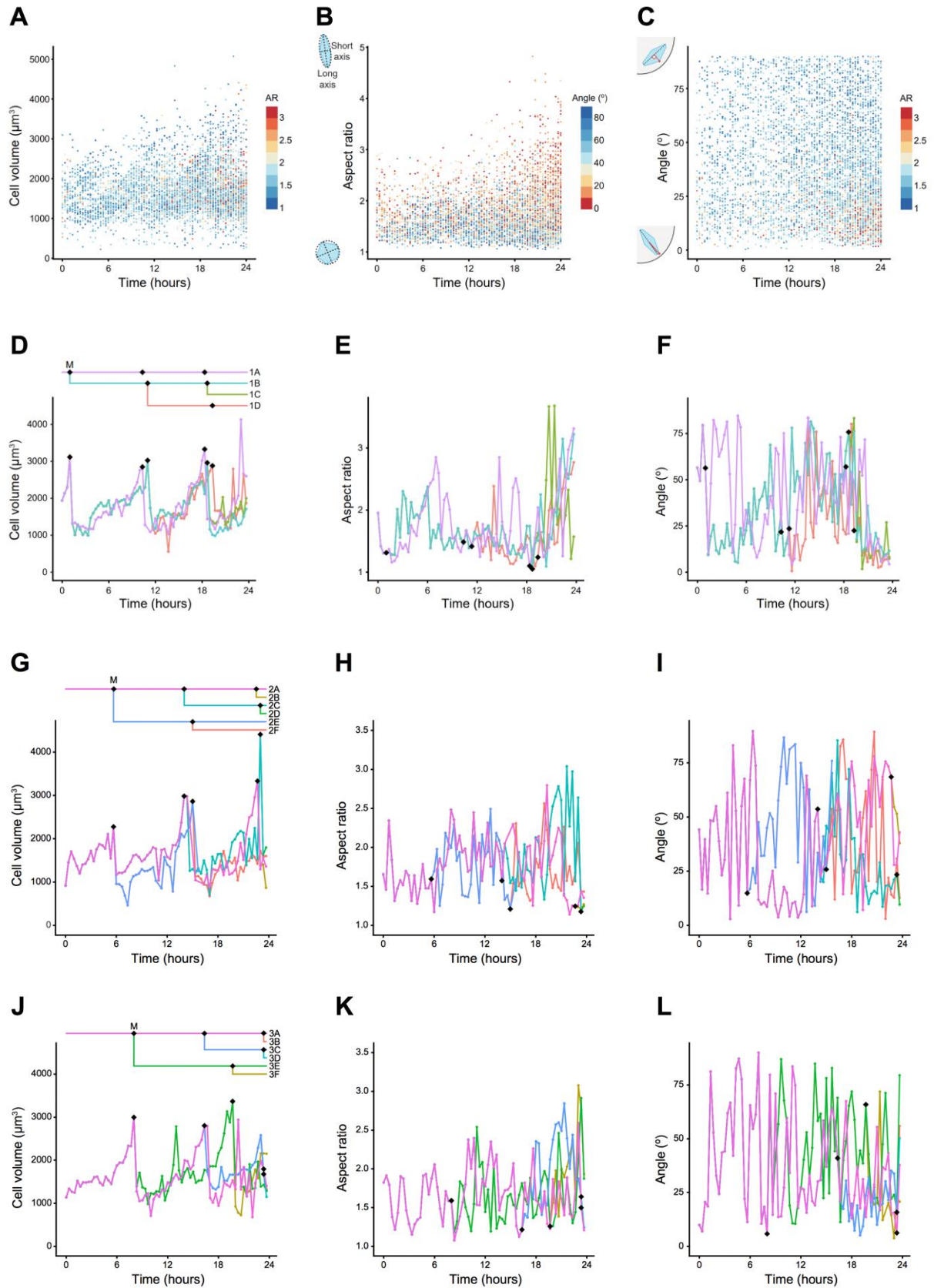
(Legends continue on next page)

Figure 4.13: Live-imaging of 3D-geec embryos coupled with machine-learning-based image segmentation enables quantitative analysis of cell dynamics in the peri-implantation EPI. Data produced jointly with Dimitri Fabrèges and Takafumi Ichikawa. Sample collection and imaging performed by Takafumi Ichikawa and Hui Ting Zhang. Data analysis pipeline constructed by Dimitri Fabrèges and Takafumi Ichikawa. Manual curation of segmentation output performed by Takafumi Ichikawa. Cell tracking, data analysis, and data visualisation performed by Hui Ting Zhang. Figure prepared by Hui Ting Zhang. Figure adapted from (Ichikawa et al., 2022).

(A—C) Measurement of volume **(A)**, aspect ratio **(B)** and alignment **(C)** of all EPI cells in a representative 3D-geec embryo.

(D—F, G—I, J—L) Measurement of volume **(D, G, J)**, aspect ratio **(E, H, K)** and alignment **(F, I, L)** of three EPI cells and their tracked descendants in the same 3D-geec embryo. The black diamonds indicate mitotic events in the lineage trees. Daughter cells that cannot be tracked with confidence are excluded from the lineage trees.

I found that the cell volume of EPI cells increased during the cell cycle and fell back to a basal volume (approximately 1000 μm^3) after each mitosis, stereotypical of somatic cell divisions (**Figure 4.13A, 4.13D, 4.13G, 4.13J**). While it appeared that, on the whole, waves of cell division took place in the EPI, more analysis is required before I can make a conclusive statement. In addition, while some cell lineages showed remarkable synchronicity in cell cycle length and division times (**Figure 4.13D, 4.13G**), this is not consistent across all lineages in the EPI (**Figure 4.13J**). Interestingly, the maximum cell volume just before mitosis takes place seemed to increase over time, though this represented only a very small subset of cells, and whether this is biologically relevant or merely an artefact of image segmentation and analysis remains to be investigated.

Overall, EPI cells showed an increase in aspect ratio (defined as the ratio of the longest axis of the cell to the mean of the shorter axes) over the 24 hours analysed (**Figure 4.13B**). While an individual cell's aspect ratio can vary significantly from timepoint to timepoint, likely due to influences from neighbouring cells (e.g. a cell undergoing mitosis will deform neighbouring cells, due to the space constraints in the EPI), EPI cells consistently exhibit a marked increase in aspect ratio during the 6 hours prior to pro-amniotic cavity formation (**Figure 4.13E, 4.13H, 4.13K**).

Finally, EPI cells show a concomitant radial alignment of their long axis, which increases with both time and aspect ratio (**Figure 4.13C, 4.13F, 4.13I, 4.13L**). Cells with high aspect ratios (AR > 2) also have higher alignment (indicated by a lower angle between their long axis and a line segment projected from the centre of the cell to their outermost voxel). It is intuitive that only cells with high aspect ratios possess a significant long axis and therefore the potential to be aligned or mis-aligned; focusing on these cells, the observation remains that these cells are consistently well-aligned – there are few cells with both high aspect ratio and high angle the population of EPI cells (**Figure 4.13C**). Analysing individual tracked cells reveals that once cells are aligned, they tended to maintain this alignment, unless undergoing mitosis (**Figure 4.13F** cells 1A, 1B, 1C,1D**, 4.13I** cells 2A, 2C**, 4.13L** cells 3A, 3C).

Neighbour-neighbour interactions and heterogeneities in the epiblast

I observed that in EPI cells, changes in cellular parameters such as aspect ratio and alignment did not correlate necessarily with lineage, i.e. not all descendants from one cell will adopt the same aspect ratio and alignment at the same rate (**Figure 4.13G—4.13I**). I observed that EPI daughter cells can be spatially distant from each other after a mitotic event, especially in early peri-implantation development upon pTE invagination (Ichikawa et al. 2022, supplementary data).

I analysed the cell tracking data I obtained from the embryo in Figure 4.13 and identified two lineage trees (**Figure 4.14A**). In one lineage tree, daughter cells remained in close proximity with each other after cell divisions (**Figure 4.14A**, cells 1A—1D). In the other lineage tree, daughter cells were distributed across the EPI tissue (**Figure 4.14A**, cells 2A, 2C, 2F). In the latter lineage tree, cell 2C was spatially closer to the cell cluster 1A—1D, while cells 2A and 2F were further away (**Figure 4.14B, 4.14C**). I observed that when cells 1A—1D underwent a drastic increase in aspect ratio (AR) starting from approximately 18 hours (**Figure 4.13E**), only cell 2C, the cell closest to the cell cluster, showed a synchronous increase in AR (**Figure 4.14B**). Similarly, when cells 1A—1D became radially aligned from approximately 20 hours (**Figure 4.13F**), cell 2C also showed a similar degree of alignment at around the same time, unlike cells 2A and 2F (**Figure 4.14C**). Taken together, this indicates that EPI cells are highly susceptible to influences from their local environment.

Regional differences within the EPI have previously been reported; for example, the proportion of EPI cells undergoing mitosis was observed to be higher towards the distal tip of the egg cylinder (Snow, 1977). In addition, heterogeneities within the EPI have also been reported, and were implicated in cell competition and regulation within the EPI during development (Bowling et al., 2018; Clavería et al., 2013; Díaz-Díaz et al., 2017; Granier et al., 2011; Mohammed et al., 2017). In agreement with these previous reports, I observed both heterogeneity and spatial differences in signalling activity within the EPI (**Figure 4.15A—C**). Live-imaging of transgenic embryos carrying fluorescent reporters of signalling pathways allowed me to visualise signalling activity in real time. I noted that these heterogeneities persisted across mitotic events (**Figure 4.15D**); furthermore, these heterogeneities could exist on top of a tissue-scale gradient across the EPI (**Figure 4.15E**).
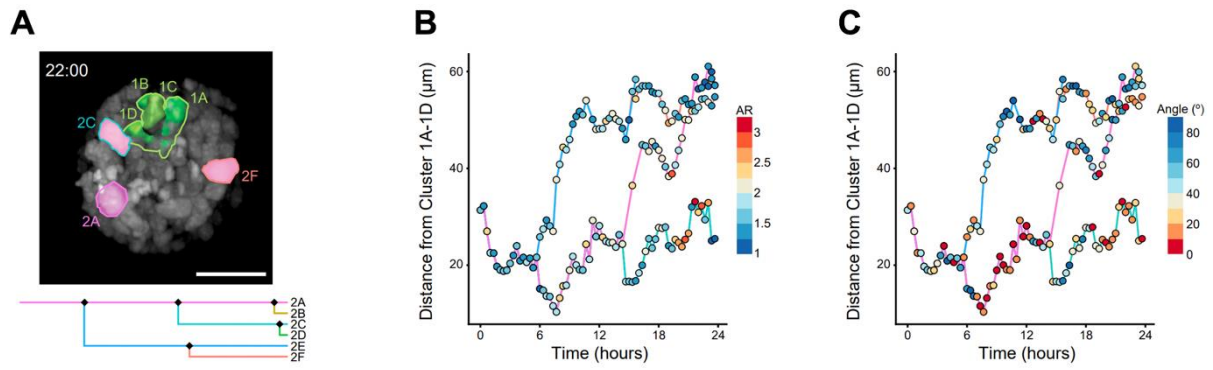
Figure 4.14: EPI cells adopt a cell shape and arrangement determined by their environment instead of their lineage. Figure adapted from (Ichikawa et al., 2022). Data produced jointly with Dimitri Fabrèges and Takafumi Ichikawa. Sample collection performed by Takafumi Ichikawa and Hui Ting Zhang. Data analysis pipeline constructed by Dimitri Fabrèges and Takafumi Ichikawa. Manual segmentation of identified cells, cell tracking, data analysis, and data visualisation performed by Hui Ting Zhang. Figure prepared by Hui Ting Zhang.

(A) EPI cells from the lineage shown in Figure 4.13D (labelled 1A—1D, filled in green) and separate lineage (labelled 2A, 2C, and 2F, filled in pink). Cells 1A—1D remained clustered throughout the time period analysed. Cell 2C (filled in pink, outlined in turquoise) is close in space to cell cluster 1A—1D, while its sisters 2A and 2F (filled in pink, outlined in magenta and coral respectively) are not.

(B, C) Change in distance from cell cluster 1A—1D over time in cells 2A, 2C, and 2F. Changes in aspect ratio (AR) **(B)** and alignment **(C)** over time in these cells are shown by colour.

Scale bar = 50 μm.
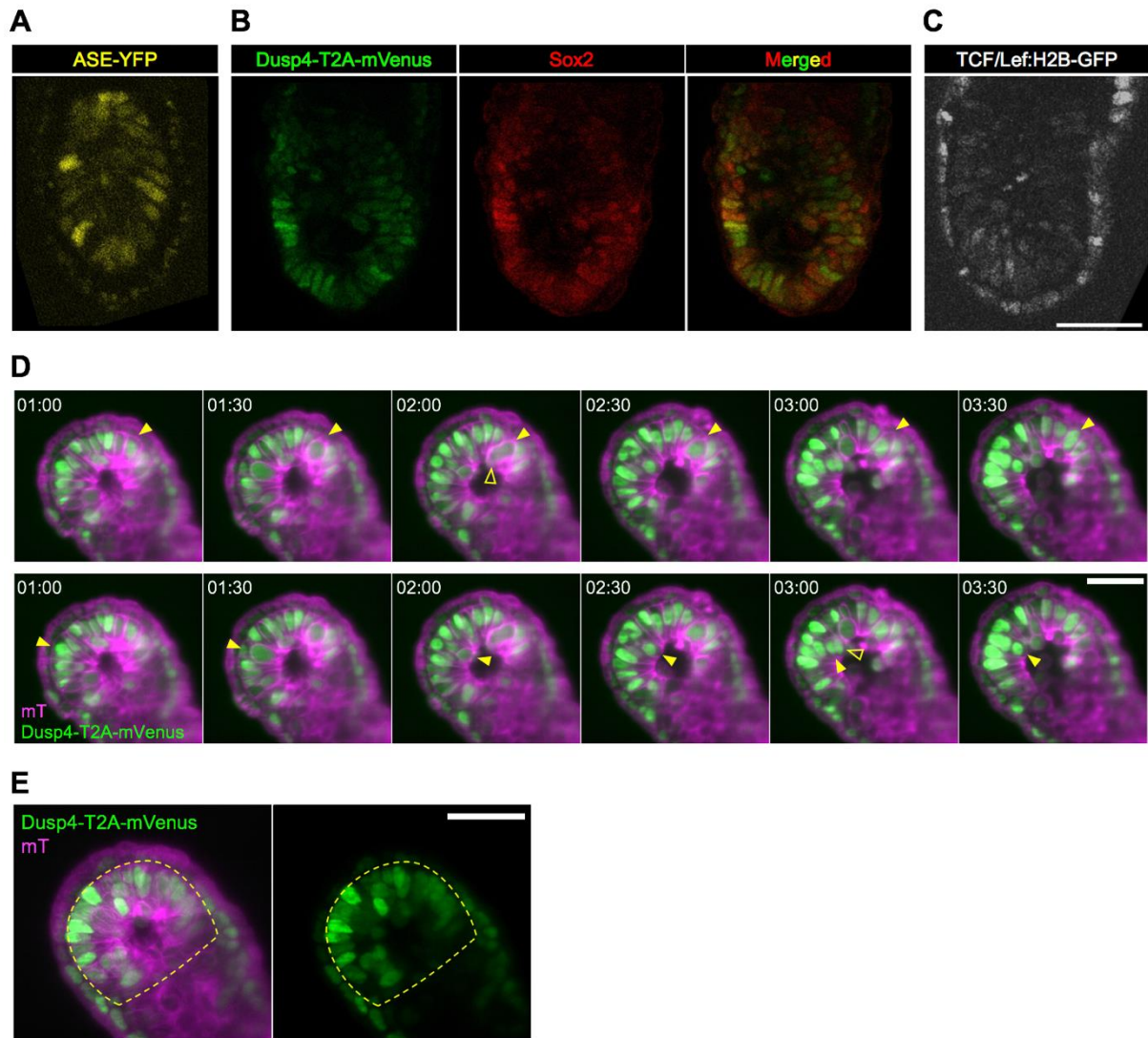
Figure 4.15: Cell-to-cell heterogeneity and spatial gradients in gene expression and signalling pathway activation across the peri-implantation EPI.

(A—C) Immunofluorescence images of cell-to-cell heterogeneity in signalling activity in the Nodal (A), FGF (B), and Wnt (C) signalling pathways, as well as gene expression (B), in *in utero*-developed E6.5 embryos. ASE-YFP, Dusp4-T2A-mVenus, and TCF/Lef:H2B-GFP expression are used as a readout for Nodal, FGF, and Wnt signalling pathway activation respectively. Embryos are additionally stained for in (B).

(D) Time-lapse images of a Dusp4-T2A-mVenus;mT embryo recovered at E5.25 and cultured and imaged *ex vivo* for short term. The solid yellow arrowheads indicate individual cells through mitotic events, and the open yellow arrowheads indicate their sister cells, which move out of frame in the *z*-axis after division.

(E) A frame of the embryo in (D). The yellow dashed line indicates the EPI tissue domain. ExE is present to the lower right, with the distal tip of the egg cylinder to the upper left.

Time = hours:minutes. Scale bar = 50 µm.

IMPACTS OF EXTRA-EMBRYONIC TISSUES ON EPIBLAST MORPHOGENESIS

The 3D-geec system has allowed unprecedented access to the mouse peri-implantation epiblast. In addition, it has also revealed the impact that extra-embryonic tissues, namely the polar trophectoderm (pTE) and its descendant the extraembryonic ectoderm (ExE), has on the development of the epiblast. We had previously shown that the invagination of the pTE after tension release was necessary for further egg cylinder development (**Figure 4.3b**; see also (Ichikawa et al., 2022). I wanted to identify mechanisms through which development of the pTE could facilitate development of the embryonic tissues.

Development of the extraembryonic ectoderm is necessary for growth and patterning of the epiblast

I cultured *in utero*-developed embryos recovered at E4.5 with and without mTE excision to study the effects of pTE invagination on the EPI (**Figure 4.16A**). In mTE- embryos, i.e. embryos cultured according to the normal 3D-geec protocol with mTE excision, the pTE was able to invaginate and develop into the ExE. In contrast, in mTE+ embryos, i.e. embryos cultured with mTE intact, the pTE remained highly stretched and a single cell layer, as expected from our previous experiments (**Figure 4.1C, 4.3**; see also (Ichikawa et al., 2022). I found that in mTE- embryos, both EPI and ExE cell numbers are higher than those in mTE+ embryos ($P = 0.0462$ and 0.0535 respectively) (**Figure 4.16B, 4.16C**). This indicated that pTE growth and morphogenesis into the ExE promoted proliferation in the EPI.

Next, I investigated how the ExE could promote EPI growth. It is known that signalling between extra-embryonic and embryonic tissues is instrumental during *in utero* development (Brennan et al., 2001b; Goldin and Papaioannou, 2003; Wilson and Hemmati-Brivanlou, 1995; Winnier et al., 1995; Yang et al., 1998)_. I compared the signalling landscape in mTE- and mTE+ embryos with respect to three signalling pathways known to be active in the mouse peri-implantation embryo, Nodal, BMP, and FGF (**Figure 4.17, 4.18**). I used the expression of Id1, A_7-Venus, and Dusp4-T2A-mVenus as reporters for these signalling pathways respectively.
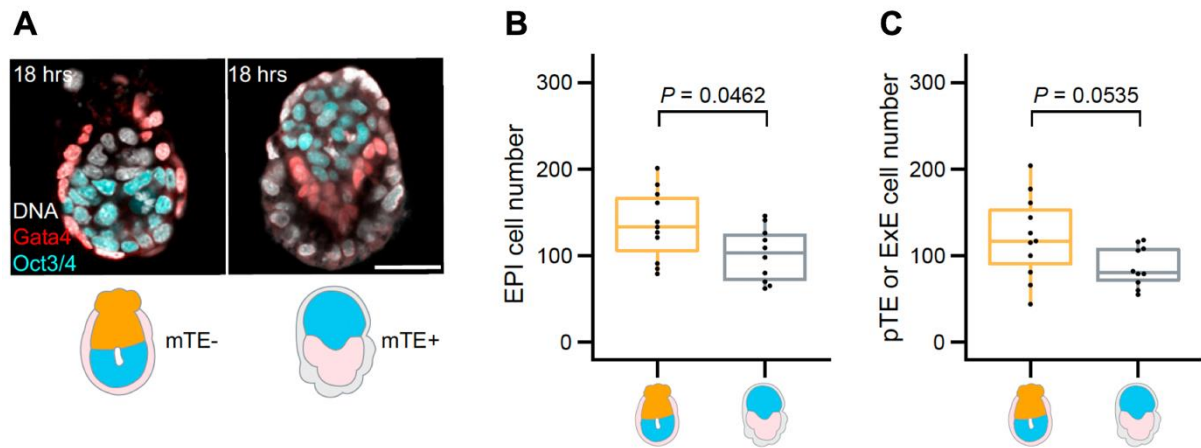
Figure 4.16: pTE invagination and growth facilitates development of the EPI. Figure adapted from (Ichikawa et al., 2022). Data produced jointly with Takafumi Ichikawa. Sample collection performed by Takafumi Ichikawa and Hui Ting Zhang. Image analysis, cell counting, data analysis, and data visualisation performed by Hui Ting Zhang. Figure prepared by Hui Ting Zhang.

(A) Immunofluorescence images of representative 3D-geec embryos after 18 hours of culture, with (left panels) or without (right panels) pTE invagination and development. Embryos are stained for Gata4$^+$ VE, Oct3/4$^+$ EPI, and DNA.

(B, C) Comparison of EPI (B) and pTE or ExE (C) cell numbers in 3D-geec embryos after 18 hours of culture, with or without pTE invagination and development. P = 0.0462 (B) and 0.0535 (C). n = 19 (mTE- embryos), 23 (mTE+ embryos).

Scale bar = 50 μm.

A

in utero | ex vivo

E4.5 | E5.0

DNA
Gata4
Oct3/4

High
Low

A₇-venus

B

in utero | ex vivo

E4.5 | E5.0

DNA
Gata4
Oct3/4

Id1

Low High

C

Proximal

Distal

Centre 60% of
epiblast cells

(%)

Id1^{high} cell/total cell

P D   P D   P D
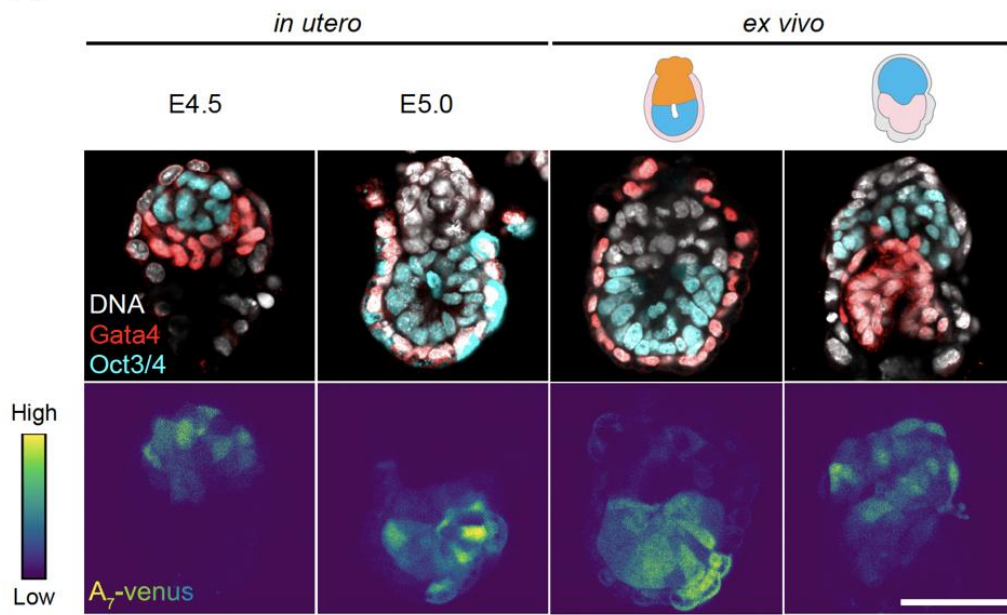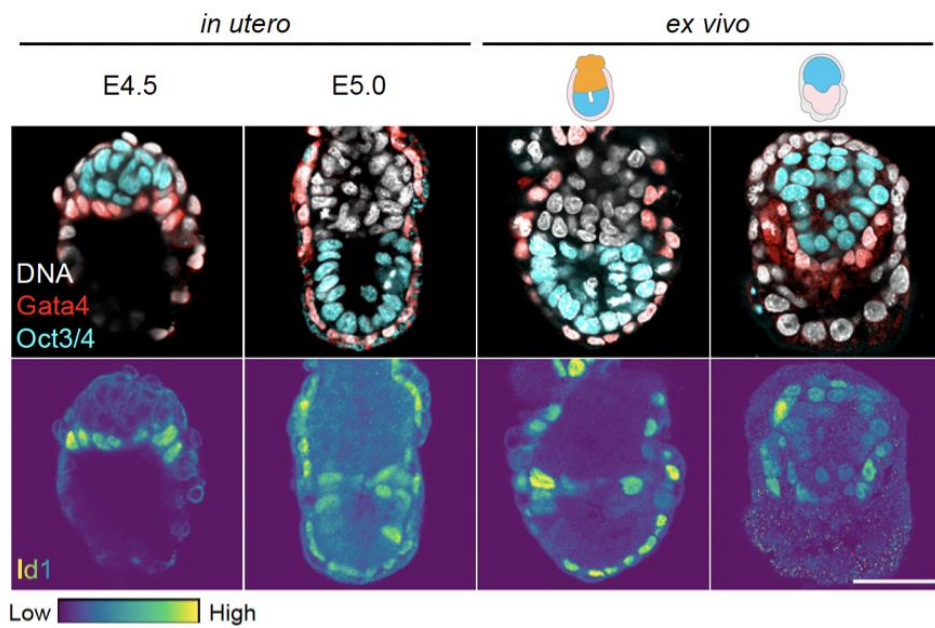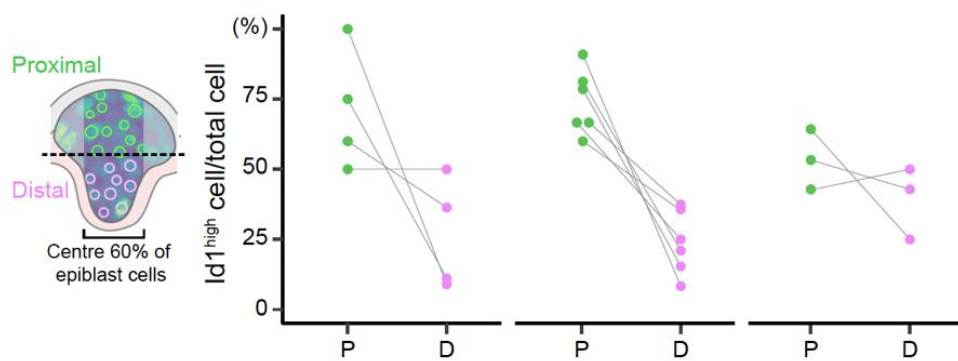
(Legends on next page)

Figure 4.17: Nodal and BMP signalling activity does not depend on ExE development. Figure adapted from (Ichikawa et al., 2022). Data produced jointly with Takafumi Ichikawa. Sample collection performed by Takafumi Ichikawa and Hui Ting Zhang. Image analysis, data analysis, and data visualisation performed by Hui Ting Zhang. Figure prepared by Hui Ting Zhang.

(A) Immunofluorescence images showing representative *in utero*-developed embryos at E4.5 and E5.0, as well as mTE- and mTE+ *ex vivo*-cultured embryos. Upper panels show cell lineages, while lower panels show Nodal signalling activity. Embryos are stained for Gata4$^+$ VE, Oct3/4$^+$ EPI, and DNA, and A$_7$-Venus expression is used as a readout for Nodal signalling pathway activation. $n = 3$, 8, 2, and 3 embryos.

(B) Immunofluorescence images showing representative *in utero*-developed embryos at E4.5 and E5.0, as well as mTE- and mTE+ *ex vivo*-cultured embryos. Upper panels show cell lineages, while lower panels show BMP signalling activity. Embryos are stained for Gata4$^+$ VE, Oct3/4$^+$ EPI, and DNA, and Id1 expression is used as a readout for BMP signalling pathway activation. $n = 4$, 16, 10, and 14 embryos.

(C) Quantification of the Id1 expression gradient in the EPI. The centre 60% of the EPI tissue at an equatorial slice is taken, and the percentages of Id1^{high} cells in the proximal (pTE or ExE-adjacent) half (green) versus in the distal half (magenta) are calculated. Measurements from the same embryo are linked by a black line segment. $n = 4$, 6, and 3 embryos.

Scale bars = 50 μm.

A

in utero | *ex vivo*

E4.5 | E5.0

DNA
Gata4
Oct3/4

Dusp4-
T2A-mVenus

Low ▮ High

B

Proximal

Distal

Centre 60% of
epiblast cells

Dusp4^high cell/total cell (%)

75
50
25
0

P D   P D   P D

C

270°

180° 0°

Linear ROI 90°

Proximal

Distal

Measure Dusp4-T2A-mVenus
and Hoechst intensities radially
with rotating linear ROI

↓

Average Dusp4:Hoechst intensity ratios
for each linear ROI

↓

Plot deviations of intensity ratios
from mean as function of angle

Distal Proximal

0   360

D

no TE/ExE | with remnant TE/ExE

DNA
Gata4
Oct3/4

Dusp4-
T2A-mVenus

Deviation

Distal Proximal

1.5
1.0
0.5
0
-0.5

1.5
1.0
0.5
0
-0.5

0 90 180 270 360   0 90 180 270 360
Angle (°)   Angle (°)

(Legends on next page)

90

Figure 4.18: FGF signalling activity is disrupted in embryos lacking ExE. Figure adapted from (Ichikawa et al., 2022). Data produced jointly with Takafumi Ichikawa. Sample collection performed by Takafumi Ichikawa and Hui Ting Zhang. Image analysis, data analysis, and data visualisation performed by Hui Ting Zhang. Figure prepared by Hui Ting Zhang.

(A) Immunofluorescence images showing representative *in utero*-developed embryos at E4.5 and E5.0, as well as mTE- and mTE+ *ex vivo*-cultured embryos. Upper panels show cell lineages, while lower panels show FGF signalling activity. Embryos are stained for Gata4$^+$ VE, Oct3/4$^+$ EPI, and DNA, and Dusp4-T2A-mVenus expression is used as a readout for FGF signalling pathway activation. $n = 4, 5, 6$, and 6 embryos.

(B) Quantification of the Dusp4-T2A-mVenus expression gradient in the EPI. The centre 60% of the EPI tissue at an equatorial slice is taken, and the percentages of Dusp4^{high} cells in the proximal (pTE or ExE-adjacent) half (green) versus in the distal half (magenta) are calculated. Measurements from the same embryo are linked by a black line segment. $n = 3, 3$, and 5 embryos.

(C) Schematic of how FGF signalling activity, as reported by Dusp4-T2A-mVenus expression, was quantified in embryos after immunosurgery. For the protocol of immunosurgery itself, see Ichikawa et al., 2022 for a full description.

(D) Quantification of FGF signalling in the EPI of embryos cultured for 18 hours after immunosurgery to remove all (left panels) or only some (right panels) TE cells. Upper panels show cell lineages, while lower panels show FGF signalling activity. Embryos are stained for Gata4$^+$ VE, Oct3/4$^+$ EPI, and DNA, and Dusp4-T2A-mVenus expression is used as a readout for FGF signalling pathway activation. $n = 8, 3$.

Scale bars = 50 µm.

I found that Nodal and BMP signalling activity are consistent between mTE- and mTE+ embryos. Specifically, Nodal signalling activity is heterogeneous within the EPI in both mTE- and mTE+ cells, with no region of the EPI exhibiting higher signalling activity overall (**Figure 4.17A**), whereas Id1 expression is high in EPI cells adjacent to ExE and pTE (**Figure 4.17B, 4.17C**). In contrast, FGF signalling activity shows both heterogeneity within the EPI, as well as a proximal-distal gradient in in utero-developed embryos and mTE- embryos (**Figure 4.18A**); in mTE+ embryos, heterogeneity remains, but the proximal-distal gradient is disrupted (**Figure 4.18B**). I experimentally removed all or some TE cells from blastocysts via immunosurgery to lyse outer cells (Ichikawa et al., 2022), and confirmed that embryos lacking TE show no local enrichment of FGF signalling activity, while embryos with remnant pTE cells post-immunosurgery recapitulated the proximal-distal gradient (**Figure 4.18C, 4.18D**). From these findings, I concluded that ExE formation is required to induce specific signalling landscapes in the EPI.

The extraembryonic ectoderm-epiblast tissue boundary potentiates pro-amniotic cavity formation

The ExE forms a sharp boundary with the EPI. This boundary differs from the one between the EPI and the PrE/VE in that it lacks Collagen IV (Ichikawa et al., 2022); as Collagen IV enables integrin-mediated adhesion between EPI cells and VE cells, the Collagen IV-free ExE-EPI boundary may possess different mechanical properties. I noticed that the formation of the pro-amniotic cavity often involved a few disparate potential nucleation sites forming transiently, before resolving into a single cavity, and in *in utero*-developed embryos, this cavity often formed at the ExE-EPI interface (67%, $n = 24$ out of 36 embryos) (**Figure 4.19A, 4.19B**).

Together with colleagues and collaborators, I investigated the potential role the ExE-EPI boundary may play in pro-amniotic cavity formation and EPI morphogenesis (see (Ichikawa et al., 2022). In brief, we modelled the formation of the pro-amniotic cavity using the theory of heterogeneous nucleation, where "an external wall or an impurity provides an additional interface for newly forming droplets" (Ichikawa et al., 2022); we hypothesised that "the neighboring ExE tissue provides an interface with properties facilitating lumen formation, analogous to heterogeneous nucleation" (Ichikawa et al., 2022).

Testing our hypothesis, we found that 3D-geec embryos with the ExE-EPI boundary were able to form a single pro-amniotic cavity robustly (90%, $n = 38$ out of 42 embryos), whereas embryos without this boundary, and even with comparable EPI cell numbers, formed one or more rosettes but failed to resolve them into a single cavity (**Figure 4.19B**). Indeed, live-imaging of 3D-geec embryos showed that rosette and subsequent pro-amniotic cavity formation occurred at the ExE-EPI boundary, with the nascent pro-amniotic cavity resembling a lumen forming and expanding via heterogeneous nucleation on a surface (Duclut et al., 2019; Ichikawa et al., 2022) (**Figure 4.19C**). From these findings, we concluded that "[pro-amniotic cavity] formation is more stable at the [ExE-EPI] tissue boundary, illustrating a mechanical contribution of the ExE in shaping the EPI" (Ichikawa et al., 2022).

In summary, 3D-geec allowed unprecedented insight into the growth, morphogenesis, and interaction of embryonic and extra-embryonic tissues in the peri-implantation mouse epiblast, including the ability to study the dynamics of developmental processes at both cell- and tissue-scale in real time.
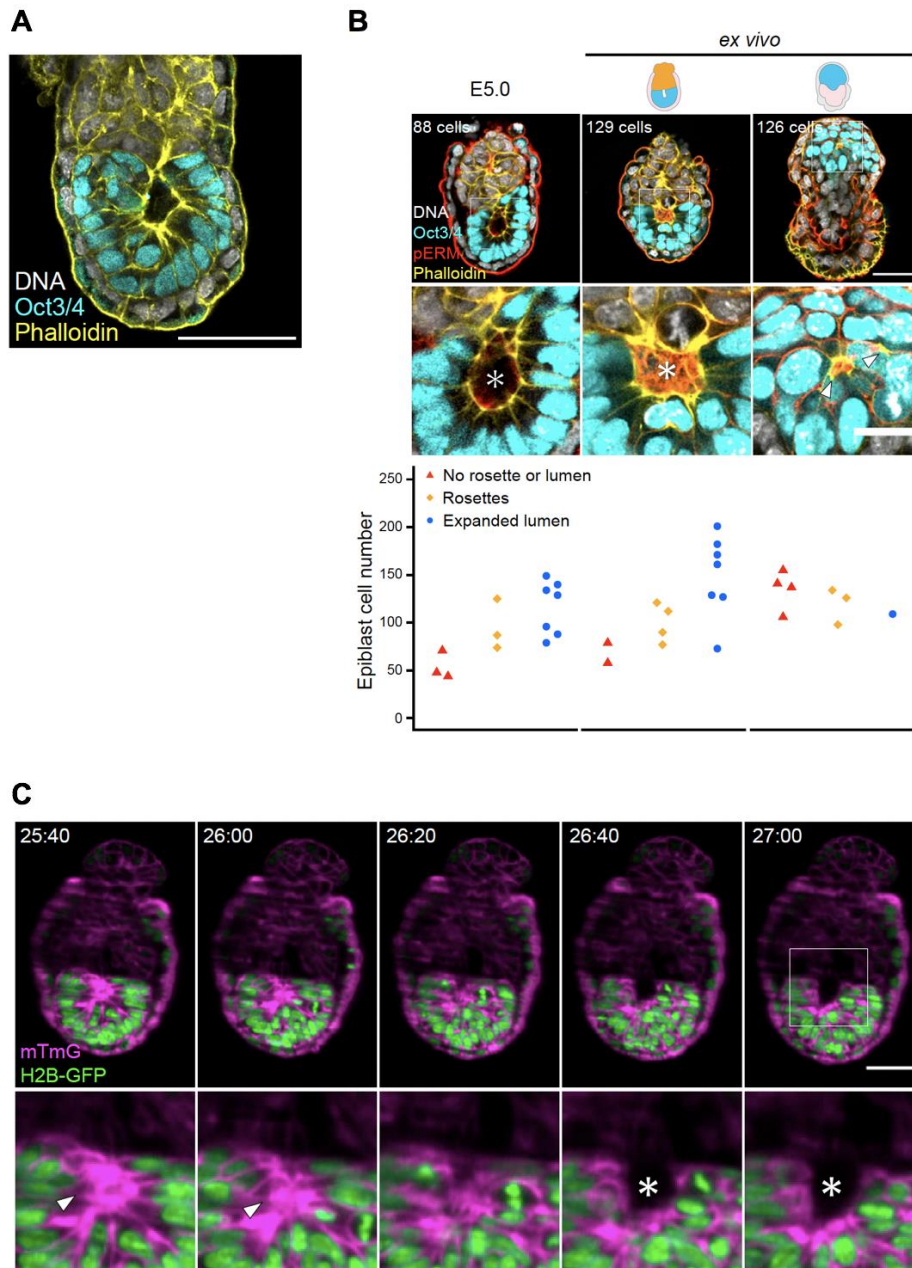
Figure 4.19: The ExE-EPI boundary facilitates robust pro-amniotic cavity formation. Figure adapted from (Ichikawa et al., 2022). Data produced jointly with Takafumi Ichikawa. Sample collection performed by Takafumi Ichikawa and Hui Ting Zhang. Image analysis, cell counting, data analysis, and data visualisation performed by Hui Ting Zhang. Figure prepared by Takafumi Ichikawa and Hui Ting Zhang.

(A) Immunofluorescence image showing representative *in utero*-developed embryo at E5.0 showing pro-amniotic cavity formation at the ExE-EPI boundary. The embryo was stained for Oct3/4[+] EPI, actin, and DNA.

(Legends continue on next page)

(B) Immunofluorescence images (upper panels) of a representative in utero-developed embryo at E5.0, and *ex vivo*-cultured embryos with and without ExE, and dot plots (lower panels) of pro-amniotic cavity formation success. Embryos were stained for Oct3/4$^+$ EPI, actin, pERM, and DNA. The white asterisk indicates the pro-amniotic cavity.

(C) Time-lapse images of a representative H2B-GFP;mT embryo showing the formation of a rosette in the EPI followed by the nascent pro-amniotic cavity. The white arrowhead indicates the rosette, and the white asterisk indicates the pro-amniotic cavity.

Time = hours:minutes. Scale bars = 50 µm.

REGULATION OF SIZE DURING PERI-IMPLANTATION DEVELOPMENT

The mouse embryo exhibits impressive capability to tolerate and compensate for size deviations. Previous work has identified the peri-implantation period to be the time frame during which compensatory growth occurs to regulate embryo body size. Past investigations into this interesting phenomenon have been limited by the relative difficulty in studying the peri-implantation period; now, with a recently-established *ex vivo* culture system for embryos of this developmental stage, I aim to revisit this topic and dissect how mouse embryos could sense size deviations and compensate for them. Naturally, the openness of the question of size regulation means that this will be an extensive project; in this section, I present my preliminary findings as a contribution towards laying the groundwork for ongoing and future investigations.

Establishment of a protocol to study compensatory growth in vivo

Past studies on compensatory growth utilised embryos at different sizes, manipulated by different experimental procedures, and analysed using different methodology (summarised in **Table 1.1**), making it difficult to conduct direct comparisons between them. I aimed to establish a protocol of embryo transfer and recapitulate the reported findings regarding the time period during which compensatory growth takes place and the mechanisms by which it can be accomplished.

Some of the earliest studies generated under-sized embryos by drug treatment or by rupturing one blastomere during early pre-implantation development; others dissociated blastomeres and re-aggregated them in specific ratios to achieve more precise control over size manipulations and to avoid non-physiological effects in the remaining blastomeres caused by unnatural cell death (**Table 1.1**). I followed the latter approach and dissociated and reaggregated blastomeres. I performed this procedure at the 4-cell stage to minimise the amount of time embryos spend in *in vitro* culture, while still ensuring that embryos do not begin compaction (**Figure 1.3**). I also restricted the current study to only double-sized and under-sized embryos, due to multiple factors: past studies reported that embryos with more drastic size deviations had a lower success rate in implantation and development (Petters and Mettus, 1984; Rands, 1986a; Rossant, 1976).

Previous studies also differed in the time when manipulated embryos were transferred into foster mothers for *in vivo* development. While multiple studies used "compacted morulae", or E2.5 embryos, (Buehr and McLaren, 1974; Lewis and Rossant, 1982; Rossant, 1976), and in theory one would expect that a shorter time spend in *ex vivo* culture would lead to a higher survival rate and better development, I found that many embryos had yet to complete compaction by the time of embryo transfer on E2.5. Embryo transfer surgeries were found empirically to yield better results if performed sooner after pseudopregnancy induction and plug detection, which limited the amount of time manipulated embryos could remain in culture before transfer on E2.5. As the embryos used in these experiments do not have a zona pellucida, poorly-compacted embryos may aggregate with each other during the transfer process and affect both embryo transfer efficiency and the actual size of the embryos upon implantation. Therefore, I chose to transfer embryos at E3.5, which had also been performed previously (Power and Tam, 1993).

Pilot experiments were low in efficiency, often with only half or fewer of the transferred embryos yielding decidua, and a significant delay in post-embryo transfer (pET) development (**Figure 4.20A**). I explored uterine transfers into foster mothers 2.5 days after vaginal plug detection (VP+2.5) instead of the standard oviduct transfers into foster mothers 0.5 days after vaginal plug detection (VP+0.5), as I hypothesised that 1) the uterine environment better matched the developmental stage of the embryos at transfer (E3.5), and 2) the loss of the zona pellucida may impede the embryos' movement through the oviduct and into the uterus. However, recent further experiments showed that uterine transfers did not significantly improve embryo survival rate (**Figure 4.21B**) or total success rate (**Figure 4.21C**), and control (unmanipulated, but with zona pellucida removed) embryos from oviduct and uterine transfers are not significantly different in embryo development in terms of EPI cell number ($P = 0.4559$, $n = 36$ and 15) (**Figure 4.21D**).

One point of note is that, due to a change in animal facility, I used different foster mother strains for the embryo transfer surgeries in the pilot experiments and recent experiments. In the pilot experiments, CD1 foster mothers were used, while current experiments used an F1 hybrid between C57BL/6 and C3H (B6C3F1). I suspected that the change in foster mother strain may explain some of the differences in embryo transfer surgery outcome, although a previous study reported no difference between Crl:CD1(ICR) and C57BL/6 strains (Lamas et al., 2020). Nevertheless, to ensure consistency, I restricted all further experiments and analyses to embryos recovered from B6C3F1 foster mothers.
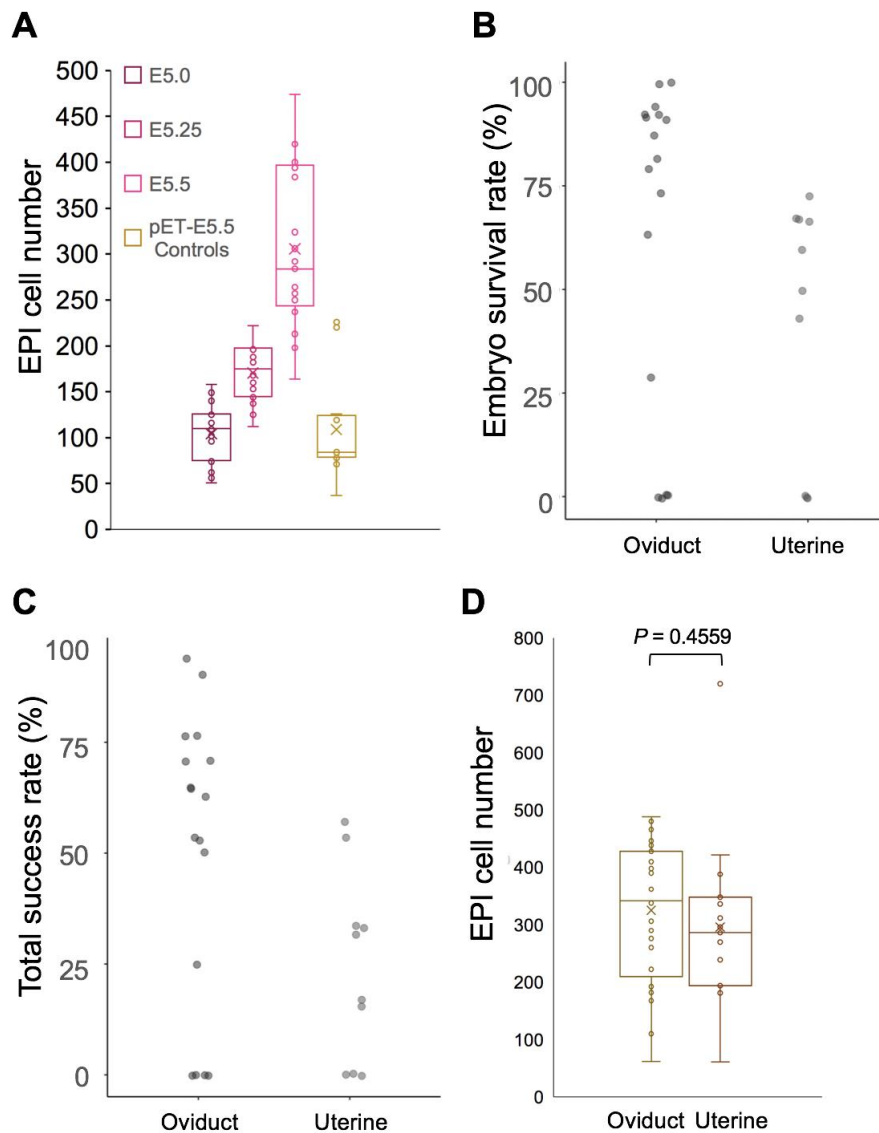
Figure 4.21: Optimisation of the embryo transfer protocol to support *in vivo* development in control pET embryos without size deviations.

(A) Boxplots of EPI cell numbers of *in utero*-developed embryos recovered at E5.0—E5.25, and pET control embryos recovered at pET-E5.5. *n* = 20, 20, 21, and 13.

(B, C) Dot plots of embryo survival rate (B) and total success rate (C) of embryos transferred by oviduct or uterine transfer. Embryo survival rate is defined as the number of embryos recovered divided by the number of decidua observed, and is used as a measure of embryo survival after implantation is initiated. Total success rate is defined as the number of embryos recovered divided by the number of embryos originally transferred into the foster mother, and is used as a measure of efficiency of the transfer protocol. *n* = 17 and 10 litters.

(D) Boxplots of EPI cell numbers of pET control embryos transferred by either oviduct or uterine transfer and recovered at pET-E5.5. *P* = 0.4559, *n* = 36 and 15.

Finally, I noted that due to technical limitations of the time, the majority of prior work was limited in the extent to which their results could be quantitatively analysed. pET embryos had been recovered at differing and irregular time points, and embryo development had been evaluated inconsistently based on volume, mass, or cell number, depending on the study. I elected to use EPI cell number as the primary determinant of embryo development, keeping consistent with methodology established in (Ichikawa et al., 2022), in addition to EPI tissue volume and expression of cell lineage markers. I also decided to use biochemical markers to assess phenomena such as cell proliferation, cell death, and gastrulation onset, instead of gross morphological traits.

In sum, I have established a protocol for manipulating embryo size and evaluating the subsequent *in vivo* development of these embryos (**Figure 4.21**), which is currently in use for ongoing experiments.
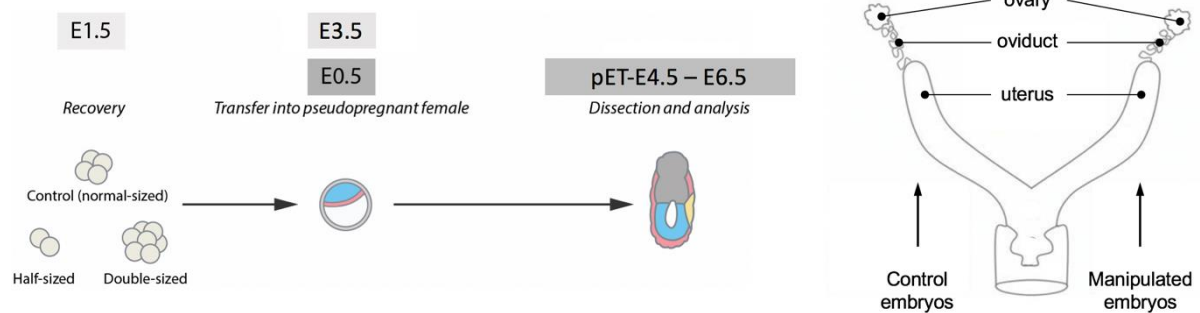
Figure 4.21: A protocol for embryo transfer to study compensatory growth *in vivo*. Post-embryo transfer (pET) days counted based on foster mother plug date, not transferred embryo age. Mouse reproductive tract schematic adapted from **(Gravina et al., 2014)**.

Variability in development of pET embryos necessitates inclusion/exclusion criteria for data analysis

I observed that, compared to *in utero*-developed embryos recovered at specific time points, pET embryos exhibited a great degree of intra- and inter-litter variation (**Figure 4.22**). For example, control pET embryos recovered at pET-E5.5 ranged from 62 to 720 cells in the EPI; in contrast, *in utero*-developed embryos recovered at E5.5 ranged from 164 to 474 cells in the EPI (**Figure 4.22A**). Furthermore, litters differed in mean EPI cell number, as did individual embryos within each litter; one litter, Ovi-7, included control pET embryos with 62 EPI cells as well as with 488 EPI cells, an almost eight-fold difference (**Figure 4.22B**). Some of these embryos clearly fell outside of physiological development, and may represent embryos that will be resorbed by the uterus later in pregnancy (Drews et al., 2020). This necessitated the development of a set of inclusion and exclusion criteria to minimise confounding effects from non-viable embryos.

A first round of exclusion criteria was applied to control pET embryos. Embryos that looked visibly aberrant (e.g. entirely lacking in one lineage) or were damaged during embryo recovery were excluded from analysis; in addition, embryos that had greater than 200% or less than 50% of the expected EPI cell number of embryos recovered at that stage were also excluded (**Figure 4.23A**). I also fitted linear regression lines to the mean EPI cell numbers at each of the six time points from E4.75 to E6.0, allowing the derivation of expected upper and lower bounds based purely on mean control EPI cell number (x_c), so that inclusion/exclusion criteria can still be applied to pET embryos recovered at time points that did not fall within one of these six. At this point, only litters that had two or more control embryos remaining were included for further analysis.

A second round of exclusion criteria was applied to manipulated pET embryos (**Figure 4.23B**). I first calculated the theoretical mean manipulated EPI cell number (x_h or x_d for half-sized and double-sized embryos respectively) one might expect a manipulated pET embryo not undergoing compensatory growth to have, i.e. 50% that of control pET embryos from the same litter for half-sized embryos, and 200% that of control pET embryos from the same litter for double-sized embryos. To account for variation that is present even in *in utero*-developed embryos, I decided to include embryos 2 standard deviations (S.D.s) away from x_h or x_d and exclude embryos that fell outside of this range. To account for embryos undergoing compensation, the upper bound for half-sized embryos and lower bound of double-sized embryos were set as $x_c + 2$ S.D.s or $x_c - 2$ S.D.s respectively.
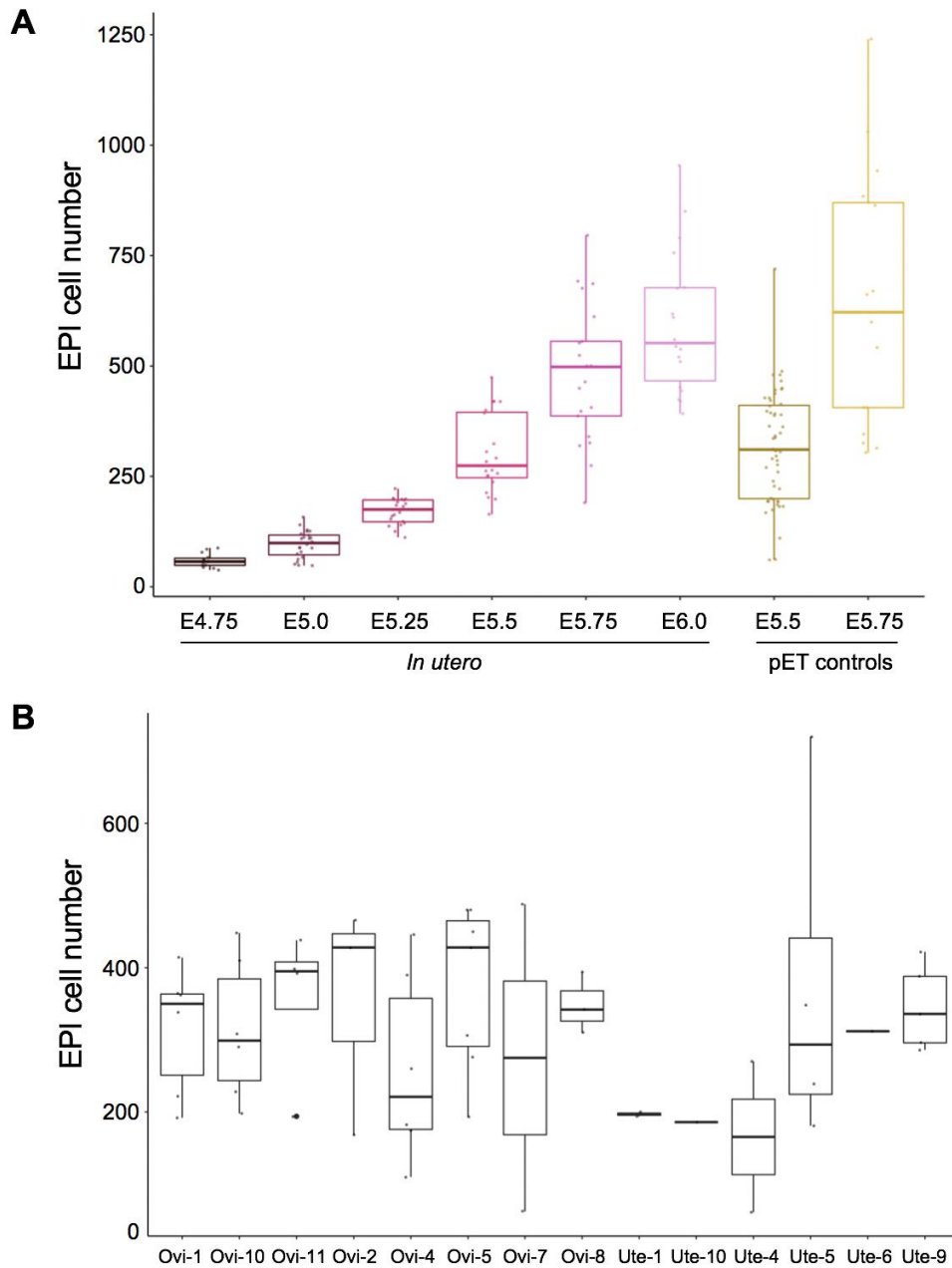
Figure 4.22: pET embryos exhibit higher variability in development than *in utero*-developed embryos.

(A) Boxplots of EPI cell numbers of in utero-developed embryos recovered at E4.75—E6.0, and pET control embryos recovered at pET-E5.5 and pET-E5.75. Embryos were transferred by either oviduct or uterine transfer (pET-E5.5) or only by oviduct transfer (pET-E5.75). $n = 21, 28, 20, 20, 21, 21, 22, 52, 17$.

(B) Boxplots of EPI cell numbers of pET control embryos recovered at pET-E5.5. Embryos were transferred by either oviduct (Ovi) or uterine (Ute) transfer. $n = 6, 6, 4, 3, 6, 7, 2, 3, 2, 1, 2, 4, 5$.

I derived upper and lower bounds for half- and double-sized embryos based on their control littermates as shown in **Table 4.1**:

Manipulation	Bound	Description	Formula based on x_c
Half	Upper	$x_h + 2$ S.D.	$1.4203x_c - 4.0554$
	Lower	$0.5x_c - 2$ S.D.	$0.2898x_c + 2.0277$
Double	Upper	$0.5x_c + 2$ S.D.	$2.8407x_c - 8.1107$
	Lower	$x_d - 2$ S.D.	$0.5797x_c + 4.0554$

Table 4.1: Derivation of upper and lower bounds for half- and double-sized embryos. x_c = mean EPI cell number of control littermates. x_h = theoretical mean EPI cell number of half littermates. x_d = theoretical mean EPI cell number of double littermates.

Using control littermates from the same foster mother accounted for inter-litter variation, which in turn could be caused by variation in maternal uterine environment due to differences in mating time/time of induction of pseudopregnancy, surgery time, or post-surgical recovery. At this point, only "complete" litters with both control and manipulated embryos were used for further analysis.

After the two rounds of inclusion and exclusion, 76 embryos remained from 145 samples, representing a total of 11 litters roughly equally divided between control:half and control:double litters (**Table 4.2**).

Litter	Stage (pET)	Controls	Halfs	Litter	Stage (pET)	Controls	Doubles
Ovi-2	E5.5	3	1	Ovi-10	E5.5	5	1
Ovi-4	E5.5	5	1	Ovi-11	E5.5	4	7
Ovi-5	E5.5	7	2	Ovi-13	E5.75	5	6
Ovi-8	E5.5	3	4	Ovi-14	E5.75	7	2
Ute-5	E5.5	3	1	Ovi-15	E5.75	2	1
Ute-9	E5.5	5	1				

Table 4.2: Remaining samples after inclusion and exclusion criteria have been applied.

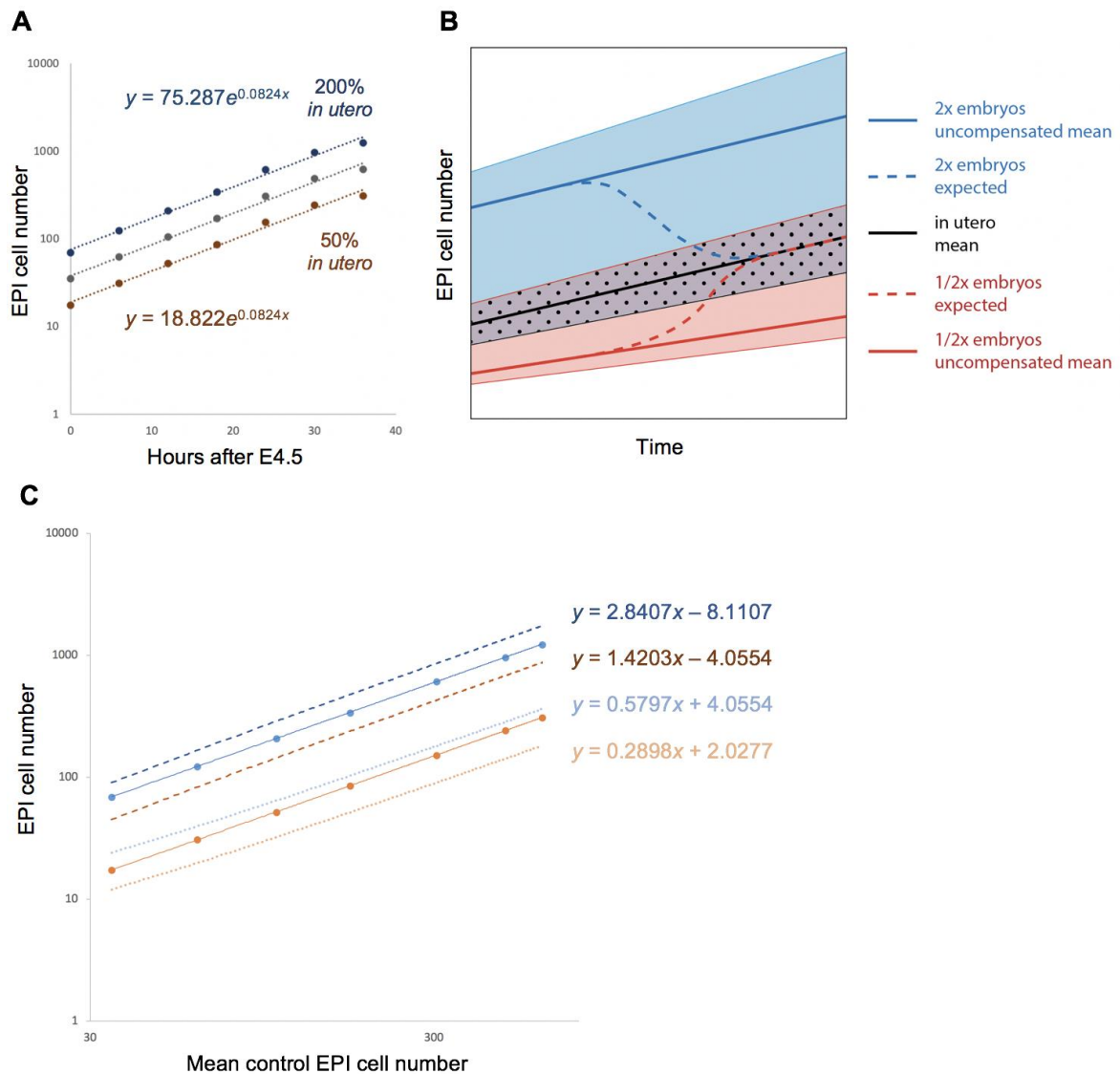
Figure 4.23: A set of inclusion/exclusion criteria for control and manipulated pET embryos.

(A) The derivation of upper and lower bounds for control pET embryos based on time of recovery. A theoretical age for the litter on the whole is calculated from the mean EPI cell number of control littermates, and the corresponding upper and lower bounds are found. Embryos with EPI cell numbers outside of these bounds are excluded. *y*-axis in log scale.

(B) Schematic indicating the derivation of inclusion and exclusion criteria for manipulated pET embryos. Figure adapted from joint unpublished work with Erica van der Maas; figure prepared by Erica van der Maas.

(C) The derivation of upper and lower bounds for manipulated pET embryos based on mean EPI cell number of control littermates. Embryos with EPI cell numbers outside of these bounds are excluded. Axes in log scale.

Compensatory growth occurs to varying degrees in peri-implantation embryos

I first analysed the EPI cell number ratios in half- and double-sized embryos (**Figure 4.24A**). I found that half-sized embryos showed no compensation at pET-E5.5, while double-sized embryos were variable and limited in compensation at pET-E5.5, and, paradoxically, even less compensation at pET-E5.75. Analysis of EPI cell numbers in pooled control and manipulated embryos showed that at pET-E5.5, half embryos had approximately 50% the number of EPI cells as control embryos ($n = 12$ and 24 respectively), and double embryos had approximately 160% that of control embryos ($n = 8$ and 9 respectively). Double embryos at pET-E5.75 had approximately 200% the number of EPI cells as control embryos ($n = 9$ and 14 respectively). Individual litters, and individual embryos within each litter, also displayed varying degrees of compensation in EPI cell number (**Figure 4.24A'**). In addition to EPI cell number, manipulated embryos also showed no consistent or progressive compensation in terms of EPI tissue volume (**Figure 4.24B, 4.24B'**) or pro-amniotic cavity volume (**Figure 4.24D, 4.24D'**).

During my pilot experiments, I had aimed to confirm if compensatory growth indeed took place within the time period reported, i.e. if manipulated embryos reached the same size as control littermates by E6.5. I found that manipulated embryos approached nearly the same EPI cell number as control littermates, indicating that compensatory growth had indeed occurred (**Table 4.2**). However, these experiments had been performed using a different foster mother strain, and these embryos exhibited a delay in development with respect to *in utero*-developed embryos (**Table 4.2, Figure 4.8**). A repeat of these experiments is currently ongoing to verify these results.

Litter	Manipulation	EPI cell number	Control:Manipulated Ratio
EMBL-1	Control	1060	
EMBL-1	Control	1000	1.02
EMBL-1	Double	800	
EMBL-2	Control	680	
EMBL-2	Control	760	*N/A*
EMBL-3	Control	660	
EMBL-3	Half	640	1.08

Table 4.3: Pilot experiments agree with reports that compensatory growth is complete by pET-E6.5.
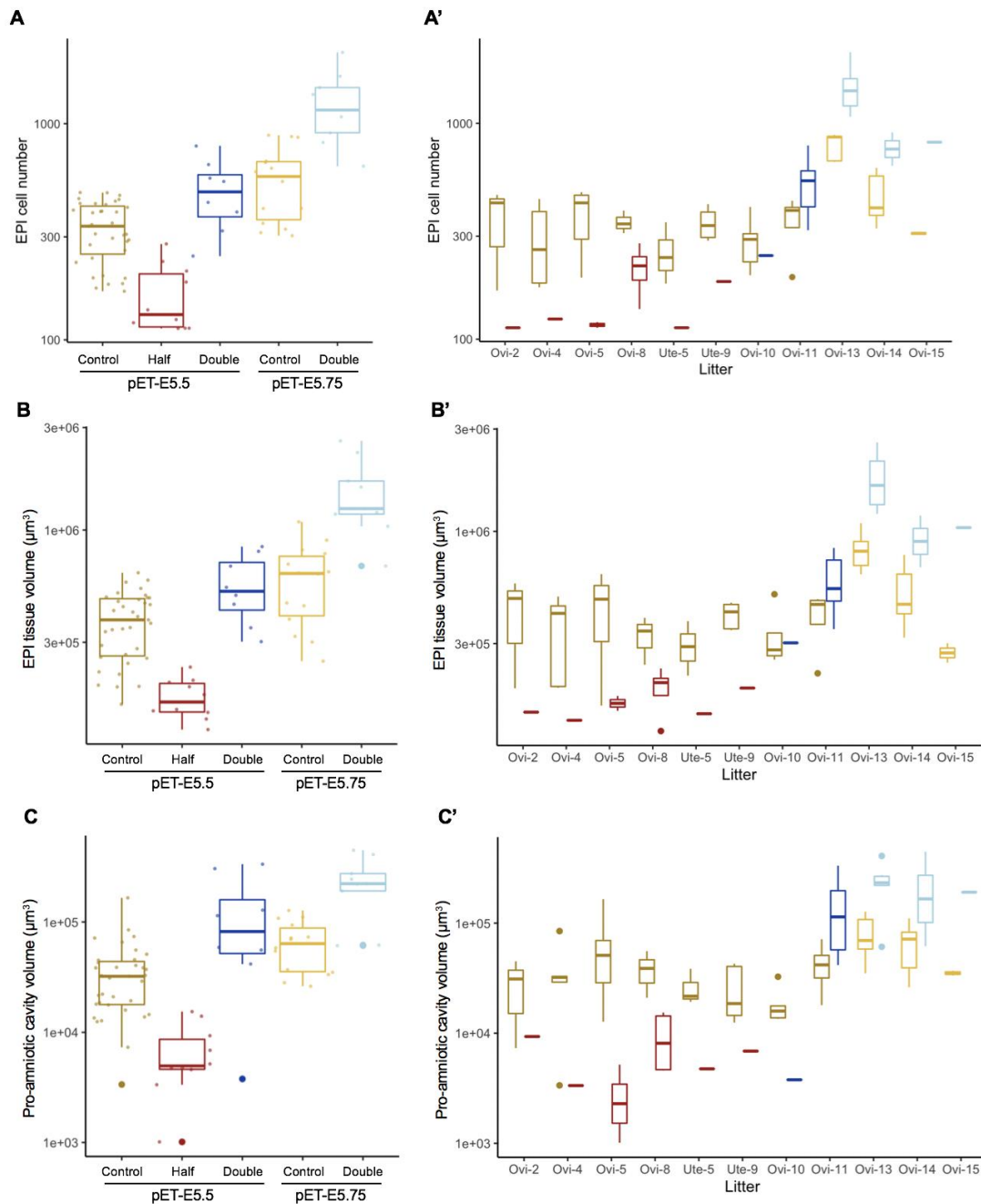
Figure 4.24: Half- and double-sized embryos do not consistently display compensation in EPI cell numbers, EPI tissue volume, or pro-amniotic cavity volume at pET-E5.5 or pET-5.75.

(A, B, C) Boxplots of EPI cell numbers (A), EPI tissue volume (B), and pro-amniotic cavity volume (C) in pooled control pET embryos, half- and double-sized pET embryos at pET-E5.5 and pET-E5.75. *y*-axis in log scale. *n* = 35 (pET-E5.5 Control), 10 (pET-E5.5 Half), 8 (pET-E5.5 Double), 14 (pET-E5.75 Control), and 9 (pET-E5.75 Double) embryos.

(A', B', C') Boxplots of EPI cell numbers (A'), EPI tissue volume (B'), and pro-amniotic cavity volume (C') in control pET embryos, half- and double-sized pET embryos at pET-E5.5 and pET-E5.75. *y*-axis in log scale. *n* = 3, 1, 5, 1, 7, 2, 3, 4, 3, 1, 5, 1, 5, 1, 4, 7, 5, 6, 7, 2, 2, and 1 embryos (see Table 4.2).

Pro-amniotic cavity formation occurs irrespective of epiblast cell number, but is less robust in double-sized embryos

Another surprising observation was that both half- and double-embryos were able to form the pro-amniotic cavity at the same time as their control littermates (**Figure 4.25A, 4.25B**); previous studies had reported delayed pro-amniotic cavity formation in both under- and over-sized embryos (Lewis and Rossant, 1982; Orietti et al., 2020). In pilot experiments, even embryos with very low EPI cell numbers were able to form the pro-amniotic cavity, including in both half-sized and double-sized embryos (**Figure 4.25C**). This finding was also recapitulated in current ongoing experiments. However, I also noted that double embryos occasionally showed non-standard EPI and pro-amniotic cavity morphology, such as masses of un-incorporated EPI cells (**Figure 4.25D**, left panel), or multiple cavities/fissures that could not resolve into a single coherent cavity (**Figure 4.25D**, right panel).

Epiblast cell and tissue parameters correlate more with epiblast cell number than chronological time

Many cell- and tissue-level parameters change during early embryonic development as the embryo undergoes growth and morphogenesis, but it is difficult to know whether it is the passage of time or the change in tissue size that determines these changes, as during normal development, chronological time and tissue size are intrinsically linked. For example, i*n utero*-developed and *ex vivo* cultured embryos exhibit progressive elongation of EPI cells along the apico-basal cell axis during and after formation of the pro-amniotic cavity (**Figure 4.12, 4.13**). I wanted to know if EPI cell elongation was dependent on time or EPI cell number. I compared how EPI cell length varied with chronological time and EPI cell number in *in utero*-developed and pET embryos. While EPI cell length increased with both parameters (**Figure 4.26A, 4.26B**), manipulated pET embryos displayed EPI cell length similar to *in utero* and control pET embryos with similar EPI cell numbers, rather than their littermates (**Figure 4.26B**), was not a cell-autonomous process entirely dependent on chronological time, but could be affected by tissue-scale changes.
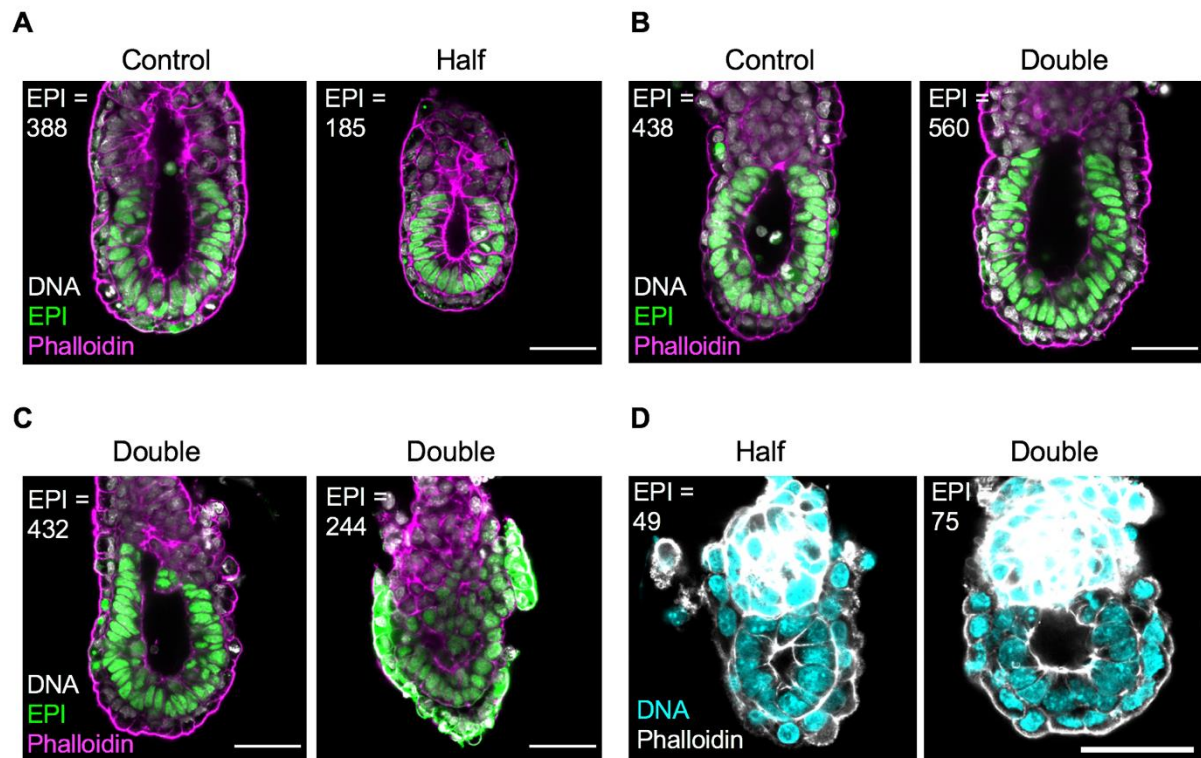
Figure 4.25: Pro-amniotic cavity formation takes place irrespective of EPI cell number, though over-sized embryos exhibit non-standard morphologies.

(A, B) Immunofluorescence image showing representative pET-E5.5 control (**A**, left panel) and half-sized (**A**, right panel) littermates, and pET-E5.5 control (**B**, left panel) and double-sized (**B**, right panel) littermates, with well-formed pro-amniotic cavities. Embryos were stained for Oct3/4[+] EPI, actin, and DNA.

(C) Immunofluorescence image showing two pET-E5.5 double-sized embryos which did not completely recapitulate *in utero* pro-amniotic cavity formation. Embryos were stained for Oct3/4[+] EPI, actin, and DNA.

(D) Immunofluorescence image showing pET-E5.5 half- and double-sized embryos with successful pro-amniotic cavity formation from pilot experiments. Embryos were stained for actin and DNA.

Scale bars = 50 μm.

A

B

Legend (B):
- *In utero*
- pET-E5.5 Control
- pET-E5.5 Double
- pET-E5.5 Half
- pET-E5.75 Control
- pET-E5.75 Double

C

$y = 0.3466x + 18.958$

$y = 4.4827x + 2.1624$

D

E

Legend (E):
- *In utero*
- pET-E5.5 Control
- pET-E5.5 Double
- pET-E5.5 Half
- pET-E5.75 Control
- pET-E5.75 Double

F

$y = 44036e^{0.0769x}$

$y = 1126.2x - 20788$

G

H

Legend (H):
- *In utero*
- pET-E5.5 Control
- pET-E5.5 Double
- pET-E5.5 Half
- pET-E5.75 Control
- pET-E5.75 Double

I

$y = 510.73e^{0.1401x}$

$y = 0.6203x^{1.7987}$

(Legends on next page)

108
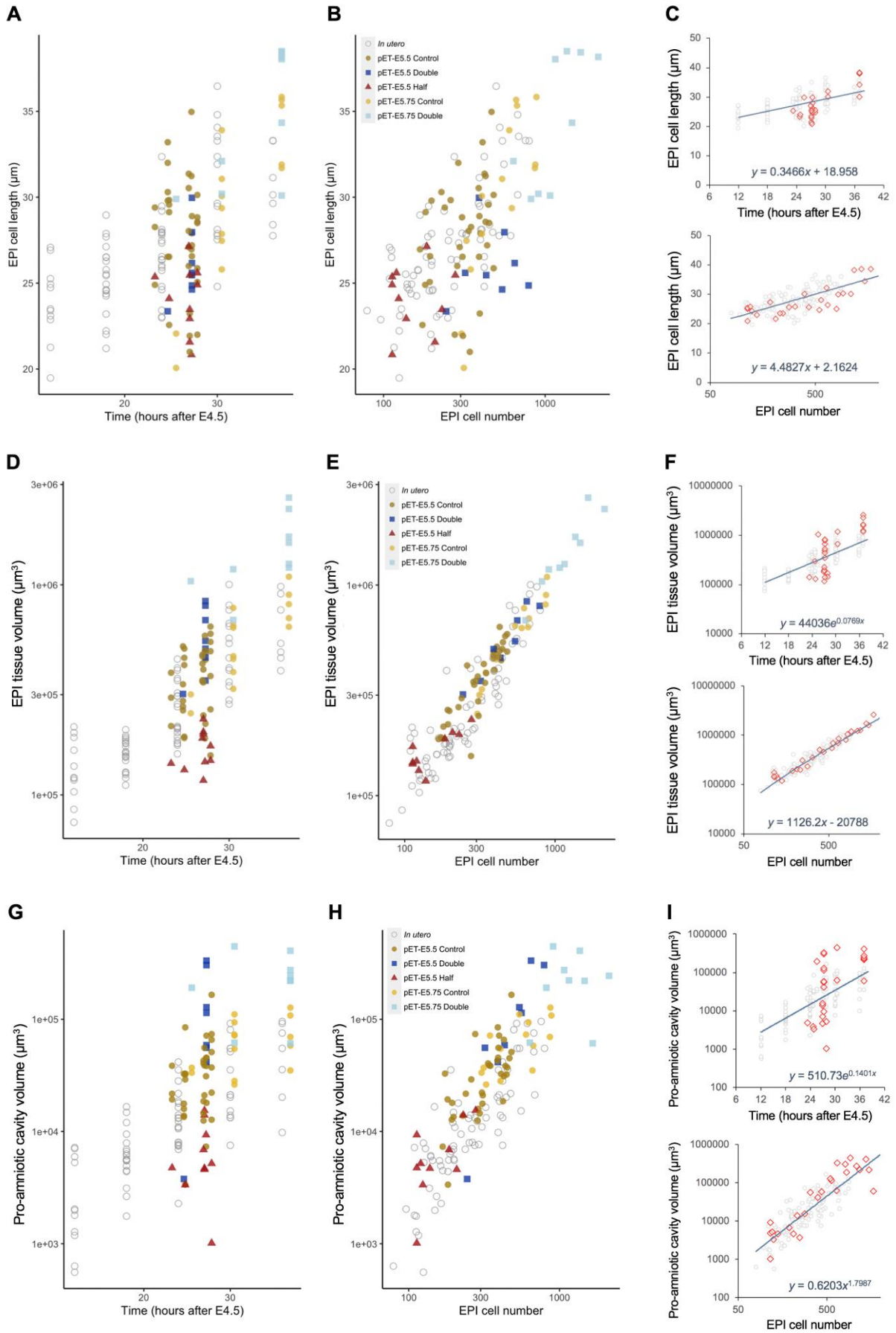
Figure 4.26: EPI cell length, EPI tissue volume, and pro-amniotic cavity volume scale more with epiblast cell number than with chronological age.

(A, B) Scatter plots of EPI cell length against chronological time **(A)** and EPI cell number **(B)** of *in utero*-developed embryos from E5.0 to E6.0 (with embryos without pro-amniotic cavity excluded) and pET embryos from pET-E5.5 to pET-E5.75. n = 11 (E5.0), 20 (E5.25), 21 (E5.5), 14 (E5.75), 7 (E6.0), 35 (pET-E5.5 Control), 8 (pET-E5.5 Double), 10 (pET-E5.5 Half), 14 (pET-E5.75 Control), and 9 (pET-E5.75 Double) embryos.

(C) Analysis of Sum of Squared Residuals (SSR) and Weighted Least Squares (WLS) of manipulated pET embryos when mapped to the regression line calculated from *in utero*-developed and control pET embryos. EPI cell number was log-transformed during calculations for linearity. Upper panel, EPI cell length against chronological time (hours after E4.5), $y = 0.3466x + 18.958$, SSR = 461.18, WLS = 15.61. Lower panel, EPI cell length against EPI cell number, $y = 4.4827x + 2.1624$, SSR = 275.25, WLS = 9.16.

(D, E) Scatter plots of EPI tissue volume against chronological time **(D)** and EPI cell number **(E)** of *in utero*-developed embryos from E5.0 to E6.0 (with embryos without pro-amniotic cavity excluded) and pET embryos from pET-E5.5 to pET-E5.75. n = 11 (E5.0), 20 (E5.25), 21 (E5.5), 14 (E5.75), 7 (E6.0), 35 (pET-E5.5 Control), 8 (pET-E5.5 Double), 10 (pET-E5.5 Half), 14 (pET-E5.75 Control), and 9 (pET-E5.75 Double) embryos.

(F) Analysis of SSR and WLS as in **(C)**. EPI tissue volume and cell number were log-transformed during calculations for linearity. Upper panel, EPI tissue volume against chronological time (hours after E4.5), $y = 44036e^{0.0769x}$, SSR = 14.88, WLS = 1.15. Lower panel, EPI tissue volume against EPI cell number, $y = 1126.2x - 20788$, SSR = 0.84, WLS = 0.067.

(G, H) Scatter plots of pro-amniotic cavity volume against chronological time **(D)** and EPI cell number **(E)** of *in utero*-developed embryos from E5.0 to E6.0 (with embryos without pro-amniotic cavity excluded) and pET embryos from pET-E5.5 to pET-E5.75. n = 11 (E5.0), 20 (E5.25), 21 (E5.5), 14 (E5.75), 7 (E6.0), 35 (pET-E5.5 Control), 8 (pET-E5.5 Double), 10 (pET-E5.5 Half), 14 (pET-E5.75 Control), and 9 (pET-E5.75 Double) embryos.

(I) Analysis of SSR and WLS as in **(C)**. Pro-amniotic cavity volume and cell number were log-transformed during calculations for linearity. Upper panel, pro-amniotic cavity volume against chronological time (hours after E4.5), $y = 510.73e^{0.1401x}$, SSR = 65.49, WLS = 6.44. Lower panel, pro-amniotic cavity volume against EPI cell number, $y = 0.6203x^{1.7987}$, SSR = 17.83, WLS = 1.68s.

I derived a regression line based on pooled *in utero*-developed and control pET embryos for EPI cell length against chronological time (**Figure 4.26C**, upper panel) and EPI cell length against EPI cell number (**Figure 4.26C**, lower panel). Chronological time for each litter of pET embryos was defined based on the mean EPI cell number of the control littermates and the regression line from Figure 4.23A. I compared the Sum of Squared Residuals (SSR) and Weighted Least Squares of the data from the manipulated pET embryos plotted with the two regression lines and found that indeed, both SSR and WLS for manipulated embryos are lower when plotted with the regression line assuming EPI cell number as the predictor ($SSR = 275.25$, $WLS = 15.61$) than that assuming chronological time ($SSR = 461.18$, $WLS = 9.16$), indicating that EPI cell number is a stronger influence on EPI cell length. I performed the same analyses for EPI tissue volume (**Figure 4.26D—F**) and pro-amniotic cavity volume (**Figure 4.26G—I**), and found that while EPI cell number is a stronger predictor of EPI tissue volume and pro-amniotic cavity volume in both cases.

In sum, I have established the protocol for investigating compensatory growth *in vivo*, and have performed experiments to quantitatively characterise this phenomenon. My findings unexpectedly contradicted what had been previously reported, highlighting that this is a topic that still needs much more study. I also conducted a preliminary survey of the cell- and tissue-scale parameters that may be implicated in either size sensing or size regulation. Current ongoing experiments focus on capturing the end of compensatory growth *in vivo*, with a subsequent plan to recover at progressively earlier time points to capture the start of compensatory growth, as well as to increase sample numbers overall to compensate for the increased variability in pET embryo development.

5.DISCUSSION

THE 3D-GEEC SYSTEM

3D-geec is a powerful resource for investigating mouse peri-implantation development. I have shown that 3D-geec does not disrupt the organisation of the egg cylinder, allowing us to recapitulate *in utero* egg cylinder morphogenesis for the first time. I developed a rubric for evaluating embryo development, using parameters independent of chronological time and more quantitative than gross morphology, and applied it to both *in utero*-developed and *ex vivo*-cultured embryos; this facilitated direct comparison between embryos developing under different circumstances. I found that 3D-geec was able to recapitulate *in utero* E4.5 to E6.0 development within 48 hours, and with an efficiency of 49%; at D2, these 3D-geec embryos show physiological lineage differentiation, patterning, tissue organisation, and axis specification. 3D-geec is also compatible with long-term live-imaging by light-sheet microscopy at high spatial and temporal resolutions, allowing the capture of transient events such as pro-amniotic cavity nucleation. The incorporation of a machine-learning based pipeline for image segmentation, analysis, and cell tracking now allows the study of the peri-implantation epiblast (EPI) on the cellular as well as the tissue scale, and gives insight to how the EPI and its surrounding extra-embryonic tissues interact to guide EPI morphogenesis.

The removal of mural trophectoderm during 3D-geec poses a challenge to studying this extra-embryonic lineage

However, one notable feature of 3D-geec is the necessity for mural trophectoderm (mTE) to be removed from the embryo so as to release tension in the trophectoderm (**Figure 4.3, 4.4**; see also Ichikawa et al., 2022). While this procedure is not unique to the 3D-geec system (Bedzhov et al., 2014b), and was shown to be necessary to allow physiological *polar* trophectoderm (pTE) development (and subsequently EPI morphogenesis), it nevertheless does not replicate *in utero* conditions. The mTE *in utero* is crucial for implantation and formation of supportive extra-embryonic tissues including the Reichert's membrane and the placenta (Cross et al., 1994; Müntener and Hsu, 1977; Salamat et al., 1995). It is yet unknown by which mechanism *in utero* embryos resolve the need to release tension in the trophectoderm while maintaining mTE survival and development, though mTE invasion into the uterine tissue may play a role (Ichikawa et al., 2022). A different *ex vivo* peri-implantation culture setup may be necessary to address this question, in conjunction with analysis of *in utero* development of these tissues during and just after implantation.

The maternal uterine environment may contribute towards robust embryo morphogenesis

Another curious observation is that embryos developed *ex vivo*, including through 3D-geec, did not always replicate *in utero* physical dimensions, and showed more developmental variability than *in utero*-developed embryos (**Figure 4.8**; see also (Bedzhov et al., 2014a; Hsu, 1973; Morris et al., 2012b). This may point to the uterine environment shaping the developing embryo during and after implantation. For example, lateral confinement due to pressure exerted by the uterus, as occurs *in utero* but not *ex vivo*, has been proposed to play a role in guiding DVE/AVE establishment at the distal tip of the egg cylinder (Hiramatsu et al., 2013; Matsuo and Hiramatsu, 2016; Ueda et al., 2020). While this hypothesis has been challenged (Bedzhov et al., 2015), and embryos can and do specify the DVE/AVE population successfully *ex vivo*, the rate of doing so (67%) is lower than *in utero*.

Functional redundancy, degeneracy, and regulatory complexity to confer robustness is common to many biological systems, including embryonic development (reviewed in Edelman and Gally, 2001; Félix and Wagner, 2008; Whitacre, 2012). While it is clear that embryos can independently recapitulate development to a remarkable extent when removed from the *in utero* context, it may be that additional input from the uterus, whether physical, mechanical, or biochemical, act to make development more robust. Indeed, no *ex vivo* culture system can recapitulate development to the same efficiency as *in utero* as of yet. Investigations into the interplay between the maternal environment and the embryo have been ongoing for decades (reviewed in Cha et al., 2012; Dey et al., 2004; Matsumoto et al., 2009; Paria et al., 2002). Synthesising findings from studying the embryo both in isolation and *in situ* will be crucial to understanding this highly exciting and complex period of development.

THE PERI-IMPLANTATION EPIBLAST

Using a combination of *in utero*-developed embryos and *ex vivo*-cultured embryos, I was able to study cell dynamics within the peri-implantation mouse epiblast. I observed that EPI cells underwent rapid and extensive changes in cell shape and arrangement, and acquired apico-basal polarity and adopted a pseudostratified epithelial organisation just before and after pro-amniotic cavity formation.

The role of cell- and tissue-scale heterogeneity in the epiblast in development

The EPI tissue is not homogeneous; it exhibits regional differences in terms of geometry and mechanical force (**Figure 4.6**, see also Hiramatsu et al., 2013), transcriptional and signalling activity (**Figure 4.17, 4.18**; see also Introduction; Cheng et al., 2019), and cell behaviour (Mathiah et al., 2020; Snow, 1977), as well as cell-to-cell variability in gene expression and signalling activity (**Figure 4.15**; see also Cheng et al., 2019; Mohammed et al., 2017). While tissue-scale gradients and local signalling centres naturally lend themselves to the idea of positional cues guiding tissue morphogenesis, the biological significance of cell-to-cell variability in the EPI is less intuitive. One reported function of heterogeneity in the EPI is that of maintenance of the EPI, where less-fit cells are eliminated through cell competition (Bowling et al., 2018; Clavería and Torres, 2016; Clavería et al., 2013; Díaz-Díaz et al., 2017; Sancho et al., 2013).

Cell-to-cell heterogeneity has been reported in mouse embryonic stem cells (ESCs), pluripotent cells derived from the ICM of the mouse blastocyst (Chambers et al., 2007), and has been proposed as a mechanism to maintain pluripotency as well as capability for differentiation (Cahan and Daley, 2013). Similarly, heterogeneities in mouse epiblast-derived stem cells (EpiSCs) have been identified and suggested to represent different subpopulations of cells with different responses to signals for lineage specification (Han et al., 2010; Song et al., 2016). In addition, heterogeneities have been found to play a role in the differentiation of blood progenitor cells (Mojtahedi et al., 2016). Given that the heterogeneities I observed in signalling activity and gene expression can occur in parallel with tissue-scale gradients, it is possible that heterogeneities in the peri-implantation EPI act to ensure that lineage specification, cell differentiation, and tissue morphogenesis take place robustly within a complex signalling landscape.

Many questions remain regarding the observation of cell- and tissue-scale heterogeneities in the EPI. For one, how do these heterogeneities arise, and how are they

preserved through rounds of cell division? EPI cells are remarkably mobile given their epithelial nature, and this mobility can be observed from pre-implantation to post-implantation (**Figure 5.1**; see also Gardner and Cockroft, 1998). It has been suggested that the pseudostratified nature of the mouse EPI contributes to this observed cell mobility, where the rounding of mitotic cells leads to transient detachment from the basal lamina, which allows the daughter cells to disperse before re-establishing basal attachment (Gardner and Cockroft, 1998; Thowfeequ et al., 2022). However, as daughter cells inherit the state of the parent cell, this seems to imply that some heterogeneities, at least, are intrinsic to each cell and not affected by their neighbours.
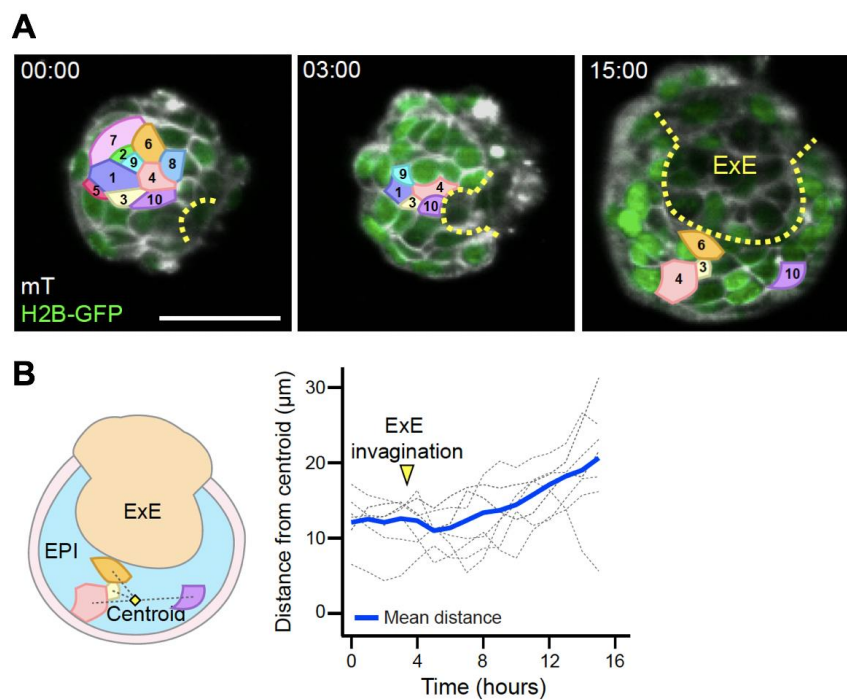
Figure 5.1: Epiblast cells are mobile during peri-implantation development. Figure adapted from (Ichikawa et al., 2022). Sample collection and image analysis performed by Takafumi Ichikawa and Hui Ting Zhang. Cell tracking and data analysis performed by Hui Ting Zhang. Figure prepared by Hui Ting Zhang.

(A) Time-lapse images of a H2B-GFP;mT embryo in 3D-geec, showing 10 cells identified for tracking. The yellow dashed line indicates the ExE-EPI boundary.

(B) The measurement of mean cell distance from centroid of tracked cells over time, as an indicator of cell dispersion.

Time = hours:minutes. Scale bar = 50 μm.

Such a statement assumes that the persistence of heterogeneities truly reflects the underlying dynamics, and is not merely an artefact inherent to the readout system. Fluorescent protein-based reporters can often affect dynamics of protein production and degradation, and may not faithfully report the dynamics of the system under study; attempts to mitigate these effects have included intentionally destabilising the fluorescent protein through the introduction of proteolytic sequences, which may be more relevant for studying heterogeneities in the EPI (Corish and Tyler-Smith, 1999; Li et al., 1998; Parasram et al., 2022; Snapp, 2009). In addition, it may also be necessary to utilise a reporter that would facilitate the tracking of individual cells and their descendants through rounds of cell division and through cell rearrangements, such as Rainbow mice (Tabansky et al., 2013), though this presents additional challenges for using a fluorescent-reporter based system to report on heterogeneities. Taken together, the observation of heterogeneities in EPI cells is exciting, though studying this phenomenon will require further technique development to accurately reflect the dynamics of the system.

Interaction between the epiblast and adjacent extra-embryonic lineages is crucial for embryo development

The interaction between the EPI and adjacent extra-embryonic tissues such as the ExE have been explored in this study, and it was found that development of the ExE was in turn necessary for development of the EPI. Both growth and patterning in the EPI were disrupted in embryos without ExE, suggesting that the ExE acted to guide the morphogenesis of the EPI through different mechanisms. Joint work with colleagues and collaborators provided insight as to how the ExE-EPI boundary is instrumental for robust pro-amniotic cavity formation, analogous to heterogeneous nucleation, while experimental removal of the ExE was observed to disrupt the establishment of the signalling landscape in the EPI. Naturally, the contribution of other extra-embryonic tissues to EPI development should also be studied. It is known that the distal visceral endoderm (DVE) and its descendant, the anterior visceral endoderm (AVE), are crucial for inducing anterior identity in the underlying EPI cells and thus establishing the first embryonic body axis. With 3D-geec now robustly recapitulating this event *ex vivo*, it may be time to revisit the topic of axis establishment, and study the interaction between DVE/AVE and EPI cells during this process.

THE REGULATION OF EMBRYO SIZE

The final part of this study presents preliminary forays into the long-standing question of size regulation in the mouse embryo, though from a hitherto unaddressed angle: does size *regulation* necessarily involve size *sensing*, and if so, how can this be accomplished? Significant attention has been directed towards consolidating disparate experimental strategies and incorporating technological advancements, so as to establish a protocol for quantitatively investigating size regulation *in vivo*. With this protocol, I have attempted to replicate previously-reported findings, and, when discrepancies arise, to address why this could be the case.

Coordination of growth with the commencement of developmental events

Two strategies of ensuring developmental events occur at the correct tissue size can be posited. One involves the maintenance of the normal "schedule" of developmental events, such as the expression of sets of genes, while cell proliferation or death are tuned; the other is directly complementary, where developmental events are accelerated or put on hold until the correct size is attained.

Pilot experiments had found both successful compensation in terms of EPI cell number by post-embryo transfer (pET) E6.5 in both half- and double-sized embryos. Moreover, embryos were able to form pro-amniotic cavities "ahead of schedule" with respect to their EPI cell numbers; embryos already possessed well-formed pro-amniotic cavities by pET-E5.5 even though their EPI cell numbers were much lower than *in utero* counterparts of the same chronological age, and before compensation could be observed (**Figure 4.25D**). These preliminary findings suggested that embryos corrected size deviations through the first strategy – by detecting that they had an "incorrect" EPI cell number upon egg cylinder morphogenesis and correcting for it over 24 hours so that by pET-E6.5, control and manipulated embryos reached comparable cell numbers. However, these findings were in opposition to those from previous studies, which proposed that embryos were able to delay morphogenetic events such as pro-amniotic cavity formation (Orietti et al., 2020) or gastrulation onset (Power and Tam, 1993). It is clear that the question of which strategy is employed during embryonic development is far from being answered.

The time frame of compensatory growth remains yet unclear

While quantitative analysis and interpretation of experimental results are limited by low sample size and high variability, I have nevertheless attempted to draw preliminary conclusions and contrast my findings with published reports. My more recent experiments are in agreement with the observations from my pilot experiments in that compensatory growth, in terms of cell number and tissue volume, has not yet begun at pET-E5.5 for half-sized embryos and is not complete for double-sized embryos (**Figure 4.24**), despite pro-amniotic cavity formation already heaving taken place in all embryos (**Figure 4.25C**). This is also in direct opposition to previous studies (Lewis and Rossant, 1982; Orietti et al., 2020; Power and Tam, 1993; Rands, 1986a). However, I did also observe, at low frequencies, manipulated pET embryos in which pro-amniotic cavity formation was not entirely comparable to *in utero* or control pET embryos. It is possible that manipulated embryos did in fact transiently encounter reported difficulties in pro-amniotic cavity formation (Orietti et al., 2020). Recovering double-sized pET embryos at pET-E5.25 or pET-E5.0 can clarify this discrepancy between my observations and those in previous studies, though the proposed theory that double-sized embryos accomplish size regulation and pro-amniotic cavity formation simultaneously still remains unsubstantiated. On the other hand, recovering half-sized pET embryos later in development will help to pinpoint the start of compensatory growth, which has not yet been observed.

One caveat is that a significant developmental delay in pET embryos was observed in these pilot experiments. In my more recent experiments, I found no such developmental delay; this may be due to a change in experiment location and foster mother strain, though the cause has not been definitively identified (Lamas et al., 2020). While this is a positive outcome in terms of protocol establishment, it does also mean that conclusions drawn from the results of the pilot experiments, as well as comparisons between those results and that of more recent experiments, should be approached with caution. As such, experiments are currently underway to replicate previous findings from the pilot experiments.

Separate mechanisms for size regulation in half- and double-sized embryos

Prior studies have reported different time windows for compensatory growth in under- and over-sized embryos, with the general consensus of over-sized embryos correcting for the size deviation substantially earlier than under-sized embryos, which may or may not involve multiple phases of correction (Rands, 1986b). Size regulation in over-sized embryos can likely be accomplished faster than in under-sized embryos for the simple reason that excess cells only need to be eliminated in over-sized embryos, while under-sized embryos will need time for

production of cellular components, cell proliferation, and tissue growth. There is a necessity to consider under- and over-sized embryos separately, where different principles of size regulation can come into play.

A previous work had reported that double-sized embryos relied on increased apoptosis to eliminate excess cells during early peri-implantation development to achieve both size regulation and morphogenesis (Orietti et al., 2020). I wanted to know if this finding could be replicated, considering that I had not observed compensation yet. I found a high degree of variation in both cell death (**Figure 5.2A**) and cell proliferation (**Figure 5.2B**) in pET-E5.5 embryos. However, while activated caspase-3 staining was very strong in apoptotic vesicles, it was difficult to correlate whether each vesicle arose from one single apoptotic cell, or if several originated from one cell (**Figure 5.2C**). This made it difficult to accurately estimate the *number* of cells undergoing apoptosis. Exploration of other methods to quantify the extent of apoptosis in the EPI is ongoing.

A framework for the sensing of size and time

Inspection of EPI cell and tissue parameters of the uncompensated manipulated embryos revealed that they resembled control or *in utero*-developed embryos of the same EPI cell number, i.e. these parameters may be better correlated with EPI cell number than chronological time (**Figure 4.26**). (Alternatively, as EPI tissue volume is tightly correlated with EPI cell number, these parameters may be determined by *tissue volume*, though it is not possible to conclude definitively which is the functionally-relevant parameter is at this point. To dissect apart this relationship, one would have to experimentally manipulate cell volume without disturbing cell number.) The scaling of cell-level parameters, such as EPI cell length, with EPI cell number is particularly exciting as this may suggest a mechanism for an individual cell to measure the size of the tissue as a whole. In conjunction with a time-determined parameter, e.g. a gene expressed at a specific time, this then suggests a way for cells to detect discrepancies between actual tissue size and expected tissue size at a given chronological time.
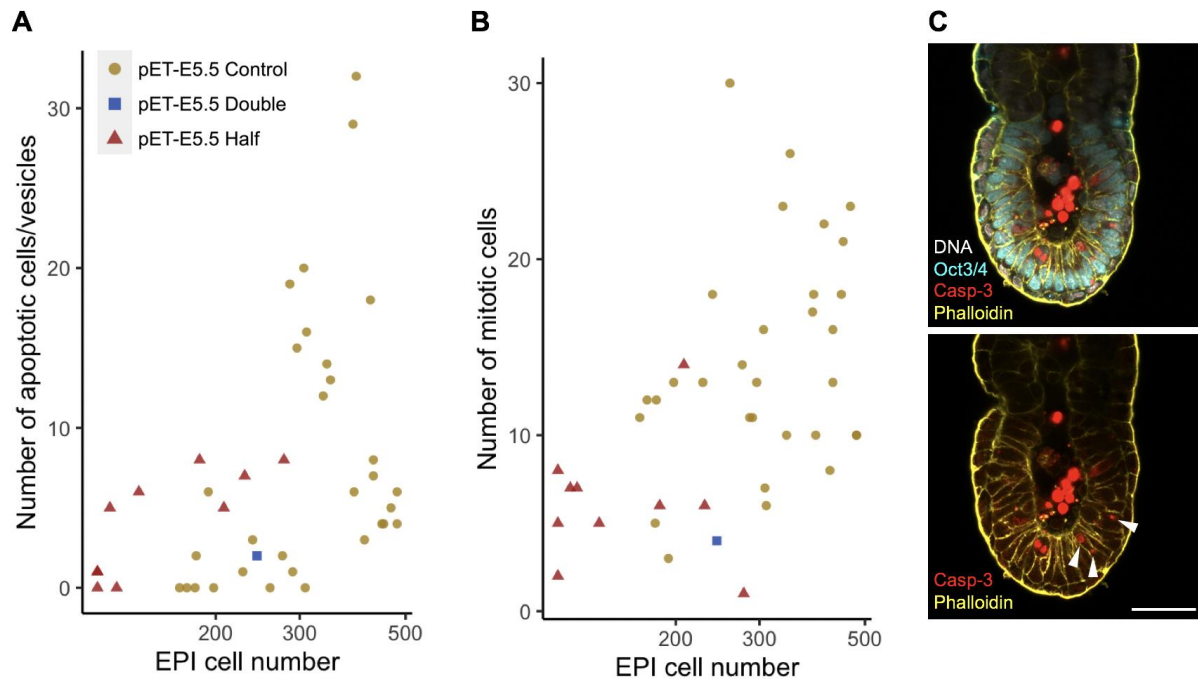
Figure 5.2: The extent of epiblast cells undergoing apoptosis or mitosis is highly variable in post-embryo transfer embryos.

(**A, B**) Scatter plots of apoptotic cells/vesicles (**A**) and mitotic cells (**B**) in the EPI against EPI cell number in pET-E5.5 embryos. $n = 42$ embryos. x-axis in log scale.

(**C**) Immunofluorescence image of a pET-E5.75 control embryo showing strong staining in apoptotic vesicles. Embryos were stained for Oct3/4$^+$ EPI, actin, and DNA, and activated caspase-3 (Casp-3) was used as a readout for apoptotic pathway activation. The solid white arrows indicate apoptotic vesicles.

Scale bar = 50 μm.

Past studies have suggested that the onset of gastrulation incorporates both time and size information in that gastrulation takes place only if a set number of hours have passed since fertilisation *and* if certain cell number is reached – over-sized embryos do not gastrulate "ahead of schedule" (Lewis and Rossant, 1982; Rands, 1986a), and under-sized embryos delay gastrulation until the appropriate cell number is reached (Power and Tam, 1993). Thus, gastrulation onset may function as a checkpoint. Joint work with a student, Adèle Micouin, has found a correlation of gastrulation onset with EPI cell number (**Figure 5.3**), but much more remains to be done to study this potential checkpoint.

Limitations of the current study

The most significant limitation of the study in its current state is low sample number, both in terms of samples collected at a time point, as well as in terms of coverage across different time points. This has been exacerbated by the fact that that data collected during two phases of the study (the pilot phase in EMBL, and the current phase in HI) are not directly comparable, and since time points selected in the current phase were based on data from the pilot phase, they do not cover the landmark morphogenetic events. As such, I have decided to strategically focus on two additional time points – around pET-E6.5, the time of gastrulation onset, and pET-E5.0, the time of pro-amniotic cavity formation – for the next experiments in this phase of the study, and further strategies will be based on data from those experiments.

Refinement of the inclusion/exclusion criteria is likely also necessary. I have assumed that half-sized embryos should never fall below 50% that of their control littermates, i.e. increase in cell number proceeds at the same rate in manipulated and control pET embryos. However, under-sized embryos may be more sensitive and less robust in development overall, and may initially experience a slower rate of growth before compensatory growth programmes kick in. This has not yet been characterised. The second exclusion criteria (for eliminating too-small manipulated embryos) may therefore exclude what I speculated were aberrant embryos that will never develop to term, but these embryos may simply represent part of the natural pathway of compensation. To safeguard against this possibility, I have still acquired images from and analysed these embryos, so that in the future, if different inclusion/exclusion criteria are set, this embryos can be included again in analyses.
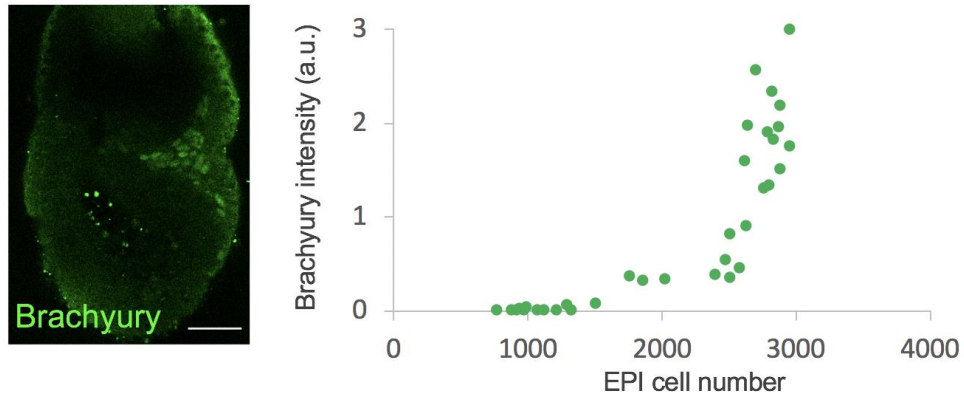
Figure 5.3: Gastrulation onset, as reported by Brachyury expression, correlates with EPI cell number. Data produced jointly with Adèle Micouin. Sample collection, image analysis, and figure preparation by Adèle Micouin. *In utero*-developed embryos at E6.5 were stained for Brachyury expression (left panel); this staining was normalised against DAPI staining to obtain Brachyury intensity (right panel). n = 34 embryos.

Scale bar = 50 μm.

As discussed above, the ability to assess the degree of cell proliferation and cell death from fixed and immunostained samples is limited. Past studies dealing with apoptosis in the mouse embryo using activated caspase-3 as a marker measured presence/absence of immunostaining signal, made qualitative statements about immunostaining signal, or measured the area of the immunostaining signal on one z-slice without drawing conclusions about number of cells. Volume of immunostaining signal may be a suitable metric in my case. However, fixed samples cannot always capture such transient processes as cell division and death, and with limited sample numbers I run the risk of under-sampling. An alternative would be to live-image and track single cells to collect data on cell cycle length, proportion of actively cycling cells, proportion of dying cells, and spatial distribution of these cells on a cellular scale. This second approach still requires further optimisation of methodology, and likely relies on size regulation being recapitulated in *ex vivo* culture systems, an assumption that is yet to be confirmed.

One last point to note is that the current study is restricted to studying what changes occur in the EPI. A natural extension of the study would be to also investigate size compensation in other cell lineages, although a past study found no difference in rate of compensation between EPI and VE (Lewis and Rossant, 1982). Nevertheless, a more quantitative analysis can be performed, to rule out any differences in extent or dynamics of compensation in cell number or tissue volume.

6.PERSPECTIVES AND CONCLUSION

FUTURE PERSPECTIVES

Bridging pre- and peri-implantation ex vivo culture systems

At the beginning of this study, robust *ex vivo* culture systems have been established for pre-implantation and post-implantation rodent embryos, with similar systems being developed for other mammalian species (Biswas and Hyun, 2021; Hickford et al., 2008; Krisher, 2012; Ozolinš, 2019; Petters and Wells, 1993; Vejlsted et al., 2006). Pre-implantation mammalian embryo culture, especially in the murine context, had been optimised for parameters such as temperature, chemical composition, and oxygenation over decades (reviewed in Behringer, 2014; Gardner and Truong, 2019; Nielsen and Ali, 2010; Vajta et al., 2010). Through these efforts, *ex vivo* culture of mouse embryos up to the blastocyst stage is now a routine methodology used in the laboratory, capable of faithfully recapitulating pre-implantation development while being compatible with experimental manipulations, chemical perturbations, and live-imaging at high spatial and temporal resolutions. Similarly, a long history of optimisation, bolstered by recent advances in culture and manipulation methodology for post-implantation rodent embryos, have enabled the study of morphogenetic events over long term with single-cell resolution (Aguilera-Castrejon et al., 2021; Ichikawa et al., 2013; McDole et al., 2018; Migeotte et al., 2010; Miura and Mishina, 2003; New, 1978; New et al., 1973; Nowotschin et al., 2019; Quinlan et al., 2008; Srinivas et al., 2004; Tam and Snow, 1980; Trichas et al., 2011), approaching what can be achieved with pre-implantation embryos. The hitherto lack of such *ex vivo* culture systems for *peri*-implantation development had forced an artificial separation between pre- and post-implantation development, and it was not possible to study process that were continuous through implantation, even though many such processes, such as the specification of the distal visceral endoderm/anterior visceral endoderm (DVE/AVE) (Takaoka et al., 2006, 2011, 2017), or the morphogenesis of the polar trophectoderm (pTE) into the extraembryonic ectoderm (ExE) (Christodoulou et al., 2019; Ichikawa et al., 2022), are integral to the development of the embryo.

3D-geec is a powerful resource that provides unprecedented access to the peri-implantation mouse embryo. However, a true continuous *ex vivo* culture system from pre-implantation to post-implantation has yet to be achieved. Notably, 3D-geec begins with E4.5 embryos; when E3.5 blastocysts cultured to E4.5 *ex vivo* are used for 3D-geec, efficiency of egg cylinder formation was drastically lower (Ichikawa et al., 2022), and it was noted that these E3.5 + 24hrs embryos were distinct from E4.5 embryos in physical dimensions, cell numbers within and between lineages, and gene expression. This suggests that the maternal uterine

environment contributes towards blastocyst maturation prior to implantation in manner(s) that are insufficiently recapitulated by *ex vivo* pre-implantation culture systems.

As mentioned previously in the Discussions, I observed that the transient nature of cell division and cell death events led to high noise in mitotic and apoptotic frequency data collected from fixed samples; in addition, the lack of a robust marker for early apoptosis made the quantitative analysis of extent of apoptosis non-trivial. While current trials are underway to find volume- or intensity- based readouts that are less subjective, I pointed out the necessity for live-imaging and tracking the behaviour of individual cells or subpopulations over time. The need to recover embryos at pre-implantation stages for size manipulations necessarily causes an incompatibility with the current 3D-geec protocol, and a preliminary trial using embryos cultured *ex vivo* from E1.5 to E4.5 in KSOM followed by 3D-geec yielded no successful egg cylinders at D2 ($n = 9$ embryos).

Current workarounds include transiently transferring manipulated embryos into foster mothers and recovering them at pET-E4.5, but such a convoluted protocol may lead to sample loss and adversely impact development of embryos. Establishing a culture system that supports blastocyst maturation *ex vivo* will be instrumental for this study. In the long term, a protocol that truly allows culture, observation, and manipulation of the same from pre- to post-implantation, while no doubt ambitious, will bring benefits to the field of mammalian embryology as a whole.

Verifying ex vivo findings in the in utero context

Following from the above, it is clear that despite the significant advancements made over the past years, *ex vivo* culture of embryos still falls short in recapitulating *in utero* development in full. Apart from the lack of continuity in culture, where each culture system only allows access to the embryo for a window of time, *ex vivo*-cultured embryos often exhibit developmental delays and variable morphologies from *in utero*-developed counterparts, and in these culture systems, not all lineages derived from the embryo, or present around the embryo *in utero* to support its development, are preserved (Bedzhov et al., 2014a; Hsu, 1973; Ichikawa et al., 2022; Morris et al., 2012a). Most importantly, embryos cultured past implantation *ex vivo* cannot be easily assessed for success of development. *Ex vivo*-cultured pre-implantation embryos can be placed back into an *in vivo* context through embryo transfer, allowed to develop to term, and the animals assessed for viability, fertility, and other aspects. This is not yet possible for peri- and post-implantation embryos. Thus, we cannot be sure that developmental

outcomes observed in *ex vivo* cultured embryos necessarily reflect *in utero* development. This then necessitates more rigorous and extensive parallel studies *in vivo* to confirm conclusions based on *ex vivo* experiments.

While it is possible to recover *in utero*-developed embryos at fixed time points and analyse these, this precludes the following of phenomena through time, and information about the dynamics of developmental processes is lost. Therefore, another approach has been to study development completely *in situ*. *In vivo* imaging technology, utilising modalities such as light microscopy, optical coherence tomography (OCT), or ultrasound, has been applied in a variety of developmental biology contexts across different species (reviewed in Gregg and Butcher, 2012). However, studying mouse peri- and post-implantation development *in situ* requires both high depth of field and high resolution. Recently, intravital imaging has been demonstrated in both pre- and post-implantation embryos, where the introduction of an imaging window in the abdomen of the mother allowed visualisation, through light microscopy or OCT, of the reproductive tract and the embryos within (Huang et al., 2020; Wang and Larina, 2021). Future work to bring the imaging time frame towards early peri-implantation should shed light on developmental processes as they occur in utero, as well as how faithfully *ex vivo* culture systems recapitulate them.

Size regulation in other biological systems

The question of size regulation is not exclusive to the mouse embryo, or indeed, to embryo development in general, or even to animals (Horiguchi and Tsukaya, 2011). The control of organ size during organogenesis (Harrison, 1924; Stanger et al., 2007) or regeneration (Bucher et al., 1951; Fausto et al., 2006; Moolten and Bucher, 1967; Muller et al., 1999) has been pursued in many contexts to understand how organisms maintain an optimal proportionality of body parts (Gokhale and Shingleton, 2015; Harrison, 1924; Lui and Baron, 2011; Lupu et al., 2001; Verheyden and Sun, 2008). On the other hand, a loss of size regulation capacity is common to many pathologies (Lui and Baron, 2011), ranging from developmental abnormalities such as over- and under-growth (Eggermann, 2010; Lui et al., 2008; Pilia et al., 1996), to uncontrolled cell proliferation and tissue growth in cancer.

In comparing size regulation across different systems, one must be cautious about over-generalisation. The individual context of each system must be carefully considered – do these systems exist in relative independence or isolation? Or, alternatively, are they subject to influences such as physical constraints imposed by rigid tissues, or biochemical or signalling

gradients from a local source? In addition, the "end-goal" of size regulation must also be considered, as this can determine which factors play the dominant role in controlling size regulation: do these systems only need to maintain a set size at the end of a period of development, or does the rate at which they reach this set size also need to be tightly controlled? Nevertheless, it is likely that principles of size regulation, derived from studying the mouse embryo, can be extended to other systems, especially those relatively self-contained, or those which exhibit a need to coordinate growth with timed events instead of simply limiting growth. *Vice versa*, findings from other systems may shed light on how size regulation is achieved during development.

CONCLUDING REMARKS

In this thesis, I have presented my contributions towards the establishment of a robust *ex vivo* culture system for peri-implantation mouse embryos, which supports physiological growth and patterning of the egg cylinder, and is compatible with setups for light-sheet live-imaging, photomanipulation, and perturbation. In addition, I have discussed the new insights we have gained regarding peri-implantation morphogenesis of the epiblast tissue, revealing that it is a highly dynamic tissue subject to a complex signalling landscape set up by internal heterogeneities and external interactions with extra-embryonic tissues. The increased accessibility of the peri-implantation stage of development brought about by this *ex vivo* culture system has led me to return to the long-standing open question of size regulation, as this period of development was identified as the time frame during which compensatory growth to correct for size deviations takes place. My preliminary results have shown that this interesting and complex question is far from resolved, and much remains to be done to identify mechanisms by which embryos can sense and correct for size deviations.

It is my hope that the 3D-geec system can be utilised by other researchers studying this exciting period of development. In parallel, I hope that my efforts to establish a robust protocol and my initial experiments on size regulation have laid a foundation and provided directions for future investigations. My experiments and findings so far have only cemented my belief that this is a highly intriguing phenomenon, rich in theoretical and practical challenges, a large part of which is yet to be explored. Further work on this topic will no doubt be rewarding, and I look forward to the new findings that will come.

REFERENCES

Aguilera-Castrejon, A., Oldak, B., Shani, T., Ghanem, N., Itzkovich, C., Slomovich, S., Tarazi, S., Bayerl, J., Chugaeva, V., Ayyash, M., et al. (2021). Ex utero mouse embryogenesis from pre-gastrulation to late organogenesis. Nature *593*, 119–124. https://doi.org/10.1038/s41586-021-03416-3.

Alarcón, V.B., and Marikawa, Y. (2005). Unbiased contribution of the first two blastomeres to mouse blastocyst development. Mol. Reprod. Dev. *72*, 354–361. https://doi.org/10.1002/mrd.20353.

Anani, S., Bhat, S., Honma-Yamanaka, N., Krawchuk, D., and Yamanaka, Y. (2014). Initiation of Hippo signaling is linked to polarity rather than to cell position in the pre-implantation mouse embryo. Development *141*, 2813–2824. https://doi.org/10.1242/dev.107276.

Antczak, M., and Van Blerkom, J. (1997). Oocyte influences on early development: the regulatory proteins leptin and STAT3 are polarized in mouse and human oocytes and differentially distributed within the cells of the preimplantation stage embryo. Mol. Hum. Reprod. *3*, 1067–1086. .

Arnold, S.J., and Robertson, E.J. (2009). Making a commitment: cell lineage allocation and axis patterning in the early mouse embryo. Nat Rev Mol Cell Biol *10*, 91–103. https://doi.org/10.1038/nrm2618.

Arora, R., Fries, A., Oelerich, K., Marchuk, K., Sabeur, K., Giudice, L.C., and Laird, D.J. (2016). Insights from imaging the implanting embryo and the uterine environment in three dimensions. Development *143*, 4749–4754. https://doi.org/10.1242/dev.144386.

Artus, J., and Chazaud, C. (2014). A close look at the mammalian blastocyst: epiblast and primitive endoderm formation. Cell. Mol. Life Sci. *71*, 3327–3338. https://doi.org/10.1007/s00018-014-1630-3.

Austin, C.R. (1961). The mammalian egg. The Mammalian Egg.

Bedzhov, I., Leung, C.Y., Bialecka, M., and Zernicka-Goetz, M. (2014a). In vitro culture of mouse blastocysts beyond the implantation stages. Nat Protoc *9*, 2732–2739. https://doi.org/10.1038/nprot.2014.186.

Bedzhov, I., Leung, C.Y., Bialecka, M., and Zernicka-Goetz, M. (2014b). In vitro culture of mouse blastocysts beyond the implantation stages. Nature Protocols *9*, 2732–2739. https://doi.org/10.1038/nprot.2014.186.

Bedzhov, I., Bialecka, M., Zielinska, A., Kosalka, J., Antonica, F., Thompson, A.J., Franze, K., and Zernicka-Goetz, M. (2015). Development of the anterior-posterior axis is a self-organizing process in the absence of maternal cues in the mouse embryo. Cell Res *25*, 1368–1371. https://doi.org/10.1038/cr.2015.104.

Behringer, R. (2014). Manipulating the mouse embryo: a laboratory manual (Cold Spring Harbor, New York: Cold Spring Harbor Laboratory Press).

Biswas, D., and Hyun, S.H. (2021). Supplementation of fetal bovine serum increased the quality of in vitro fertilized porcine embryo. J Adv Vet Anim Res *8*, 589–596. https://doi.org/10.5455/javar.2021.h549.

Bowling, S., Di Gregorio, A., Sancho, M., Pozzi, S., Aarts, M., Signore, M., D. Schneider, M., Martinez-Barbera, J.P., Gil, J., and Rodríguez, T.A. (2018). P53 and mTOR signalling determine fitness selection through cell competition during early mouse embryonic development. Nat Commun *9*. https://doi.org/10.1038/s41467-018-04167-y.

Brennan, J., Lu, C.C., Norris, D.P., Rodriguez, T.A., Beddington, R.S.P., and Robertson, E.J. (2001a). Nodal signalling in the epiblast patterns the early mouse embryo. Nature *411*, 965–969. https://doi.org/10.1038/35082103.

Brennan, J., Lu, C.C., Norris, D.P., Rodriguez, T.A., Beddington, R.S., and Robertson, E.J. (2001b). Nodal signalling in the epiblast patterns the early mouse embryo. Nature *411*, 965–969. https://doi.org/10.1038/35082103.

Bucher, N.L.R., Scott, J.F., and Aub, J.C. (1951). Regeneration of the liver in parabiotic rats. Cancer Res *11*, 457–465. .

Buehr, M., and McLaren, A. (1974). Size regulation in chimaeric mouse embryos. Development *31*, 229–234. .

Bulletti, C., and de Ziegler, D. (2005). Uterine contractility and embryo implantation. Current Opinion in Obstetrics and Gynecology *17*, 265–276. https://doi.org/10.1097/01.gco.0000169104.85128.0e.

Cahan, P., and Daley, G.Q. (2013). Origins and implications of pluripotent stem cell variability and heterogeneity. Nat Rev Mol Cell Biol *14*, 357–368. https://doi.org/10.1038/nrm3584.

Carson, D.D., Bagchi, I., Dey, S.K., Enders, A.C., Fazleabas, A.T., Lessey, B.A., and Yoshinaga, K. (2000). Embryo implantation. Dev Biol *223*, 217–237. https://doi.org/10.1006/dbio.2000.9767.

Cha, J., Sun, X., and Dey, S.K. (2012). Mechanisms of implantation: strategies for successful pregnancy. Nature Medicine *18*, nm.3012. https://doi.org/10.1038/nm.3012.

Chambers, I., Silva, J., Colby, D., Nichols, J., Nijmeijer, B., Robertson, M., Vrana, J., Jones, K., Grotewold, L., and Smith, A. (2007). Nanog safeguards pluripotency and mediates germline development. Nature *450*, 1230. https://doi.org/10.1038/nature06403.

Chazaud, C., and Yamanaka, Y. (2016). Lineage specification in the mouse preimplantation embryo. Development *143*, 1063–1074. https://doi.org/10.1242/dev.128314.

Chazaud, C., Yamanaka, Y., Pawson, T., and Rossant, J. (2006). Early lineage segregation between epiblast and primitive endoderm in mouse blastocysts through the Grb2-MAPK pathway. Dev. Cell *10*, 615–624. https://doi.org/10.1016/j.devcel.2006.02.020.

Cheng, S., Pei, Y., He, L., Peng, G., Reinius, B., Tam, P.P.L., Jing, N., and Deng, Q. (2019). Single-Cell RNA-Seq Reveals Cellular Heterogeneity of Pluripotency Transition and X Chromosome Dynamics during Early Mouse Development. Cell Rep *26*, 2593-2607.e3. https://doi.org/10.1016/j.celrep.2019.02.031.

Chisholm, J.C., and Houliston, E. (1987). Cytokeratin filament assembly in the preimplantation mouse embryo. Development *101*, 565–582. .

Christodoulou, N., Kyprianou, C., Weberling, A., Wang, R., Cui, G., Peng, G., Jing, N., and Zernicka-Goetz, M. (2018). Sequential formation and resolution of multiple rosettes drive embryo remodelling after implantation. Nat Cell Biol *20*, 1278–1289. https://doi.org/10.1038/s41556-018-0211-3.

Christodoulou, N., Weberling, A., Strathdee, D., Anderson, K.I., Timpson, P., and Zernicka-Goetz, M. (2019). Morphogenesis of extra-embryonic tissues directs the remodelling of the mouse embryo at implantation. Nat Commun *10*, 3557. https://doi.org/10.1038/s41467-019-11482-5.

Clavería, C., and Torres, M. (2016). Cell Competition: Mechanisms and Physiological Roles. Annu Rev Cell Dev Biol *32*, 411–439. https://doi.org/10.1146/annurev-cellbio-111315-125142.

Clavería, C., Giovinazzo, G., Sierra, R., and Torres, M. (2013). Myc-driven endogenous cell competition in the early mammalian embryo. Nature *500*, 39–44. https://doi.org/10.1038/nature12389.

Cole, R.J. (1967). Cinemicrographic observations on the trophoblast and zona pellucida of the mouse blastocyst. J Embryol Exp Morphol *17*, 481–490. .

Conlon, I., and Raff, M. (1999). Size control in animal development. Cell *96*, 235–244. https://doi.org/10.1016/s0092-8674(00)80563-2.

Copp, A.J. (1979). Interaction between inner cell mass and trophectoderm of the mouse blastocyst. II. The fate of the polar trophectoderm. J Embryol Exp Morphol *51*, 109–120. .

Copp, A.J. (1981). The mechanism of mouse egg-cylinder morphogenesis in vitro. J Embryol Exp Morphol *61*, 277–287. .

Corish, P., and Tyler-Smith, C. (1999). Attenuation of green fluorescent protein half-life in mammalian cells. Protein Eng *12*, 1035–1040. https://doi.org/10.1093/protein/12.12.1035.

Cross, J.C., Werb, Z., and Fisher, S.J. (1994). Implantation and the placenta: key pieces of the development puzzle. Science *266*, 1508–1518. https://doi.org/10.1126/science.7985020.

Dey, S.K., Lim, H., Das, S.K., Reese, J., Paria, B.C., Daikoku, T., and Wang, H. (2004). Molecular cues to implantation. Endocr Rev *25*, 341–373. https://doi.org/10.1210/er.2003-0020.

Díaz-Díaz, C., Manuel, L.F. de, Jimenez-Carretero, D., Montoya, M.C., Clavería, C., and Torres, M. (2017). Pluripotency Surveillance by Myc-Driven Competitive Elimination of Differentiating Cells. Developmental Cell *42*, 585-599.e4. https://doi.org/10.1016/j.devcel.2017.08.011.

Drews, B., Landaverde, L.F., Kühl, A., and Drews, U. (2020). Spontaneous embryo resorption in the mouse is triggered by embryonic apoptosis followed by rapid removal via maternal sterile purulent inflammation. BMC Developmental Biology *20*, 1. https://doi.org/10.1186/s12861-019-0201-0.

Duclut, C., Sarkar, N., Prost, J., and Jülicher, F. (2019). Fluid pumping and active flexoelectricity can promote lumen nucleation in cell assemblies. Proc Natl Acad Sci U S A *116*, 19264–19273. https://doi.org/10.1073/pnas.1908481116.

Edelman, G.M., and Gally, J.A. (2001). Degeneracy and complexity in biological systems. Proc Natl Acad Sci U S A *98*, 13763–13768. https://doi.org/10.1073/pnas.231499798.

Eggermann, T. (2010). Russell-Silver syndrome. Am J Med Genet C Semin Med Genet *154C*, 355–364. https://doi.org/10.1002/ajmg.c.30274.

Faure, E., Savy, T., Rizzi, B., Melani, C., Stašová, O., Fabrèges, D., Špir, R., Hammons, M., Čúnderlík, R., Recher, G., et al. (2016). A workflow to process 3D+time microscopy images of developing organisms and reconstruct their cell lineage. Nat Commun *7*, 8674. https://doi.org/10.1038/ncomms9674.

Fausto, N., Campbell, J.S., and Riehle, K.J. (2006). Liver regeneration. Hepatology *43*, S45-53. https://doi.org/10.1002/hep.20969.

Fazleabas, A.T., and Strakova, Z. (2002). Endometrial function: cell specific changes in the uterine environment. Mol Cell Endocrinol *186*, 143–147. https://doi.org/10.1016/s0303-7207(01)00655-4.

Félix, M.-A., and Wagner, A. (2008). Robustness and evolution: concepts, insights and challenges from a developmental model system. Heredity (Edinb) *100*, 132–140. https://doi.org/10.1038/sj.hdy.6800915.

Ferrer-Vaquer, A., Piliszek, A., Tian, G., Aho, R.J., Dufort, D., and Hadjantonakis, A.-K. (2010). A sensitive and bright single-cell resolution live imaging reporter of Wnt/ß-catenin signaling in the mouse. BMC Dev. Biol. *10*, 121. https://doi.org/10.1186/1471-213X-10-121.

Flores, D., Madhavan, M., Wright, S., and Arora, R. (2020). Mechanical and signaling mechanisms that guide pre-implantation embryo movement. Development *147*, dev193490. https://doi.org/10.1242/dev.193490.

Frankenberg, S., Shaw, G., Freyer, C., Pask, A.J., and Renfree, M.B. (2013). Early cell lineage specification in a marsupial: a case for diverse mechanisms among mammals. Development *140*, 965–975. https://doi.org/10.1242/dev.091629.

Gardner, D.K., and Truong, T.T. (2019). Culture of the Mouse Preimplantation Embryo. In Comparative Embryo Culture: Methods and Protocols, J.R. Herrick, ed. (New York, NY: Springer), pp. 13–32.

Gardner, R.L., and Cockroft, D.L. (1998). Complete dissipation of coherent clonal growth occurs before gastrulation in mouse epiblast. Development *125*, 2397–2402. https://doi.org/10.1242/dev.125.13.2397.

Gokhale, R.H., and Shingleton, A.W. (2015). Size control: the developmental physiology of body and organ size regulation. WIREs Developmental Biology *4*, 335–356. https://doi.org/10.1002/wdev.181.

Goldin, S.N., and Papaioannou, V.E. (2003). Paracrine action of FGF4 during periimplantation development maintains trophectoderm and primitive endoderm. Genesis *36*, 40–47. https://doi.org/10.1002/gene.10192.

Gomer, R.H. (2001). Not being the wrong size. Nat Rev Mol Cell Biol *2*, 48–54. https://doi.org/10.1038/35048058.

Gong, S., Zheng, C., Doughty, M.L., Losos, K., Didkovsky, N., Schambra, U.B., Nowak, N.J., Joyner, A., Leblanc, G., Hatten, M.E., et al. (2003). A gene expression atlas of the central nervous system based on bacterial artificial chromosomes. Nature *425*, 917–925. https://doi.org/10.1038/nature02033.

Granier, C., Gurchenkov, V., Perea-Gomez, A., Camus, A., Ott, S., Papanayotou, C., Iranzo, J., Moreau, A., Reid, J., Koentges, G., et al. (2011). Nodal cis-regulatory elements reveal epiblast and primitive endoderm heterogeneity in the peri-implantation mouse embryo. Dev Biol *349*, 350–362. https://doi.org/10.1016/j.ydbio.2010.10.036.

Gravina, F.S., Helden, D.F. van, Kerr, K.P., Oliveira, R.B. de, and Jobling, P. (2014). Phasic Contractions of the Mouse Vagina and Cervix at Different Phases of the Estrus Cycle and during Late Pregnancy. PLOS ONE *9*, e111307. https://doi.org/10.1371/journal.pone.0111307.

Gregg, C.L., and Butcher, J.T. (2012). Quantitative in vivo imaging of embryonic development: opportunities and challenges. Differentiation *84*, 149–162. https://doi.org/10.1016/j.diff.2012.05.003.

Guo, G., Huss, M., Tong, G.Q., Wang, C., Li Sun, L., Clarke, N.D., and Robson, P. (2010). Resolution of cell fate decisions revealed by single-cell gene expression analysis from zygote to blastocyst. Dev. Cell *18*, 675–685. https://doi.org/10.1016/j.devcel.2010.02.012.

Hadjantonakis, A.K., and Papaioannou, V.E. (2004). Dynamic in vivo imaging and cell tracking using a histone fluorescent protein fusion in mice. BMC Biotechnology *4*, 1–14. https://doi.org/10.1186/1472-6750-4-33.

Han, D.W., Tapia, N., Joo, J.Y., Greber, B., Araúzo-Bravo, M.J., Bernemann, C., Ko, K., Wu, G., Stehling, M., Do, J.T., et al. (2010). Epiblast stem cell subpopulations represent mouse embryos of distinct pregastrulation stages. Cell *143*, 617–627. https://doi.org/10.1016/j.cell.2010.10.015.

Harris, C. (2012). Rodent whole embryo culture. Methods Mol Biol *889*, 215–237. https://doi.org/10.1007/978-1-61779-867-2_13.

Harrison, R.G. (1924). Some Unexpected Results of the Heteroplastic Transplantation of Limbs. Proc Natl Acad Sci U S A *10*, 69–74. .

Hermitte, S., and Chazaud, C. (2014). Primitive endoderm differentiation: from specification to epithelium formation. Philos Trans R Soc Lond B Biol Sci *369*. https://doi.org/10.1098/rstb.2013.0537.

Hickford, D., Shaw, G., and Renfree, M.B. (2008). In vitro culture of peri-gastrulation embryos of a macropodid marsupial. J Anat *212*, 180–191. https://doi.org/10.1111/j.1469-7580.2007.00846.x.

Hiramatsu, R., Matsuoka, T., Kimura-Yoshida, C., Han, S.-W., Mochida, K., Adachi, T., Takayama, S., and Matsuo, I. (2013). External Mechanical Cues Trigger the Establishment of the Anterior-Posterior Axis in Early Mouse Embryos. Developmental Cell *27*, 131–144. https://doi.org/10.1016/j.devcel.2013.09.026.

Hirate, Y., Hirahara, S., Inoue, K.-I., Suzuki, A., Alarcon, V.B., Akimoto, K., Hirai, T., Hara, T., Adachi, M., Chida, K., et al. (2013). Polarity-dependent distribution of angiomotin localizes Hippo signaling in preimplantation embryos. Curr. Biol. *23*, 1181–1194. https://doi.org/10.1016/j.cub.2013.05.014.

Horiguchi, G., and Tsukaya, H. (2011). Organ Size Regulation in Plants: Insights from Compensation. Front Plant Sci *2*, 24. https://doi.org/10.3389/fpls.2011.00024.

Hsieh, C.-S., Ko, C.-Y., Chen, S.-Y., Liu, T.-M., Wu, J.-S., Hu, C.-H., and Sun, C.-K. (2008). In vivo long-term continuous observation of gene expression in zebrafish embryo nerve systems by using harmonic generation microscopy and morphant technology. J Biomed Opt *13*, 064041. https://doi.org/10.1117/1.3050423.

Hsu, Y.C. (1971). Post-blastocyst differentiation in vitro. Nature *231*, 100–102. https://doi.org/10.1038/231100a0.

Hsu, Y.C. (1972). Differentiation in vitro of mouse embryos beyond the implantation stage. Nature *239*, 200–202. .

Hsu, Y.-C. (1973). Differentiation in vitro of mouse embryos to the stage of early somite. Developmental Biology *33*, 403–411. https://doi.org/10.1016/0012-1606(73)90145-0.

Huang, Q., Cohen, M.A., Alsina, F.C., Devlin, G., Garrett, A., McKey, J., Havlik, P., Rakhilin, N., Wang, E., Xiang, K., et al. (2020). Intravital imaging of mouse embryos. Science *368*, 181–186. https://doi.org/10.1126/science.aba0210.

Ichikawa, T., Nakazato, K., Keller, P.J., Kajiura-Kobayashi, H., Stelzer, E.H.K., Mochizuki, A., and Nonaka, S. (2013). Live Imaging of Whole Mouse Embryos during Gastrulation: Migration Analyses of Epiblast and Mesodermal Cells. PLoS ONE *8*, e64506. https://doi.org/10.1371/journal.pone.0064506.

Ichikawa, T., Zhang, H.T., Panavaite, L., Erzberger, A., Fabrèges, D., Snajder, R., Wolny, A., Korotkevich, E., Tsuchida-Straeten, N., Hufnagel, L., et al. (2022). An ex vivo system to study cellular dynamics underlying mouse peri-implantation development. Dev Cell *57*, 373-386.e9. https://doi.org/10.1016/j.devcel.2021.12.023.

Johnson, M.H., and McConnell, J.M.L. (2004). Lineage allocation and cell polarity during mouse embryogenesis. Seminars in Cell & Developmental Biology *15*, 583–597. https://doi.org/10.1016/j.semcdb.2004.04.002.

Johnson, M.H., and Ziomek, C.A. (1981). Induction of polarity in mouse 8-cell blastomeres: specificity, geometry, and stability. J. Cell Biol. *91*, 303–308. .

Jones, E. a. V., Baron, M.H., Fraser, S.E., and Dickinson, M.E. (2004). Measuring hemodynamic changes during mammalian development. Am J Physiol Heart Circ Physiol *287*, H1561-1569. https://doi.org/10.1152/ajpheart.00081.2004.

Kang, M., Piliszek, A., Artus, J., and Hadjantonakis, A.-K. (2013). FGF4 is required for lineage restriction and salt-and-pepper distribution of primitive endoderm factors but not their initial expression in the mouse. Development *140*, 267–279. https://doi.org/10.1242/dev.084996.

Kang, M., Garg, V., and Hadjantonakis, A.-K. (2017). Lineage Establishment and Progression within the Inner Cell Mass of the Mouse Blastocyst Requires FGFR1 and FGFR2. Developmental Cell *41*, 496-510.e5. https://doi.org/10.1016/j.devcel.2017.05.003.

Karreman, M.A., Hyenne, V., Schwab, Y., and Goetz, J.G. (2016). Intravital Correlative Microscopy: Imaging Life at the Nanoscale. Trends in Cell Biology *26*, 848–863. https://doi.org/10.1016/j.tcb.2016.07.003.

Kierszenbaum, A.L. (2001). Decidualization and implantation: embryo-uterine bioinformatics at work. Mol Reprod Dev *59*, 123–125. https://doi.org/10.1002/mrd.1014.

Korotkevich, E., Niwayama, R., Courtois, A., Friese, S., Berger, N., Buchholz, F., and Hiiragi, T. (2017). The Apical Domain Is Required and Sufficient for the First Lineage Segregation in the Mouse Embryo. Dev Cell *40*, 235-247.e7. https://doi.org/10.1016/j.devcel.2017.01.006.

Koutsourakis, M., Langeveld, A., Patient, R., Beddington, R., and Grosveld, F. (1999). The transcription factor GATA6 is essential for early extraembryonic development. Development *126*, 723–732. .

Krawchuk, D., Honma-Yamanaka, N., Anani, S., and Yamanaka, Y. (2013). FGF4 is a limiting factor controlling the proportions of primitive endoderm and epiblast in the ICM of the mouse blastocyst. Dev. Biol. *384*, 65–71. https://doi.org/10.1016/j.ydbio.2013.09.023.

Krisher, R.L. (2012). Utility of animal models for human embryo culture development: domestic species. Methods Mol Biol *912*, 27–37. https://doi.org/10.1007/978-1-61779-971-6_3.

Krupa, M., Mazur, E., Szczepańska, K., Filimonow, K., Maleszewski, M., and Suwińska, A. (2014). Allocation of inner cells to epiblast vs primitive endoderm in the mouse embryo is biased but not determined by the round of asymmetric divisions (8→16- and 16→32-cells). Dev. Biol. *385*, 136–148. https://doi.org/10.1016/j.ydbio.2013.09.008.

Kurotaki, Y., Hatta, K., Nakao, K., Nabeshima, Y.-I., and Fujimori, T. (2007). Blastocyst axis is specified independently of early cell lineage but aligns with the ZP shape. Science *316*, 719–723. https://doi.org/10.1126/science.1138591.

Kyvelidou, C., Tserevelakis, G.J., Filippidis, G., Ranella, A., Kleovoulou, A., Fotakis, C., and Athanassakis, I. (2011). Following the course of pre-implantation embryo patterning by non-linear microscopy. J Struct Biol *176*, 379–386. https://doi.org/10.1016/j.jsb.2011.09.007.

Lamas, S., Franquinho, F., Morgado, M., Mesquita, J.R., Gärtner, F., and Amorim, I. (2020). C57BL/6J and B6129F1 Embryo Transfer: Unilateral and Bilateral Transfer, Embryo Number and Recipient Female Background Control for the Optimization of Embryo Survival and Litter Size. Animals (Basel) *10*, E1424. https://doi.org/10.3390/ani10081424.

Larina, I.V., Furushima, K., Dickinson, M.E., Behringer, R.R., and Larin, K.V. (2009). Live imaging of rat embryos with Doppler swept-source optical coherence tomography. J Biomed Opt *14*, 050506. https://doi.org/10.1117/1.3241044.

Lauber, D.T., Fülöp, A., Kovács, T., Szigeti, K., Máthé, D., and Szijártó, A. (2017). State of the art in vivo imaging techniques for laboratory animals. Lab Anim *51*, 465–478. https://doi.org/10.1177/0023677217695852.

Lewis, N.E., and Rossant, J. (1982). Mechanism of size regulation in mouse embryo aggregates. Development *72*, 169–181. .

Li, X., Zhao, X., Fang, Y., Jiang, X., Duong, T., Fan, C., Huang, C.C., and Kain, S.R. (1998). Generation of destabilized green fluorescent protein as a transcription reporter. J Biol Chem *273*, 34970–34975. https://doi.org/10.1074/jbc.273.52.34970.

Littwin, T., and Denker, H.-W. (2011). Segregation during cleavage in the mammalian embryo? A critical comparison of whole-mount/CLSM and section immunohistochemistry casts doubts on segregation of axis-relevant leptin domains in the rabbit. Histochem Cell Biol *135*, 553–570. https://doi.org/10.1007/s00418-011-0816-0.

Louvet-Vallée, S., Vinot, S., and Maro, B. (2005). Mitotic spindles and cleavage planes are oriented randomly in the two-cell mouse embryo. Curr. Biol. *15*, 464–469. https://doi.org/10.1016/j.cub.2004.12.078.

Lui, J.C., and Baron, J. (2011). Mechanisms limiting body growth in mammals. Endocr Rev *32*, 422–440. https://doi.org/10.1210/er.2011-0001.

Lui, J.C., Finkielstain, G.P., Barnes, K.M., and Baron, J. (2008). An imprinted gene network that controls mammalian somatic growth is down-regulated during postnatal growth deceleration in multiple organs. Am J Physiol Regul Integr Comp Physiol *295*, R189–R196. https://doi.org/10.1152/ajpregu.00182.2008.

Lupu, F., Terwilliger, J.D., Lee, K., Segre, G.V., and Efstratiadis, A. (2001). Roles of growth hormone and insulin-like growth factor 1 in mouse postnatal growth. Dev Biol *229*, 141–162. https://doi.org/10.1006/dbio.2000.9975.

Ma, W., Song, H., Das, S.K., Paria, B.C., and Dey, S.K. (2003). Estrogen is a critical determinant that specifies the duration of the window of uterine receptivity for implantation. Proc Natl Acad Sci U S A *100*, 2963–2968. https://doi.org/10.1073/pnas.0530162100.

Maître, J.-L., Niwayama, R., Turlier, H., Nédélec, F., and Hiiragi, T. (2015). Pulsatile cell-autonomous contractility drives compaction in the mouse embryo. Nature Cell Biology *17*, 849. https://doi.org/10.1038/ncb3185.

Maître, J.-L., Turlier, H., Illukkumbura, R., Eismann, B., Niwayama, R., Nédélec, F., and Hiiragi, T. (2016). Asymmetric division of contractile domains couples cell positioning and fate specification. Nature *536*, 344–348. https://doi.org/10.1038/nature18958.

Markert, C.L., and Petters, R.M. (1978). Manufactured Hexaparental Mice Show That Adults Are Derived from Three Embryonic Cells. Science *202*, 56–58. https://doi.org/10.1126/science.694518.

Mathiah, N., Despin-Guitard, E., Stower, M., Nahaboo, W., Eski, E.S., Singh, S.P., Srinivas, S., and Migeotte, I. (2020). Asymmetry in the frequency and position of mitosis in the mouse embryo epiblast at gastrulation. EMBO Rep *21*, e50944. https://doi.org/10.15252/embr.202050944.

Matsumoto, H. (2017). Molecular and cellular events during blastocyst implantation in the receptive uterus: clues from mouse models. J Reprod Dev *63*, 445–454. https://doi.org/10.1262/jrd.2017-047.

Matsumoto, H., Fukui, E., and Yoshizawa, M. (2009). Differential Interactions between Embryo and Uterus During Implantation in Laboratory Animals. Jmor *26*, 111–115. https://doi.org/10.1274/jmor.26.111.

Matsuo, I., and Hiramatsu, R. (2016). Mechanical perspectives on the anterior-posterior axis polarization of mouse implanted embryos. Mech. Dev. https://doi.org/10.1016/j.mod.2016.09.002.

McDole, K., and Zheng, Y. (2012). Generation and live imaging of an endogenous Cdx2 reporter mouse line. Genesis *50*, 775–782. https://doi.org/10.1002/dvg.22049.

McDole, K., Guignard, L., Amat, F., Berger, A., Malandain, G., Royer, L.A., Turaga, S.C., Branson, K., and Keller, P.J. (2018). In Toto Imaging and Reconstruction of Post-Implantation Mouse Development at the Single-Cell Level. Cell *175*, 859-876.e33. https://doi.org/10.1016/j.cell.2018.09.031.

McMullen, N.M., Zhang, F., Hotchkiss, A., Bretzner, F., Wilson, J.M., Ma, H., Wafa, K., Brownstone, R.M., and Pasumarthi, K.B.S. (2009). Functional characterization of cardiac progenitor cells and their derivatives in the embryonic heart post-chamber formation. Dev Dyn *238*, 2787–2799. https://doi.org/10.1002/dvdy.22112.

de Medeiros, G., Kromm, D., Balazs, B., Norlin, N., Günther, S., Izquierdo, E., Ronchi, P., Komoto, S., Krzic, U., Schwab, Y., et al. (2020). Cell and tissue manipulation with ultrashort infrared laser pulses in light-sheet microscopy. Scientific Reports *10*, 1942. https://doi.org/10.1038/s41598-019-54349-x.

Migeotte, I., Omelchenko, T., Hall, A., and Anderson, K.V. (2010). Rac1-Dependent Collective Cell Migration Is Required for Specification of the Anterior-Posterior Body Axis of the Mouse. PLoS Biol *8*. https://doi.org/10.1371/journal.pbio.1000442.

Mintz, B. (1964). FORMATION OF GENETICALLY MOSAIC MOUSE EMBRYOS, AND EARLY DEVELOPMENT OF "LETHAL (T12/T12)-NORMAL" MOSAICS. J Exp Zool *157*, 273–292. https://doi.org/10.1002/jez.1401570210.

Mintz, B. (1965). GENETIC MOSAICISM IN ADULT MICE OF QUADRIPARENTAL LINEAGE. Science *148*, 1232–1233. https://doi.org/10.1126/science.148.3674.1232.

Mishra, A., and Seshagiri, P.B. (2000). Evidence for the involvement of a species-specific embryonic protease in zona escape of hamster blastocysts. Mol Hum Reprod *6*, 1005–1012. https://doi.org/10.1093/molehr/6.11.1005.

Mitsui, K., Tokuzawa, Y., Itoh, H., Segawa, K., Murakami, M., Takahashi, K., Maruyama, M., Maeda, M., and Yamanaka, S. (2003). The homeoprotein Nanog is required for maintenance of pluripotency in mouse epiblast and ES cells. Cell *113*, 631–642. .

Miura, S., and Mishina, Y. (2003). Whole-embryo culture of E5.5 mouse embryos: development to the gastrulation stage. Genesis *37*, 38–43. https://doi.org/10.1002/gene.10229.

Mohammed, H., Hernando-Herraez, I., Savino, A., Scialdone, A., Macaulay, I., Mulas, C., Chandra, T., Voet, T., Dean, W., Nichols, J., et al. (2017). Single-Cell Landscape of Transcriptional Heterogeneity and Cell Fate Decisions during Mouse Early Gastrulation. Cell Rep *20*, 1215–1228. https://doi.org/10.1016/j.celrep.2017.07.009.

Mojtahedi, M., Skupin, A., Zhou, J., Castaño, I.G., Leong-Quong, R.Y.Y., Chang, H., Trachana, K., Giuliani, A., and Huang, S. (2016). Cell Fate Decision as High-Dimensional Critical State Transition. PLoS Biol *14*, e2000640. https://doi.org/10.1371/journal.pbio.2000640.

Molè, M.A., Weberling, A., and Zernicka-Goetz, M. (2020). Chapter Four - Comparative analysis of human and mouse development: From zygote to pre-gastrulation. In Current Topics in Developmental Biology, L. Solnica-Krezel, ed. (Academic Press), pp. 113–138.

Molotkov, A., Mazot, P., Brewer, J.R., Cinalli, R.M., and Soriano, P. (2017). Distinct Requirements for FGFR1 and FGFR2 in Primitive Endoderm Development and Exit from Pluripotency. Developmental Cell *41*, 511-526.e4. https://doi.org/10.1016/j.devcel.2017.05.004.

Moolten, F.L., and Bucher, N.L. (1967). Regeneration of rat liver: transfer of humoral agent by cross circulation. Science *158*, 272–274. https://doi.org/10.1126/science.158.3798.272.

Moore, N.W., Adams, C.E., and Rowson, L.E. (1968). Developmental potential of single blastomeres of the rabbit egg. J Reprod Fertil *17*, 527–531. https://doi.org/10.1530/jrf.0.0170527.

Morris, S.A., Teo, R.T.Y., Li, H., Robson, P., Glover, D.M., and Zernicka-Goetz, M. (2010). Origin and formation of the first two distinct cell types of the inner cell mass in the mouse embryo. Proc. Natl. Acad. Sci. U.S.A. *107*, 6364–6369. https://doi.org/10.1073/pnas.0915063107.

Morris, S.A., Grewal, S., Barrios, F., Patankar, S.N., Strauss, B., Buttery, L., Alexander, M., Shakesheff, K.M., and Zernicka-Goetz, M. (2012a). Dynamics of anterior-posterior axis formation in the developing mouse embryo. Nat Commun *3*, 673. https://doi.org/10.1038/ncomms1671.

Morris, S.A., Grewal, S., Barrios, F., Patankar, S.N., Strauss, B., Buttery, L., Alexander, M., Shakesheff, K.M., and Zernicka-Goetz, M. (2012b). Dynamics of anterior–posterior axis formation in the developing mouse embryo. Nature Communications *3*, 673. https://doi.org/10.1038/ncomms1671.

Motosugi, N., Bauer, T., Polanski, Z., Solter, D., and Hiiragi, T. (2005). Polarity of the mouse embryo is established at blastocyst and is not prepatterned. Genes Dev *19*, 1081–1092. https://doi.org/10.1101/gad.1304805.

Muller, T.L., Ngo-Muller, V., Reginelli, A., Taylor, Gail, Anderson, R., and Muneoka, K. (1999). Regeneration in higher vertebrates: Limb buds and digit tips. Seminars in Cell & Developmental Biology *10*, 405–413. https://doi.org/10.1006/scdb.1999.0327.

Müntener, M., and Hsu, Y.C. (1977). Development of trophoblast and placenta of the mouse. A reinvestigation with regard to the in vitro culture of mouse trophoblast and placenta. Acta Anat (Basel) *98*, 241–252. .

Muzumdar, M.D., Tasic, B., Miyamichi, K., Li, L., and Luo, L. (2007). A global double-fluorescent Cre reporter mouse. Genesis *45*, 593–605. https://doi.org/10.1002/dvg.20335.

Negrón-Pérez, V.M., and Hansen, P.J. (2017). The bovine embryo hatches from the zona pellucida through either the embryonic or abembryonic pole. J Assist Reprod Genet *34*, 725–731. https://doi.org/10.1007/s10815-017-0933-3.

New, D. a. T. (1978). Whole-Embryo Culture and the Study of Mammalian Embryos During Organogenesis. Biological Reviews *53*, 81–122. https://doi.org/10.1111/j.1469-185X.1978.tb00993.x.

New, D. a. T., Coppola, P.T., and Terry, S. (1973). CULTURE OF EXPLANTED RAT EMBRYOS IN ROTATING TUBES. Reproduction *35*, 135–138. https://doi.org/10.1530/jrf.0.0350135.

Nielsen, H.I., and Ali, J. (2010). Embryo Culture Media, Culture Techniques and Embryo Selection: A Tribute to Wesley Kingston Whitten. Journal of Reproductive and Stem Cell Biotechnology *1*, 1–29. https://doi.org/10.1177/205891581000100102.

Nishioka, N., Inoue, K., Adachi, K., Kiyonari, H., Ota, M., Ralston, A., Yabuta, N., Hirahara, S., Stephenson, R.O., Ogonuki, N., et al. (2009). The Hippo signaling pathway components Lats and Yap pattern Tead4 activity to distinguish mouse trophectoderm from inner cell mass. Dev. Cell *16*, 398–410. https://doi.org/10.1016/j.devcel.2009.02.003.

Nowotschin, S., Garg, V., Piliszek, A., and Hadjantonakis, A.-K. (2019). Ex Utero Culture and Imaging of Mouse Embryos. Methods Mol Biol *1920*, 163–182. https://doi.org/10.1007/978-1-4939-9009-2_11.

O'Grady, J.E., and Heald, P.J. (1969). The position and spacing of implantation sites in the uterus of the rat during early pregnancy. J Reprod Fertil *20*, 407–412. https://doi.org/10.1530/jrf.0.0200407.

Ohnishi, Y., Huber, W., Tsumura, A., Kang, M., Xenopoulos, P., Kurimoto, K., Oleś, A.K., Araúzo-Bravo, M.J., Saitou, M., Hadjantonakis, A.-K., et al. (2014a). Cell-to-cell expression variability followed by signal reinforcement progressively segregates early mouse lineages. Nat Cell Biol *16*, 27–37. https://doi.org/10.1038/ncb2881.

Ohnishi, Y., Huber, W., Tsumura, A., Kang, M., Xenopoulos, P., Kurimoto, K., Oleś, A.K., Araúzo-Bravo, M.J., Saitou, M., Hadjantonakis, A.-K., et al. (2014b). Cell-to-cell expression variability followed by signal reinforcement progressively segregates early mouse lineages. Nature Cell Biology *16*, 27–37. https://doi.org/10.1038/ncb2881.

Orietti, L.C., Rosa, V.S., Antonica, F., Kyprianou, C., Mansfield, W., Marques-Souza, H., Shahbazi, M.N., and Zernicka-Goetz, M. (2020). Embryo Size Regulates the Timing and Mechanism of Pluripotent Tissue Morphogenesis. Stem Cell Reports https://doi.org/10.1016/j.stemcr.2020.09.004.

O'Sullivan, C.M., Rancourt, S.L., Liu, S.Y., and Rancourt, D.E. (2001). A novel murine tryptase involved in blastocyst hatching and outgrowth. Reproduction *122*, 61–71. https://doi.org/10.1530/rep.0.1220061.

Ozolinš, T.R.S. (2019). Rabbit Whole Embryo Culture. Methods Mol Biol *1965*, 219–233. https://doi.org/10.1007/978-1-4939-9182-2_15.

Panavaite, L. (2018). Emergence of cellular heterogeneity and body plan in early mammalian development. Dissertation. Heidelberg University.

Parasram, K., Bachetti, D., Carmona-Alcocer, V., and Karpowicz, P. (2022). Fluorescent Reporters for Studying Circadian Rhythms in Drosophila melanogaster. Methods Mol Biol *2482*, 353–371. https://doi.org/10.1007/978-1-0716-2249-0_24.

Paria, B.C., Huet-Hudson, Y.M., and Dey, S.K. (1993). Blastocyst's state of activity determines the "window" of implantation in the receptive mouse uterus. Proc Natl Acad Sci U S A *90*, 10159–10162. https://doi.org/10.1073/pnas.90.21.10159.

Paria, B.C., Lim, H., Wang, X.N., Liehr, J., Das, S.K., and Dey, S.K. (1998). Coordination of differential effects of primary estrogen and catecholestrogen on two distinct targets mediates embryo implantation in the mouse. Endocrinology *139*, 5235–5246. https://doi.org/10.1210/endo.139.12.6386.

Paria, B.C., Reese, J., Das, S.K., and Dey, S.K. (2002). Deciphering the cross-talk of implantation: advances and challenges. Science *296*, 2185–2188. https://doi.org/10.1126/science.1071601.

Penzo-Méndez, A.I., and Stanger, B.Z. (2015). Organ-Size Regulation in Mammals. Cold Spring Harb Perspect Biol *7*. https://doi.org/10.1101/cshperspect.a019240.

Perona, R.M., and Wassarman, P.M. (1986). Mouse blastocysts hatch in vitro by using a trypsin-like proteinase associated with cells of mural trophectoderm. Dev Biol *114*, 42–52. https://doi.org/10.1016/0012-1606(86)90382-9.

Petters, R.M., and Mettus, R.V. (1984). Survival rate to term of chimeric morulae produced by aggregation of five to nine embryos in the mouse, Mus musculus. Theriogenology *22*, 167–174. https://doi.org/10.1016/0093-691x(84)90429-1.

Petters, R.M., and Wells, K.D. (1993). Culture of pig embryos. J Reprod Fertil Suppl *48*, 61–73. .

Pilia, G., Hughes-Benzie, R.M., MacKenzie, A., Baybayan, P., Chen, E.Y., Huber, R., Neri, G., Cao, A., Forabosco, A., and Schlessinger, D. (1996). Mutations in GPC3, a glypican gene, cause the Simpson-Golabi-Behmel overgrowth syndrome. Nat Genet *12*, 241–247. https://doi.org/10.1038/ng0396-241.

Plusa, B., Piliszek, A., Frankenberg, S., Artus, J., and Hadjantonakis, A.-K. (2008). Distinct sequential cell behaviours direct primitive endoderm formation in the mouse blastocyst. Development *135*, 3081–3091. https://doi.org/10.1242/dev.021519.

Posfai, E., Petropoulos, S., de Barros, F.R.O., Schell, J.P., Jurisica, I., Sandberg, R., Lanner, F., and Rossant, J. (2017). Position- and Hippo signaling-dependent plasticity during lineage segregation in the early mouse embryo. Elife *6*. https://doi.org/10.7554/eLife.22906.

Power, M.-A., and Tam, P.P.L. (1993). Onset of gastrulation, morphogenesis and somitogenesis in mouse embryos displaying compensatory growth. Anat Embryol *187*, 493–504. https://doi.org/10.1007/BF00174425.

Qi, Q.-R., Xie, Q.-Z., Liu, X.-L., and Zhou, Y. (2014). Osteopontin is expressed in the mouse uterus during early pregnancy and promotes mouse blastocyst attachment and invasion in vitro. PLoS One *9*, e104955. https://doi.org/10.1371/journal.pone.0104955.

Quinlan, G.A., Khoo, P.-L., Wong, N., Trainor, P.A., and Tam, P.P.L. (2008). Cell grafting and labeling in postimplantation mouse embryos. Methods Mol Biol *461*, 47–70. https://doi.org/10.1007/978-1-60327-483-8_6.

Rad, R., Saeedi, P., Au, J., and Havelock, J. (2018). Blastomere Cell Counting and Centroid Localization in Microscopic Images of Human Embryo. 2018 IEEE 20th International Workshop on Multimedia Signal Processing (MMSP) https://doi.org/10.1109/MMSP.2018.8547107.

Raff, M.C. (1996). Size control: the regulation of cell numbers in animal development. Cell *86*, 173–175. https://doi.org/10.1016/s0092-8674(00)80087-2.

Rands, G.F. (1986a). Size regulation in the mouse embryo: I. The development of quadruple aggregates. Development *94*, 139–148. .

Rands, G.F. (1986b). Size regulation in the mouse embryo: II. The development of half embryos. Development *98*, 209–217. .

Rossant, J. (1976). Postimplantation development of blastomeres isolated from 4- and 8-cell mouse eggs. J Embryol Exp Morphol *36*, 283–290. .

Rossant, J., and Lis, W.T. (1979). The possible dual origin of the ectoderm of the chorion in the mouse embryo. Dev. Biol. *70*, 249–254. .

Rossant, J., and Tam, P.P.L. (2004). Emerging Asymmetry and Embryonic Patterning in Early Mouse Development. Developmental Cell *7*, 155–164. https://doi.org/10.1016/j.devcel.2004.07.012.

Rossant, J., and Tam, P.P.L. (2009). Blastocyst lineage formation, early embryonic asymmetries and axis patterning in the mouse. Development *136*, 701–713. https://doi.org/10.1242/dev.017178.

Rossant, J., and Vijh, K.M. (1980). Ability of outside cells from preimplantation mouse embryos to form inner cell mass derivatives. Dev. Biol. *76*, 475–482. .

Ryan, A.Q., Chan, C.J., Graner, F., and Hiiragi, T. (2019). Lumen Expansion Facilitates Epiblast-Primitive Endoderm Fate Specification during Mouse Blastocyst Formation. Dev Cell *51*, 684-697.e4. https://doi.org/10.1016/j.devcel.2019.10.011.

Saiz, N., Williams, K.M., Seshan, V.E., and Hadjantonakis, A.-K. (2016). Asynchronous fate decisions by single cells collectively ensure consistent lineage composition in the mouse blastocyst. Nature Communications *7*, 13463. https://doi.org/10.1038/ncomms13463.

Saiz, N., Mora-Bitria, L., Rahman, S., George, H., Herder, J.P., Garcia-Ojalvo, J., and Hadjantonakis, A.-K. (2020). Growth-factor-mediated coupling between lineage size and cell fate choice underlies robustness of mammalian development. ELife *9*, e56079. https://doi.org/10.7554/eLife.56079.

Salamat, M., Miosge, N., and Herken, R. (1995). Development of Reichert's membrane in the early mouse embryo. Anat Embryol (Berl) *192*, 275–281. https://doi.org/10.1007/BF00184752.

Samarage, C.R., White, M.D., Álvarez, Y.D., Fierro-González, J.C., Henon, Y., Jesudason, E.C., Bissiere, S., Fouras, A., and Plachta, N. (2015). Cortical Tension Allocates the First Inner Cells of the Mammalian Embryo. Dev. Cell *34*, 435–447. https://doi.org/10.1016/j.devcel.2015.07.004.

Sancho, M., Di-Gregorio, A., George, N., Pozzi, S., Sánchez, J.M., Pernaute, B., and Rodríguez, T.A. (2013). Competitive Interactions Eliminate Unfit Embryonic Stem Cells at the Onset of Differentiation. Developmental Cell *26*, 19–30. https://doi.org/10.1016/j.devcel.2013.06.012.

Sawada, H., Yamazaki, K., and Hoshi, M. (1990). Trypsin-like hatching protease from mouse embryos: evidence for the presence in culture medium and its enzymatic properties. J Exp Zool *254*, 83–87. https://doi.org/10.1002/jez.1402540112.

Schindelin, J., Arganda-Carreras, I., Frise, E., Kaynig, V., Longair, M., Pietzsch, T., Preibisch, S., Rueden, C., Saalfeld, S., Schmid, B., et al. (2012). Fiji: an open-source platform for biological-image analysis. Nature Methods *9*, 676–682. https://doi.org/10.1038/nmeth.2019.

Schulz, L.C., and Roberts, R.M. (2011). Dynamic changes in leptin distribution in the progression from ovum to blastocyst of the pre-implantation mouse embryo. Reproduction *141*, 767–777. https://doi.org/10.1530/REP-10-0532.

Seshagiri, P.B., Sen Roy, S., Sireesha, G., and Rao, R.P. (2009). Cellular and molecular regulation of mammalian blastocyst hatching. J Reprod Immunol *83*, 79–84. https://doi.org/10.1016/j.jri.2009.06.264.

Shahbazi, M.N., and Zernicka-Goetz, M. (2018). Deconstructing and reconstructing the mouse and human early embryo. Nat Cell Biol *20*, 878–887. https://doi.org/10.1038/s41556-018-0144-x.

Shen, C., Lamba, A., Zhu, M., Zhang, R., Zernicka-Goetz, M., and Yang, C. (2022). Stain-free detection of embryo polarization using deep learning. Sci Rep *12*, 2404. https://doi.org/10.1038/s41598-022-05990-6.

Sheng, G. (2015). Epiblast morphogenesis before gastrulation. Developmental Biology *401*, 17–24. https://doi.org/10.1016/j.ydbio.2014.10.003.

Simunovic, M., and Brivanlou, A.H. (2017). Embryoids, organoids and gastruloids: new approaches to understanding embryogenesis. Development *144*, 976–985. https://doi.org/10.1242/dev.143529.

Skreb, N., Solter, D., and Damjanov, I. (1991). Developmental biology of the murine egg cylinder. Int J Dev Biol *35*, 161–176. .

Snapp, E.L. (2009). Fluorescent Proteins: A Cell Biologist's User Guide. Trends Cell Biol *19*, 649–655. https://doi.org/10.1016/j.tcb.2009.08.002.

Snow, M. (1977). Gastrulation in Mouse - Growth and Regionalization of Epiblast. Journal of Embryology and Experimental Morphology *42*, 293–303. .

Solter, D. (2016). Preformation Versus Epigenesis in Early Mammalian Development. Curr. Top. Dev. Biol. *117*, 377–391. https://doi.org/10.1016/bs.ctdb.2015.11.006.

Song, H., Han, K., and Lim, H. (2007). Progesterone supplementation extends uterine receptivity for blastocyst implantation in mice. Reproduction *133*, 487–493. https://doi.org/10.1530/REP-06-0330.

Song, L., Chen, J., Peng, G., Tang, K., and Jing, N. (2016). Dynamic Heterogeneity of Brachyury in Mouse Epiblast Stem Cells Mediates Distinct Response to Extrinsic Bone

Morphogenetic Protein (BMP) Signaling. J Biol Chem *291*, 15212–15225. https://doi.org/10.1074/jbc.M115.705418.

Srinivas, S., Rodriguez, T., Clements, M., Smith, J.C., and Beddington, R.S.P. (2004). Active cell migration drives the unilateral movements of the anterior visceral endoderm. Development *131*, 1157–1164. https://doi.org/10.1242/dev.01005.

Stanger, B.Z. (2008). The biology of organ size determination. Diabetes Obes Metab *10 Suppl 4*, 16–22. https://doi.org/10.1111/j.1463-1326.2008.00938.x.

Stanger, B.Z., Tanaka, A.J., and Melton, D.A. (2007). Organ size is limited by the number of embryonic progenitor cells in the pancreas but not the liver. Nature *445*, 886–891. https://doi.org/10.1038/nature05537.

Stower, M.J., and Srinivas, S. (2018). The Head's Tale: Anterior-Posterior Axis Formation in the Mouse Embryo. Curr. Top. Dev. Biol. *128*, 365–390. https://doi.org/10.1016/bs.ctdb.2017.11.003.

Strnad, P., Gunther, S., Reichmann, J., Krzic, U., Balazs, B., de Medeiros, G., Norlin, N., Hiiragi, T., Hufnagel, L., and Ellenberg, J. (2016). Inverted light-sheet microscope for imaging mouse pre-implantation development. Nat Methods *13*, 139–142. https://doi.org/10.1038/nmeth.3690.

Sun, C.-K., Chu, S.-W., Chen, S.-Y., Tsai, T.-H., Liu, T.-M., Lin, C.-Y., and Tsai, H.-J. (2004). Higher harmonic generation microscopy for developmental biology. J Struct Biol *147*, 19–30. https://doi.org/10.1016/j.jsb.2003.10.017.

Tabansky, I., Lenarcic, A., Draft, R.W., Loulier, K., Keskin, D.B., Rosains, J., Rivera-Feliciano, J., Lichtman, J.W., Livet, J., Stern, J.N., et al. (2013). Developmental bias in cleavage-stage mouse blastomeres. Curr Biol *23*, 21–31. https://doi.org/10.1016/j.cub.2012.10.054.

Takaoka, K., Yamamoto, M., Shiratori, H., Meno, C., Rossant, J., Saijoh, Y., and Hamada, H. (2006). The Mouse Embryo Autonomously Acquires Anterior-Posterior Polarity at Implantation. Developmental Cell *10*, 451–459. https://doi.org/10.1016/j.devcel.2006.02.017.

Takaoka, K., Yamamoto, M., and Hamada, H. (2011). Origin and role of distal visceral endoderm, a group of cells that determines anterior-posterior polarity of the mouse embryo. Nat Cell Biol *13*, 743–752. https://doi.org/10.1038/ncb2251.

Takaoka, K., Nishimura, H., and Hamada, H. (2017). Both Nodal signalling and stochasticity select for prospective distal visceral endoderm in mouse embryos. Nat Commun *8*, 1492. https://doi.org/10.1038/s41467-017-01625-x.

Tam, P.P., and Snow, M.H. (1980). The in vitro culture of primitive-streak-stage mouse embryos. J Embryol Exp Morphol *59*, 131–143. .

Tarkowski, A.K. (1959). Experiments on the Development of Isolated Blastomeres of Mouse Eggs. Nature *184*, 1286. https://doi.org/10.1038/1841286a0.

Tarkowski, A.K. (1961). Mouse Chimæras Developed from Fused Eggs. Nature *190*, 857–860. https://doi.org/10.1038/190857a0.

Tarkowski, A.K., and Wróblewska, J. (1967). Development of blastomeres of mouse eggs isolated at the 4- and 8-cell stage. Development *18*, 155–180. .

Thomas, P.Q., Brown, A., and Beddington, R.S.P. (1998). Hex: A homeobox gene revealing peri-implantation asymmetry in the mouse embryo and an early transient marker of endothelial cell precursors. Development *125*, 85–94. .

Thowfeequ, S., Stower, M.J., and Srinivas, S. (2022). Epithelial dynamics during early mouse development. Current Opinion in Genetics & Development *72*, 110–117. https://doi.org/10.1016/j.gde.2021.11.006.

Toralova, T., Kinterova, V., Chmelikova, E., and Kanka, J. (2020). The neglected part of early embryonic development: maternal protein degradation. Cell. Mol. Life Sci. *77*, 3177–3194. https://doi.org/10.1007/s00018-020-03482-2.

Trichas, G., Joyce, B., Crompton, L.A., Wilkins, V., Clements, M., Tada, M., Rodriguez, T.A., and Srinivas, S. (2011). Nodal Dependent Differential Localisation of Dishevelled-2 Demarcates Regions of Differing Cell Behaviour in the Visceral Endoderm. PLoS Biol *9*, e1001019. https://doi.org/10.1371/journal.pbio.1001019.

Ueda, Y., Kimura-Yoshida, C., Mochida, K., Tsume, M., Kameo, Y., Adachi, T., Lefebvre, O., Hiramatsu, R., and Matsuo, I. (2020). Intrauterine Pressures Adjusted by Reichert's Membrane Are Crucial for Early Mouse Morphogenesis. Cell Reports *31*. https://doi.org/10.1016/j.celrep.2020.107637.

Vajta, G., Rienzi, L., Cobo, A., and Yovich, J. (2010). Embryo culture: can we perform better than nature? Reprod Biomed Online *20*, 453–469. https://doi.org/10.1016/j.rbmo.2009.12.018.

Valadão, L., Silva, H.M. da, and Silva, F.M. da (2018). Bovine Embryonic Development to Implantation (IntechOpen).

Vejlsted, M., Du, Y., Vajta, G., and Maddox-Hyttel, P. (2006). Post-hatching development of the porcine and bovine embryo--defining criteria for expected development in vivo and in vitro. Theriogenology *65*, 153–165. https://doi.org/10.1016/j.theriogenology.2005.09.021.

Verheyden, J.M., and Sun, X. (2008). An Fgf/Gremlin Inhibitory Feedback Loop Triggers Termination of Limb Bud Outgrowth. Nature *454*, 638–641. https://doi.org/10.1038/nature07085.

Vianello, S., and Lutolf, M.P. (2019). Understanding the Mechanobiology of Early Mammalian Development through Bioengineered Models. Developmental Cell *48*, 751–763. https://doi.org/10.1016/j.devcel.2019.02.024.

Wang, H., and Dey, S.K. (2006). Roadmap to embryo implantation: clues from mouse models. Nature Reviews Genetics *7*, 185–199. https://doi.org/10.1038/nrg1808.

Wang, S., and Larina, I.V. (2021). In vivo dynamic 3D imaging of oocytes and embryos in the mouse oviduct. Cell Rep *36*, 109382. https://doi.org/10.1016/j.celrep.2021.109382.

Wennekamp, S., Mesecke, S., Nédélec, F., and Hiiragi, T. (2013). A self-organization framework for symmetry breaking in the mammalian embryo. Nat Rev Mol Cell Biol *14*, 452–459. https://doi.org/10.1038/nrm3602.

Whitacre, J.M. (2012). Biological Robustness: Paradigms, Mechanisms, and Systems Principles. Front Genet *3*, 67. https://doi.org/10.3389/fgene.2012.00067.

Wilson, P.A., and Hemmati-Brivanlou, A. (1995). Induction of epidermis and inhibition of neural fate by Bmp-4. Nature *376*, 331–333. https://doi.org/10.1038/376331a0.

Winnier, G., Blessing, M., Labosky, P.A., and Hogan, B.L. (1995). Bone morphogenetic protein-4 is required for mesoderm formation and patterning in the mouse. Genes Dev *9*, 2105–2116. https://doi.org/10.1101/gad.9.17.2105.

Wolny, A., Cerrone, L., Vijayan, A., Tofanelli, R., Barro, A.V., Louveaux, M., Wenzl, C., Strauss, S., Wilson-Sánchez, D., Lymbouridou, R., et al. (2020). Accurate and versatile 3D segmentation of plant tissues at cellular resolution. ELife *9*, 1–34. https://doi.org/10.7554/eLife.57613.

Yamanaka, Y. (2011). Response: Cell fate in the early mouse embryo--sorting out the influence of developmental history on lineage choice. Reprod. Biomed. Online *22*, 525–527; discussion 528. https://doi.org/10.1016/j.rbmo.2011.03.011.

Yamanaka, Y., Ralston, A., Stephenson, R.O., and Rossant, J. (2006). Cell and molecular regulation of the mouse blastocyst. Dev. Dyn. *235*, 2301–2314. https://doi.org/10.1002/dvdy.20844.

Yamanaka, Y., Lanner, F., and Rossant, J. (2010). FGF signal-dependent segregation of primitive endoderm and epiblast in the mouse blastocyst. Development *137*, 715–724. https://doi.org/10.1242/dev.043471.

Yang, X., Li, C., Xu, X., and Deng, C. (1998). The tumor suppressor SMAD4/DPC4 is essential for epiblast proliferation and mesoderm induction in mice. Proc Natl Acad Sci U S A *95*, 3667–3672. https://doi.org/10.1073/pnas.95.7.3667.

Yoshinaga, K. (1988). Uterine receptivity for blastocyst implantation. Ann N Y Acad Sci *541*, 424–431. https://doi.org/10.1111/j.1749-6632.1988.tb22279.x.

Zhang, H.T., and Hiiragi, T. (2018). Symmetry Breaking in the Mammalian Embryo. Annu. Rev. Cell Dev. Biol. *34*, 405–426. https://doi.org/10.1146/annurev-cellbio-100617-062616.

Zhang, Y., Conti, M.A., Malide, D., Dong, F., Wang, A., Shmist, Y.A., Liu, C., Zerfas, P., Daniels, M.P., Chan, C.-C., et al. (2012). Mouse models of MYH9-related disease: mutations in nonmuscle myosin II-A. Blood *119*, 238–250. https://doi.org/10.1182/blood-2011-06-358853.

Zhu, M., Leung, C.Y., Shahbazi, M.N., and Zernicka-Goetz, M. (2017). Actomyosin polarisation through PLC-PKC triggers symmetry breaking of the mouse embryo. Nature Communications *8*, 921. https://doi.org/10.1038/s41467-017-00977-8.

ACKNOWLEDGEMENTS

Looking back from where I stand now, at the end of my PhD, I am amazed by how it feels – paradoxically – like both an entire century and a blink of an eye. It has been an unexpectedly long and convoluted story, not in the least due to wrangling with an ever-evolving project during a lab move and a pandemic. To the following people and organisations, who have supported me during this incredible journey, I owe my most sincere gratitude:

Takashi, the best advisor I could have asked for. I am immensely grateful for this opportunity to have joined your group for my PhD. Thank you for your constant encouragement, for your incisive discussions, and for your unwavering support. I cannot overstate how much I have learnt from you and how much I appreciate your mentorship.

The **Hiiragi group**, both past and current members, who have welcomed me, given me advice and assistance when I struggled, listened to me complain, celebrated my successes with me, and who I will miss very *very* much when I go – Laura, Allyson, Esther, Prachiti, and Vlad; Takafumi, Dimitri, Ritsuya, and Joe; Steffi, Ramona, Wibke, Lidia, and Erica; Alison, Vera, Nisha, Adèle, Jim, and Julie.

Thank you especially, to Takafumi, with whom I have worked closely and who is an excellent mentor *and* friend; to Esther, for always being there for me (and for feeding us delicious, delicious baked goods); to Dimitri, for support regarding microscopy, image analysis, cell tracking, and various philosophical discussions and cat-related inquiries outside of work; to Erica, to whom I pass the torch; and to Lidia, Steffi, and Ramona, for supporting the lab so well – and for being my German teachers outside of evening class, and for putting us up for the night during the lab retreat in Sitges!

My **Thesis Advisory Committee** – Aissam Ikmi, Steffen Lemke, Robert Prevedel, and Ben Steventon – for not only much-valued scientific guidance but also support and encouragement during our TAC meetings.

The **EMBL Laboratory Animal Resource (LAR)** and **Advanced Light Microscopy Facility (ALMF)**, who have naturally been indispensable during my project. To them I owe my deepest gratitude for the truly excellent level of care and support; they are also some of the kindest people I have had the pleasure to meet. I would especially like to thank Sandro, George, Ivan, Erik, and Isabel from the LAR, for accommodating me regarding the embryo transfer experiments – allowing me to take up lab space and mouse supplies, and patiently teaching me the surgical techniques to ensure that I learn everything the right way.

The **Developmental Biology Unit** at EMBL, for being great colleagues and fantastic friends. I am grateful for the opportunity for me to present and receive feedback on my work during the unit seminars. I would like to thank the Aulehla and Ikmi lab members for so kindly sharing with me mouse lines, reagents, techniques, and tools, and for thoughtful discussions during our self-organisation meetings. I would also like to thank Anthi, Anna, and Ale, who have helped me so much with administration matters, especially during the last year of my PhD when the lab move was happening.

EMBL, for hosting me for the majority of my PhD years. I would like to thank the EIPP administrators and Graduate Office for assisting me with every step of my PhD, and to the institute in general for fostering such an open and supportive atmosphere.

The **Hubrecht Institute**, for taking in our mice, machines, and microscopes, and doing their best to make our move to the Netherlands a smooth one. Thank you especially to the Kops and Sonnen groups, for generously sharing their resources and expertise when we were just setting up, and the Animal Care Team at Hubrecht, for assisting with our demands for superovulations and plug checks. Special thanks to Jeroen Korving, Miranda Buter, and Mark Reijnen.

My dear, dear **friends and fellow predocs**, who have made the worst parts of PhD life more bearable and the best parts truly unforgettable. Thank you for being by my side. I wish you every success and happiness in life. (To my beloved little egestlets (you know who you are), I hope you all have a dopé time – until we next cross paths!)

Finally, my **family**, for giving me endless support and love, through spotty signal and bad WIFI, from a continent away. I can't wait to see you all again.

To **everyone**, much love, and a massive thank you one more time!